UNIVERSITA' DEGLI STUDI DI MESSINA
XXIX CICLO DOTTORATO DI RICERCA IN FISICA

EFFECTS OF INSTRUMENTAL ENERGY RESOLUTION ON THE MEASURED MSD AS OBTAINED BY ELASTIC INCOHERENT NEUTRON SCATTERING DATA

Thesis of:
Dr. Salvina Coppolino

Tutor: Chiar.mo Prof. Salvatore Magazù

PhD Coordinator: Chiar.mo Prof. Lorenzo Torrisi

Triennio 2013-2016

Table of contents

Introduction

The introductory chapter presents the work motivation and concludes with a brief description of the thesis.

Motivation

The main focus of the present thesis is Elastic Incoherent Neutron Scattering (EINS) experimental data collected for dry and hydrated (H_2O and D_2O) lysozyme samples; this study was performed as a function of the exchanged wave vector.

Later, the analysis of mean square displacement on the collected elastically scattered intensity data as a function of the exchanged wavevector has been performed.

What has been done to make a comparison between the values of mean square displacement obtained with different instruments.

In particular the data analyzed were obtained at the Institute Laue Langevin (Grenoble, France) by using two spectrometers, IN13 and IN10 working at the energy resolution value of 8 μeV, corresponding to an elastic time resolution of 516 ps, and at the energy resolution value of 1 μeV, corresponding to an elastic time resolution of 4136 ps.

Since the experimentally obtained neutron scattering data depend on the employed spectrometer instrumental characteristics, the system observables as mean square displacement (MSD), are influenced by instrumental effects.

Then, there is the problem of comparing data from spectrometers with different instrumental resolutions.

In order to do this, we faced the problem of normalization of data, which allow to solve it comparing the MSD system.

There are many ways in which we can address the problem of normalization but, after careful analysis, we deduced that only a few of them do not change the value of the MSD.

The comparison, in particular, is performed at very low temperatures (T < 80 K). In such a case occur only vibrational motions and the MSD system can be considered almost constant $\langle r^2 \rangle (t) \rightarrow \langle r^2 \rangle^{(V)}$.

Thesis outline

The current thesis is organized as follows:

- Chapter 1, **Complementary approaches for the characterization of molecular motions in condensed matter systems**. This chapter deals with the use of complementary spectroscopic techniques and numerical techniques for the study of systems of biophysical interest. In particular, the focus is addressed on laser light scattering, infrared absorption, neutron scattering for the characterization of the space-time correlations of physical systems.

- Chapter 2, **Recent Development on Elastic Incoherent Neutron Scattering and Resolution Elastic Neutron Scattering (RENS).** It deals with the collection of elastic neutron scattering intensity both as a function of temperature (EINS) and resolution (RENS).

- Chapter 3, **Mean Square Displacement (MSD).** After an introduction on the Brownian motion, it describes the concept of MSD and the SDF procedure: a recipe for the MSD evaluation from EINS experiments.

- Chapter 4, **Investigated systems and methods**. A description of the investigated systems is reported. More specifically, these are dry and hydrated (H_2O and D_2O) lysozyme samples. In addition, the description of the protein structure and of IN10 and IN13 spectrometers is given.

- Chapter 5, **Results and discussion**. It shows the different normalization procedures applicable to data obtained experimentally in laboratory, so that they can be compared. In particular, it focuses on those useful for normalization of MSD.The results obtained from applied approaches with different normalizzation procedures and the obtained values of MSD for dry and hydrated (H_2O and D_2O) lysozyme are reported.

Chapter 1

Characterization of molecular motions in condensed matter systems using complementary techniques

1.1 General introduction to molecular dynamics and spectroscopic techniques

The spectroscopy experiments and molecular dynamics calculations allow us to approach the study of molecular motions in liquids in two complementary ways [1].

By means of spectroscopic techniques, it is possible to use a probe as electromagnetic waves (e.m.), centrifugal, neutrons, ..., prepared in a known state, that interacts with the degrees of freedom of the investigated system. The probe state changes are due to the interaction, (for example the e.m. wave is dispersed) and such a change reflects the dynamic properties of the system. The result appears normally in the form of a spectrum of energy that must be interpreted in terms of molecular motions. As will be seen below, each spectrum is proportional to the time Fourier transform of a well-defined correlation function (c.f). A c.f is the average balance of the set of two molecular dynamics variables product taken at time 0 and the time t. A means now widely used to extract the physical information from a spectrum is to use the concept of a dynamic model. This model is characterized by one or more equations that govern the rates of evolution of molecular dynamics variables. These equations allow to calculate the correlation functions and, after Fourier transforming, the theoretical spectrum. The parameters of the model may be deducted (jump time, gyration radius...) and the experimental spectrum are compared with the spectrum obtained

If, however, we face the problem by molecular dynamics, we examine about N = 1000 rigid molecules, we consider the potential intermolecular coupling, and we choose the boundary and initial conditions (i.e. the volume and energy) and numerically solve the coupled equations 6N of motion. Based on these results it can generally calculate a physical quantity associated with the system (balance amount as well as time dependent). But the method is limited by computer memory and time; this method can not be very good to test long-standing and long-range phenomena, as described, for example, from hydrodynamic theory theory and critical phenomena. This in particular because:

- N is always small compared to the number of particles in a real sample (the volume of sample tested is always very small) ;
- the number of integration steps is necessarily finished then the time scale is relatively small.

The restriction to pair potentials and to classical mechanics is the other limitation of this method. Consequently a quantum description is therefore necessary as important phenomena such as vibration can not be included. The main interest of the molecular dynamics method is to give typical results that can be compared to results obtained from experiments on real liquids.

1.2 Models for translational and rotational diffusive motions and for vibration motions

To describe molecular translation, rotation and vibration [1] a large number of models have been developed and the main ones are listed below:

1. Translation

- **Langevin model** describes the molecular centre of mass. Then the particle is assumed to be submitted to two forces: a viscous force and a random force. In the limits of very weak and very strong viscosity, one finds the *free translation* and the *uniform translational diffusion*, respectively. In the latter case, the motion is characterized by a single diffusion coefficient D_t (isotropic medium). On the other hand, collective translational motions are usually described in terms of longitudinal acoustic waves and thermal diffusivity in a hydrodynamic theory.

2. Rotation

- In this case many models have been devised and can be summarized in two major groups inertial and stochastic models.

  The **inertial models** are plausible in low density compounds from spheroidal molecules systems infact the molecules are essentially rotating, but undergo random collisions that modify their dynamic state. Examples of inertial models are: the free rotation model (collisions) and diffusion models extended (so-called J and Gordon M models) where, during the collision, the orientation of molecules do not change but their angular

momentum J is randomized.

- The **stochastic models** are plausible in highly condensed systems. In this case the molecules are essentially non rotating, the motions occurring by rapid rotational jumps over barriers. An example is the Debye model (isotropic diffusion characterized by a single diffusion coefficient Dr) so the anisotropic diffusion model and the model of Ivanov (jumps of isotropic finite angle). The distinction between inertial and stochastic models is not clear, especially when the time between jumps or collisions is of the order of (kBT / I) 1/2, the average time to jump to thermal motion rotation. In this case, the model should combine both aspects as is the case for example, in the Langevin model for the rotation. Other models in which they are combined translation and rotation have been imagined. For example, remember the violent collision model in which molecules move freely, except during collisions that instant randomize both the position and the angular momentum. As for the collective rotational motions, some recent experiments of diffusion of light seem to require a description in terms of coupling between shear waves and molecular rotations.

3. Vibrations

   Regarding the molecular vibrations, little is known so far. However, it appears that a large number of mechanism may be the cause for the vibrational relaxation, in particular coupling with all the other degrees of freedom: rotation, translation and other vibrations.

   Obviously this does not exhaust the study of the subject which is much more extensive than we treated

1.3 The principle of a spectroscopic experiment: definitions

Given a system (i.e. a molecular liquid) which we call reservoir R, formed by N particles, in thermal equilibrium T. This reservoir is characterized by its Hamiltonian H_R whose eigenvalues and eigenstates are $E_{m'}$ and $|m'\rangle$ respectively [1].

We wonder how the molecular properties of this system vary with time. For this reason, we consider another system (e.g. the e.m. field, the neutron field, a spin system) which

we call the probe P. It is characterized by its Hamiltonian H_P whose eigenvalues and eigenstates are labelled E_m and $|m\rangle$.

The probe has the ability to join with the dynamical variables of the reservoir and this coupling is characterized by an Hamiltonian H_C.

1.3.1 First step: *Probe-system coupling*

Initially, we consider the probe in a defined dynamical state $|m\rangle$ (e.g. e.m. waves or neutrons are collimated and monochromatized). Being at thermal equilibrium, the reservoir R can be in any state $|m'\rangle$ with the probability p_m, given by the Boltzmann law:

$$p_{m'} = \frac{1}{Z_R}\exp(-\beta E_{m'}) \tag{1.1}$$

with

$$Z_R = \sum_{m'}\exp(-\beta E_{m'}) \tag{1.2}$$

and

$$\beta = \frac{1}{k_B T} \tag{1.3}$$

Where k_B is the Boltzmann constant.

The figure below shows a sketch of a spectroscopic experiment.

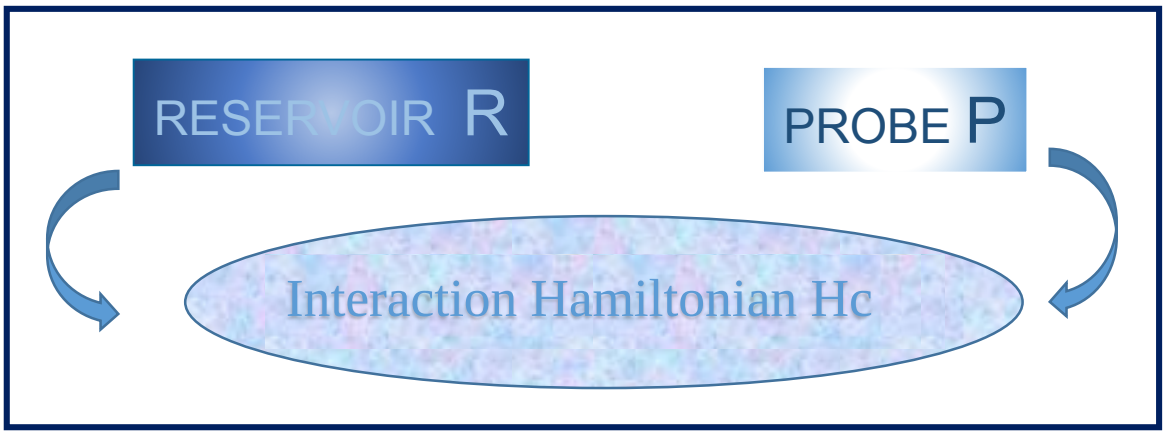

Figure 1.1 Sketch of a spectroscopic experiment

Because of the interaction hc turned on, the state of the probe P can change with time from the inistial state $|m\rangle$ to a final state $|n\rangle$. If H_C is small compared to H_P and H_R, in the linear approximation this change can be characterized by a probability per unit time

W_{nm}. The purpose of any spectroscopic experiment is to measure a quantity which is proportional to W_{nm} as a function of $|n\rangle$ or $|m\rangle$. This because W_{nm} measurement yields information about what is happening in R (e.g. the molecular motions) being that W_{nm} is a function of operators of R. Then what we need to do is to calculate W_{nm} and relating it to a measurable quantity.

1.3.2 Second step: *Calculation of W_{nm}*

The calculation of W_{nm} goes made considering the total system formed by the probe plus the reservoir. The corresponding eigenstates are symbolized by $|m\rangle\,|m'\rangle$.
In the linear approximation, we have:

$$W_{nm} = \sum_{m'n'} W_{mm'nn'} p_{m'} \tag{1.4}$$

where $W_{n'nm'm}$ is the probability for unit time that this total system changes from the state $|m\rangle\,|m'\rangle$ to the state $|n\rangle\,|n'\rangle$ due to H_C and its value is given by the following Fermi rule .

$$W_{mm'nn'} = \frac{2\pi}{\hbar}\left|\langle n'|\langle n|H_C|m\rangle|m'\rangle\right|^2 \delta\left(E_{m'} + E_m - E_{n'} - E_n\right) \tag{1.5}$$

The delta function that we see is obtainable by the energy conservation principle. Defining $\overline{H}_C$ as the average of H_C between the initial and final state of the probe:

$$\overline{H}_C = \langle n|H_{\text{int}}|m\rangle \tag{1.6}$$

Defined in this way, $\overline{H}_C$ is an operator that acts on the states of the reservoir only. With the following definitions:

$$\hbar\omega = E_m - E_n \tag{1.7}$$
$$\hbar\omega = E_{n'} - E_{m'} \tag{1.8}$$

considering the equation written above, the probability W_{nm} is written:

$$W_{nm} = \frac{2\pi}{\hbar^2}\sum_{m'n'}\frac{\exp(-\beta E_{m'})}{Z_R}\left|\langle n'|H_C|m'\rangle\right|^2 \delta(\omega_{n'm'} - \omega) \tag{1.9}$$

This expression is suitable to describe discrete peaks in a spectrum, as is the case for a purely quantum system, thanks to the presence of the δ function [1].

Using the fact that $\overline{H}_C$ is an hermitian operator and by using the integral expression for the δ function is possible using another equivalent expression for W_{nm} for describing more complicated system.

We have:

$$\left|\langle n'|\overline{H}_C|m'\rangle\right|^2 = \langle n'|\overline{H}_C|m'\rangle\langle m'|\overline{H}^+{}_C|n'\rangle \tag{1.10a}$$

and

$$\delta(\omega_{n'm'}-\omega)\frac{1}{2\pi}\int_{-\infty}^{+\infty} dt e^{i(\omega_{n'm'}-\omega)t} \tag{1.10b}$$

inserting eqs. (1.10a) and (1.10b) in eq.(1.9) and using Eq. (1.8), we obtain

$$W_{nm} = \frac{1}{\hbar^2}\int_{-\infty}^{+\infty} dt \sum_{n'm'} \frac{e^{-\beta E_{m'}}}{Z_R}\langle m'|H_C{}^+|n'\rangle\langle n'|e^{-i\frac{E_n}{\hbar}t}\overline{H}_C e^{+i\frac{E_{m'}}{\hbar}t}|m'\rangle e^{-i\omega t} \tag{1.11}$$

The double sum is simply the expression of a trace in the R Hilbert space. We thus have:

$$W_{nm} = \frac{1}{\hbar^2}\int_{-\infty}^{+\infty} dt Tr\left\{\rho_R H_C{}^+(0)H_C(t)\right\}e^{-i\omega t} \tag{1.12}$$

where ρ_R is the density matrix of R at thermal equilibrium:

$$\rho_R = \frac{e^{-\beta H_R}}{Tr\left[e^{-\beta H_R}\right]} \tag{1.13}$$

and $\overline{H}_C(t)$ is the Heisenberg representation of operator $\overline{H}_C$:

$$\overline{H}_C(t) = e^{-i\frac{E_n}{\hbar}t}\overline{H}_C e^{+i\frac{E_{m'}}{\hbar}t} \tag{1.14}$$

The quantity

$$C_{\overline{H}_C\overline{H}_C} = Tr\left\{\rho_R \overline{H}_C{}^+(0)\overline{H}_C(t)\right\} = \left\langle \overline{H}_C{}^+(0)\overline{H}_C(t)\right\rangle \tag{1.15}$$

is the quantum expression for the autocorrelation function of $\overline{H}_C$.

If the reservoir is classical, then $\overline{H}_C$ is a classical function of the variables of R and $C_{\overline{H}_C\overline{H}_C}(t)$ should be replaced by its classical equivalent. Defining the spectral density $C_{\overline{H}_C\overline{H}_C}(\omega)$ as the time Fourier transform of $C_{\overline{H}_C\overline{H}_C}(t)$:

$$C_{\overline{H}_C\overline{H}_C}(\omega) = \frac{1}{2\pi}\int_{-\infty}^{+\infty} C_{\overline{H}_C\overline{H}_C}(t)e^{-i\omega t}dt \tag{1.16}$$

and using eq.(1.12), the probability of transition W_{nm} is finally written:

$$W_{nm} = \frac{2\pi}{\hbar^2} C_{\overline{H}_C\overline{H}_C}(\omega) \tag{1.17}$$

An important point is to relate the probabilities for the direct transition W_{nm} and the inverse transition W_{mn} is finally. Changing ω into $-\omega$ in the above equations, after a little algebra, we obtain:

$$W_{mn} = e^{-\beta\hbar\omega}W_{nm} \tag{1.18}$$

This is the Kubo-Ayant theorem which means that, in the linear approximation, the probability per unit time for the transition from one level to another is proportional to the population of this level.

In summary, to describe any spectroscopic experiment, we are led to define the reservoir, the probe, the interaction H_C and calculate the average value $\overline{H}_C$, its correlation function $C_{\overline{H}_C\overline{H}_C}(t)$ and the probability W_{nm}. To be complete, we must relate W_{nm} to a measurable quantity. However, this relationship is clearly dependent on the type and details of the experiment (e.g. an absorption experiment, a scattering experiment, a relaxation experiment) and no general formula can be given. We shall thus establish it for each particular case treated below.

1.4 Neutron Scattering

In this part we will talk about neutron, describing how they can be used to study molecular motions. We begin first remembering the properties and associated concepts, then describe the principles of a neutron scattering experiment, deduce the relevant correlation function, relate it to the scattered intensity and give some illustrative examples [1].

1.4.1 Properties of the neutron probe

The free neutron [1] is an elementary particle with zero charge and spin ½, liberated for example during the process of fission of a heavy nucleus. In a nuclear reactor, the neutrons are thermalized by the atoms of the moderator, yielding a Maxwellian distribution of velocities v peaked at some $\bar{v}$ such that the average (kinetic) energy $\overline{E}$ is

$$E = \frac{1}{2} m_n \bar{v}^2 = \frac{3}{2} k_B T \tag{1.19}$$

where m_n is the mass of the neutron.

Neutrons can also be considered as plane waves of wave number $\vec{k}$ or wavelength $\lambda = 2\pi/k$. The relationships between particle and wave aspects are:

$$E = \frac{\hbar^2 k^2}{2m_n} \tag{1.20}$$

and

$$v = \frac{\hbar k}{m_n} \tag{1.21}$$

For thermal neutrons (T=300K), we have $\overline{E}$ =26 meV and $\bar{\lambda}$=1.8 Å. It is important to note that these values have the same order of magnitude as the intermolecular energies and molecular dimensions, respectively. In fig. 1.2 the spatial scales interested by neutron probe are reported.

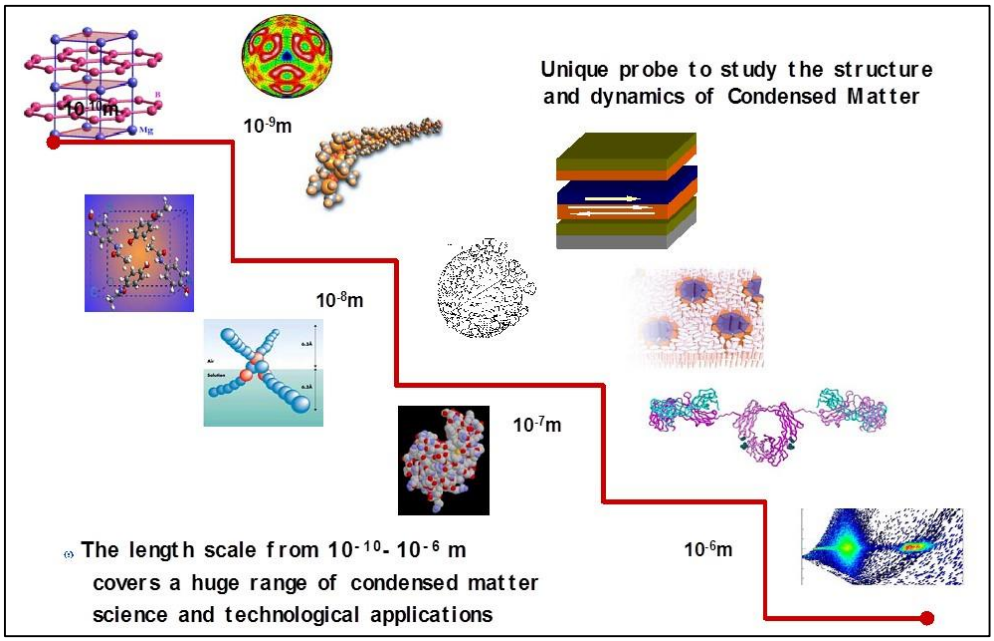

Fig. 1.2: Spatial scales interested by the neutron probe.

Finally, considered as quantum objects, neutrons are characterized by wave functions $|k\rangle$ such that

$$|k\rangle = \frac{1}{\sqrt{V}} e^{i\vec{k}\vec{r}} \tag{1.22}$$

where V is the "volume of quantization" to be identified with the volume of the irradiated sample. In this volume, the density of states of momentum $\vec{k}$ is given by

$$\rho(\vec{k}) = \frac{V}{(2\pi)^3} \tag{1.23}$$

Using the expression below of the volume element in spherical coordinates:

$$d\vec{k} = k^2 d\vec{k} d\Omega \tag{1.24}$$

with:

$d\Omega$ = the solid angle corresponding to $d\vec{k}$ around $\vec{k}$

we deduce that the number of independent neutron states between $\vec{k}$ and $\vec{k} + d\vec{k}$ is:

$$\rho(\vec{k}) d\vec{k} = \frac{V}{(2\pi)^3} k^2 d\vec{k} d\Omega \tag{1.25}$$

In fig. 1.3 a neutron "identity card" is reported.

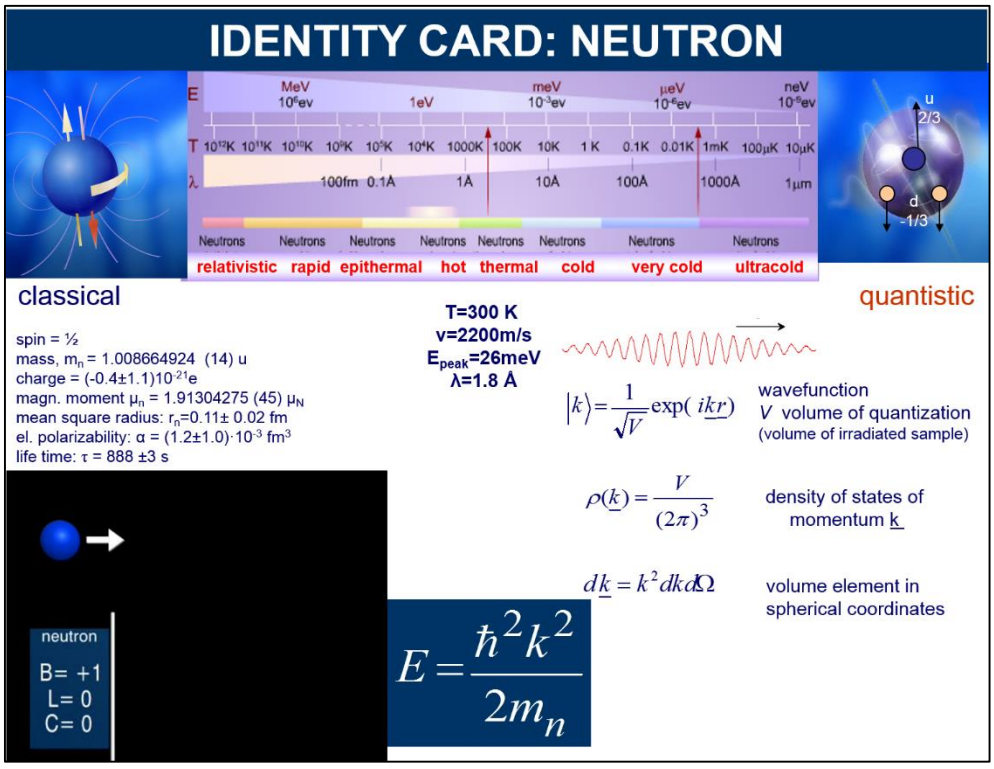

Fig. 1.3: "Identity card" of neutron

1.4.2 Nature of the neutron-nucleus interaction

A neutron interacts with a nucleus through nuclear and magnetic forces. Concerning the nuclear part, since nuclear interactions are very short range compared to the (thermal) neutron wavelength, it can be shown that the interaction potential between a neutron located at $\vec{r}$ and a nucleus located at $\vec{r}_i$ can be written as

$$V(\vec{r}) = \frac{2\pi\hbar^2}{m_n} b_i \delta(\vec{r} - \vec{r}_i) \tag{1.26}$$

In the expression we have written now (the so-called Fermi pseudo-potential), the scattering length b_i characterizes the interaction and is independent of neutron energy. b_i can be positive or negative depending on the attractive or repulsive nature of the interaction. Is so difficult theoretically calculate the value of b_i and for this reason it is calculated experimentally

For the magnetic interaction, the neutron interacts with the spins through the dipole-dipole coupling. Compared to the nuclear interaction, for diamagnetic systems it is always insignificant and shall not be considered in the following. fig. 1.4 shows the Maxwell neutron velocity distribution.

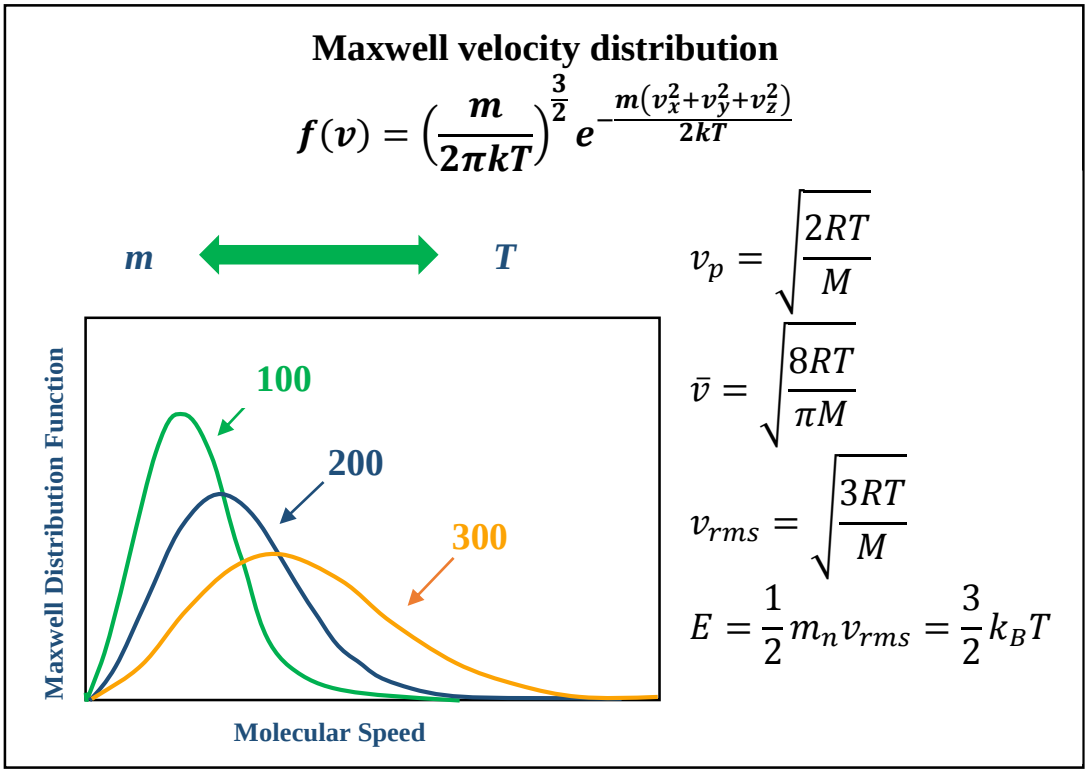

Fig. 1.4: Neutron velocity distribution

1.4.3 Coherent and incoherent scattering contributions and relative cross -sections

Consider a set of a given atomic species, i, in which many isotopes possessing a nuclear spin. The scattering length, b_i , will alter from one atom to another, since the interaction depends on the nature of the nucleus and on the total spin state of the nucleus-neutron system.

The average $\langle b_i \rangle$ of b_i over all the isotopes and spin states is called *coherent scattering length*. The mean square deviation of b_i from $\langle b_i \rangle$ is called the *incoherent scattering length*. We thus have

$$b_i^{coh} = \langle b_i \rangle \tag{1.27}$$

$$b_i^{incoh} = \left[\langle b_i \rangle^2 - \langle b_i \rangle^2 \right]^{1/2} \tag{1.28}$$

From these definitions, it is clear that b_i^{coh} and b_i^{incoh} can be modified simply by changing the relative concentration of the various isotopes. This has a great practical importance in

neutron experiment (isotopic substitution). The coherent and incoherent scattering cross-section are defined by

$$\sigma_i^{coh} = 4\pi b_i^{2\,coh} \tag{1.29}$$

$$\sigma_i^{incoh} = 4\pi b_i^{2\,incoh} \tag{1.30}$$

In the following table we list the values of these quantities in barns (1barn=10^{-24} cm^2) for a few atom:

Element	Z	Weight number	s	σ_{coh} (barn)	σ_{inc} (barn)	σ (barn)	σ_{ass} (barn)	NOTE
H	1	1.0079	1/2	1.7568	80.26	82.02	0.3326	σ_{inc} much larger than other elements. Privileged to study individual motion in hydrogenated compounds
D	1	2.0144	1	5.592	2.05	7.64	0.000519	Advantage of a selective deuteration
C	6	12.0107	0	5.551	0.001	5.551	0.0035	
O	8	15.9994	0	4.232	0.0008	4.232	0.00019	
Al	13	26.9815	5/2	1.495	0.0082	1.503	0.231@1.8Å	Weak absorber. Sample containers, windows and high pressure cells
V	23	50.9415	7/2	0.0184	5.08	5.1	5.08	Scattering nearly purely incoherent. Instrument calibration (relative efficiency of detectors, instrument resolution)
Cd	48	112.411	1/2	3.04	3.46	6.5	2520@1.8Å	Strong absorber. Shields against parasitic reflections or slits to delimit the shape and dimensions of neutron beams
Gd	64	157.25	3/2	29.3	151	180	29400@1.8Å	Strong absorber as Cd

Table 1.1: Values of coherent and incoherent scattering cross-section in barns for a few common elements

In fig. 1.5 elements' neutron total cross section values are reported.

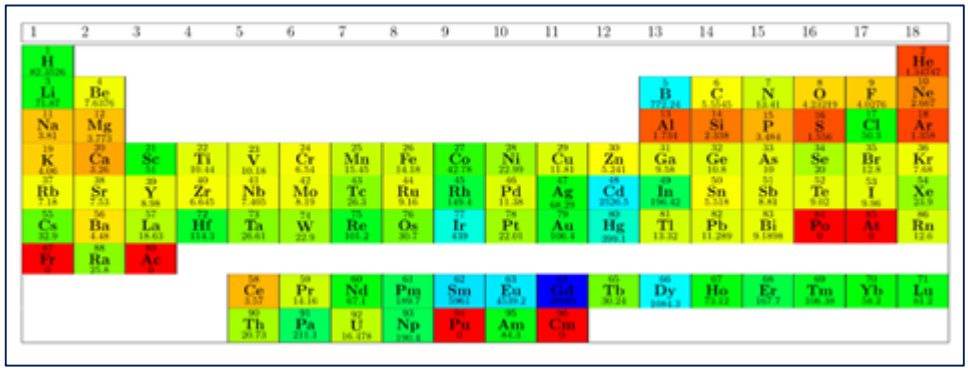

Fig. 1.5: Elements' neutron total cross section

1.4.4 Neutron scattering experiment

Is necessary, to describe the principles of a neutron experiment, first of all define the probe P, the reservoir R, and the interaction H_C. The probe P is constituted by the neutron plane waves which are characterized by their wave functions $|k\rangle$. The reservoir R is made up of N particles located at $|\vec{r}_i\rangle$. The interaction H_C between P and R is given by Eq. (26) summed over all the particles *i*:

$$H_C = \left(\frac{2\pi\hbar^2}{m_n}\right)\sum_i b_i \delta(\vec{r} - \vec{r}_i) \tag{1.31}$$

Subsequently a quantistic description, one looks for the probability of the neutrons to be scattered from a well defined initial state $|m>=|k_0>$ to a final state $|n>=|k_1>$. The average of H_C between these two states is:

$$\overline{H}_C = \langle \underline{k}_0 | H_C | \underline{k}_1 \rangle = \frac{1}{V}\left(\frac{2\pi\hbar^2}{m_n}\right)\sum_i b_i e^{i\underline{Q}\cdot r_i} \tag{1.32}$$

where

$$\underline{Q} = \underline{k}_0 - \underline{k}_1 \tag{1.33}$$

is the neutron momentum transfer.

Calling *V* the scattering volume, based on what was said, the correlation function is simply obtained:

$$C_{H_C H_C}(t) = \frac{1}{V^2}\left(\frac{2\pi\hbar^2}{m_n}\right)^2 \sum_{ij} \left\langle b_i b_j \exp\left\{i\underline{Q}\cdot\left[\underline{r}_i(t) - \underline{r}_j(0)\right]\right\}\right\rangle \tag{1.34}$$

Based on the equation 1.17 the Fourier transform of equation (1.34), one obtains the corresponding probability transition $W_{k_1 k_0}$ that is to be related to a measurable quantity. Indicating I_0 as the number of incident neutron per cm^2 and per second and I as the number of neutron scattered per second between $\underline{k}_1$ and $\underline{k}_1 + d\underline{k}_1$, we have:

$$\frac{I}{I_0} \propto W_{k_1 k_0} k_1^{\,2} dk_1 d\Omega \tag{1.35}$$

Starting from the equations (1.21), (1.17), (1.34) and (1.25) and using the definition of the energy E_1 of the scattered neutron:

$$E_1 = \hbar\omega_1 = \frac{\hbar^2 k_1^{\,2}}{2m_n} \tag{1.36}$$

in the end we get:

$$\frac{I}{I_0} = \left(\frac{d^2\sigma}{d\Omega dE'}\right) d\Omega dE' = \left(\frac{d^2\sigma}{d\Omega d\omega}\right) d\Omega d\omega_1 = \frac{|\underline{k}_1|}{|\underline{k}_0|} N\left(\frac{\sigma}{4\pi} S\ (Q,\omega)\right) d\Omega d\omega_1' \tag{1.37}$$

The double differential scattering cross-section, $\frac{d^2\sigma}{d\Omega d\omega}$ present in equation (1.37), represents the normalized scattered intensity per unit energy and per unit solid angle and is a measure of the number of neutrons scattered per second into a solid angle dΩ about $\underline{k}_1$ with energies in a range dE' about E', with

$$S\ (\underline{Q},\omega) = \frac{1}{2\pi} \int_{-\infty}^{+\infty} I\ (\underline{Q},t) \exp(-i\omega t) dt \tag{1.38}$$

and

$$I\ (\underline{Q},t) = \frac{1}{N} \sum_{i,j} < b_i\, b_j \exp\{i\underline{Q} \cdot [\underline{r}_i(t) - \underline{r}_j(0)]\} > \tag{1.39}$$

From eq. (1.39) we can see that neutron scattering reflects molecular motions through the variation of the position of the scattering particles. By making explicit the average in eqn. (1.39), we can say out more about the nature of these motions. This average can be carried out on $b_i\, b_j$ and or also on the exponential. The explanation for this is that the actual scattering length of every nucleus is evidently independent of its position. According to equations (1.27) and (1.28) in equation (1.39) we can write:

$$I(\underline{Q},t) = I_p(\underline{Q},t) + I_s(\underline{Q},t) \tag{1.40}$$

with

$$I_p(\underline{Q},t) = \frac{1}{N}\sum_{i,j} b_i^{\,coh} b_j^{\,coh} \left\langle e^{i\vec{Q}[\vec{r}_i(t)-\vec{r}_j(0)]} \right\rangle \tag{1.41}$$

$$I_s(Q,t) = \frac{1}{N}\sum_{i,j} b_i^{\,2incoh} \left\langle e^{i\underline{Q}[\underline{r}_i(t)-\underline{r}_j(0)]} \right\rangle \tag{1.42}$$

and by analogy

$$S(\underline{Q},\omega) = S_p(\underline{Q},\omega) + S_s(\underline{Q},\omega) \tag{1.43}$$

These equations show that we have two types of scattering: a coherent part and an incoherent part.

If the system is composed of molecules that do not contain hydrogen atoms (e.g. a simple liquid) then

$$b_i^{\,coh} >> b_i^{\,incoh}$$

and the scattering is mainly coherent. $I_p(\underline{Q},t)$ is a pair correlation function and thus the spectra mainly reflect collective atomic motions. If, instead, it is in the system of hydrogen atoms then (e.g. most molecular liquids) then

$$b_i^{\,incoh} >> b_i^{\,coh}$$

and the scattering is mainly incoherent. $I_s(\underline{Q},t)$ is a self correlation function and thus the spectra mainly reflect the individual atomic motions. From here on we shall consider only the latter case

In fig. 1.6 the accessible wavevector-energy region of neutrons is reported.

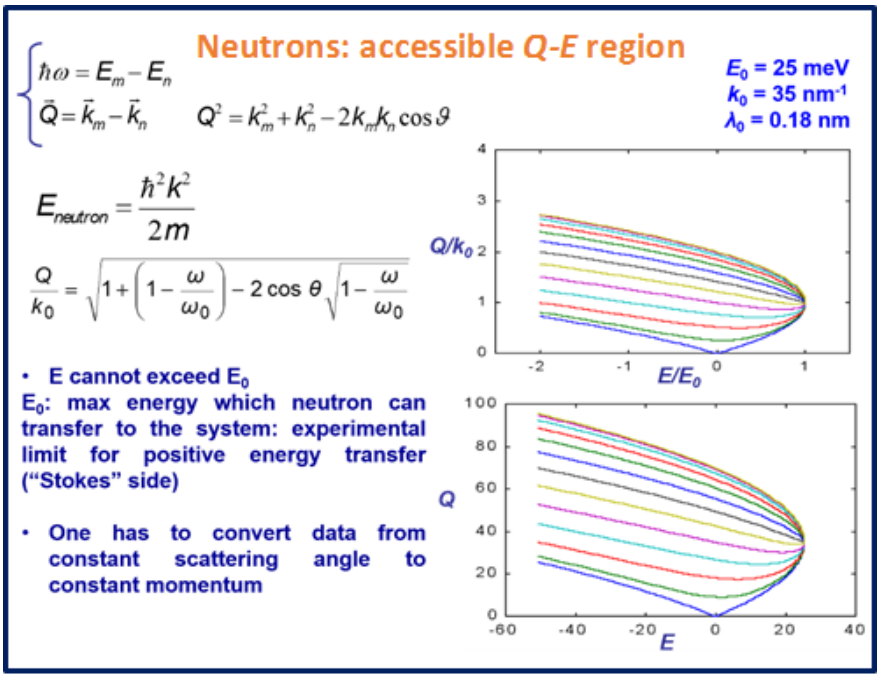

Fig. 1.6: Neutron accessible wavevector-energy region

1.4.5 Scattering from incoherent scatterers

Let us consider a system made of identical molecules that contain, for simplicity, only one hydrogen atom. Since the scattering is almost completely incoherent, we have

$$I(\underline{Q},t) = I_s(\underline{Q},t) = const\left\langle e^{i\underline{Q}[\underline{r}_i(t) - \underline{r}_j(0)]}\right\rangle \tag{1.44}$$

In fig. 1.7 a scheme of typical molecular motions is shown.

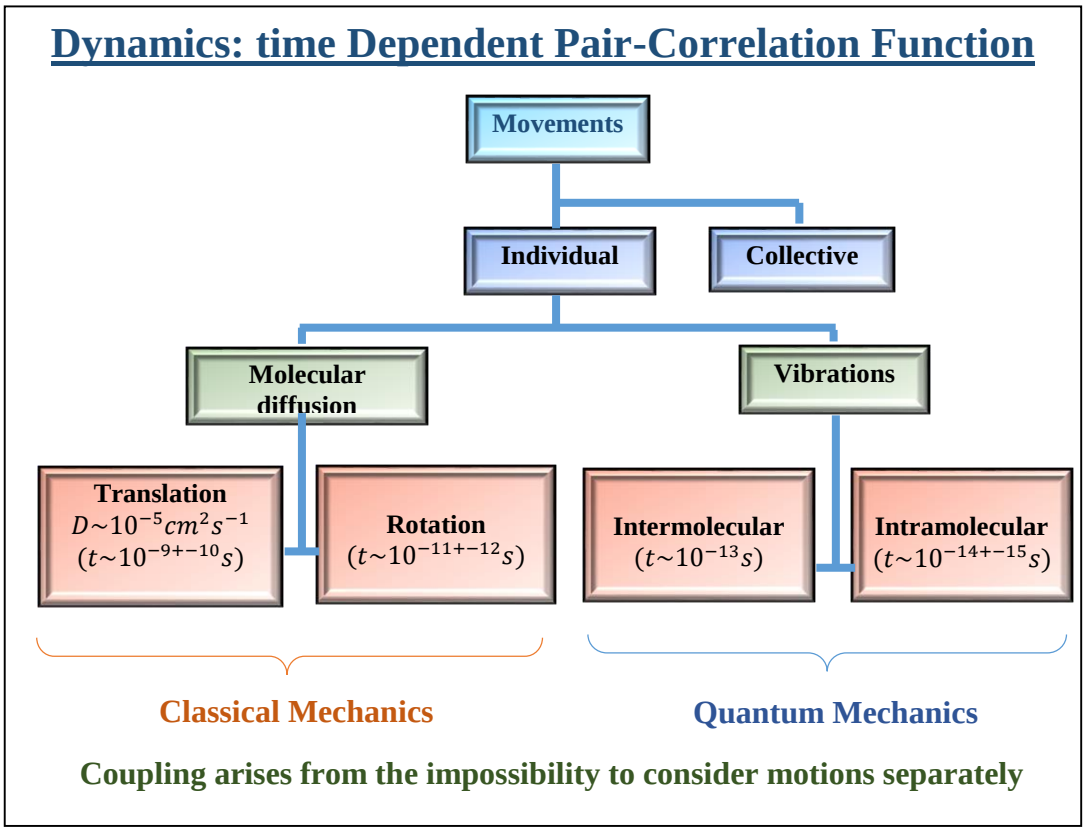

Fig. 1.7: Scheme of molecular motions.

Hereafter we use for simplicity normalized functions by doing the constant equal to 1. Let us write

$$\underline{r} = \underline{d} + \underline{\rho} + \underline{u} \tag{1.45}$$

Where:

$\underline{d}$ is the molecular centre of mass (c.o.m.)

$\underline{\rho}$ is the position of the proton with respect to the c.o.m. and stands for the vibrational

displacement around the average position.

We have, in the classical approximation:

$$\left\langle e^{i\underline{Q}(\underline{r}-\underline{r}_0)} \right\rangle = \left\langle e^{i\underline{Q}(\underline{d}-\underline{d}_0)} \right\rangle \left\langle e^{i\underline{Q}(\underline{\rho}-\underline{\rho}_0)} \right\rangle \left\langle e^{i\underline{Q}(\underline{u}-\underline{u}_0)} \right\rangle \tag{1.46}$$

If the translation (i.e. motion of $\underline{d}$), rotation (i.e. motion of $\vec{\rho}$) and vibration (i.e. motion of $\vec{u}$) are not combined, then can be carried out individually the average on the three exponentials in eq. (1.46) and we have, with evident notations:

$$I_s = I_s^{trans} I_s^{rot} I_s^{vib} \tag{1.47}$$

$$S_s(\underline{Q},\omega) = S_s^{trans}(\underline{Q},\omega) \otimes S_s^{rot}(\underline{Q},\omega) \otimes S_s^{vib}(\underline{Q},\omega) \tag{1.48}$$

If the motions are independent this result implies that the total incoherent scattering law is the convolution product of the scattering laws for the three elementary motions. In fig. 1.8 a sketch of autocorrelation, cross-correlation and convolution is shown.

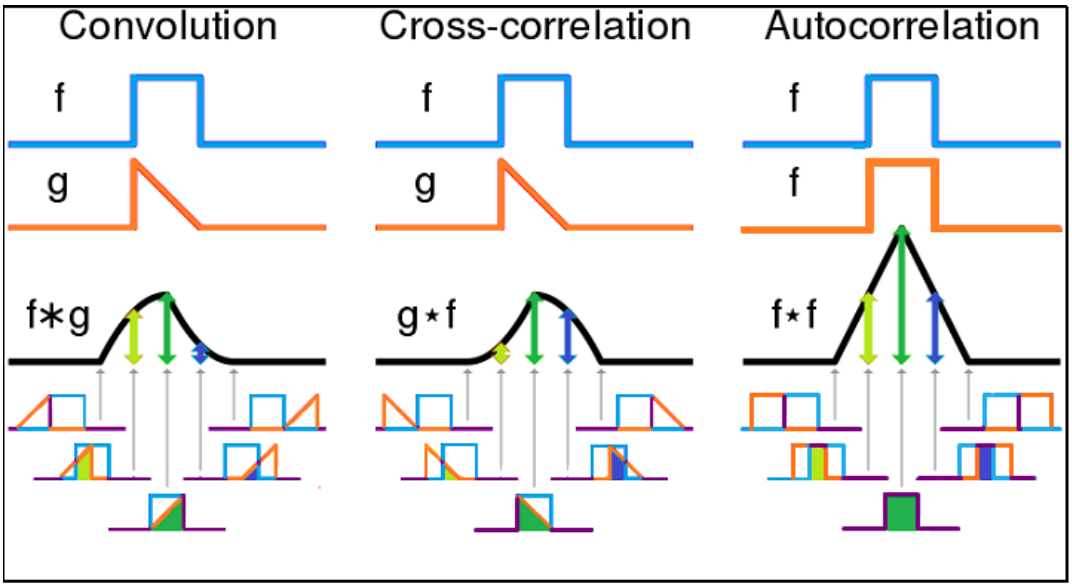

Fig.1.8: Sketch of autocorrelation, cross-correlation and convolution

If now the molecules have inside inequivalent protons, the equations that we saw earlier should be averaged over these protons. In this case, the spectra reflect the superposition of the motions of the different protons. A way to separate them is to use several partially deuterated specimens in order to make invisible to neutrons afterwards each kind of proton. This approach was successfully utilized in the field of liquid crystals.

1.4.6 Incoherent "Quasi-elastic" Spectra

In this part, we discuss calculations, that are simple in some cases, to make obvious the main features of incoherent spectra reflecting pure rotation, pure translation and a combination of both. Since these spectra are centered around $\omega = 0$, they are usually qualified as "quasi-elastic".

1.4.6.1 Rotation and diffusion spectral contribution

Let us examine the simple case of isotropic rotational diffusion on a sphere of radius ρ. The position of the particle is characterized by a vector $\underline{\rho}$ (t). The probability distribution G_s of its orientation Ω is governed by the following rate equation

$$\frac{\partial G_S}{\partial t} = D_r \nabla^2_{\Omega} G_S \tag{1.49}$$

In which:

$G_s(\Omega, \Omega_0, t)$ is the probability of finding the orientation at Ω at time t if it was at Ω_0 at zero time

D_r is the rotational diffusion coefficient.

The solution of this equation is

$$G_s(\Omega, \Omega_0, t) = 4\pi \sum_{l=0}^{\infty} e^{-Drl(l+1)t} \sum_{m=-l}^{+l} Y_m^l(\Omega) Y_m^{l*}(\Omega_0) \tag{1.50}$$

From eqn. (1.44) we get:

$$I_s(\underline{Q}, t) = \frac{1}{4\pi} \int e^{i\vec{Q}(\vec{\rho}-\vec{\rho}_0)} G_S d\Omega d\Omega_0 = j_0^2(Q\rho) + \sum_{l=1}^{\infty} (2l+1) j_l^2(Q\rho) e^{-Drl(l+1)t} \tag{1.51}$$

And by Fourier transforming

$$S_s(\underline{Q}, \omega)\, j_0^2(Q\rho)\delta(\omega) + \frac{1}{\pi} \sum_{l=1}^{\infty} (2l+1) j_l^2(Q\rho) \frac{D_r l(l+1)}{\left[D_r l(l+1)\right]^2 + \omega^2} \tag{1.52}$$

Where the j_l are the spherical Bessel functions.

The scattering law (1.52) is composed of a sharp $\delta(\omega)$ peak superimposed on a broadened component (composed of various Lorentzians) whose width is of the order of a few D_r (fig.1.9), and whose intensity depends on Q. For more complicated models, it can be shown that these key characteristics are preserved. For example a $\delta(\omega)$ peak and

broadened components whose widths are Q-independent, but other characteristics (e.g. side peaks or humps) appear if the rotation becomes relatively free.

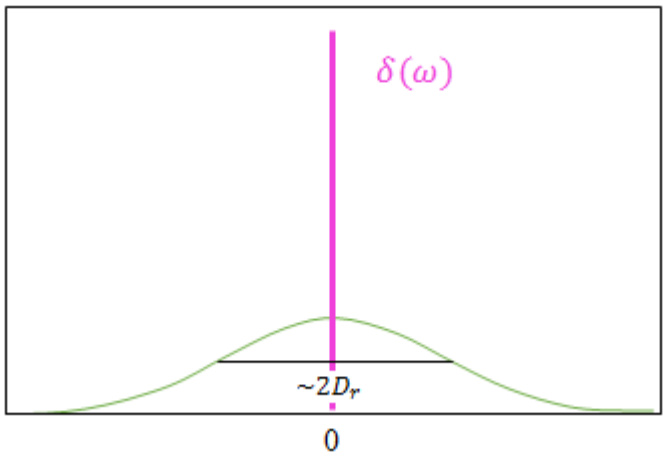

Fig.1.9: Theoretical incoherent neutron quasi-elastic scattering spectrum for a purely rotational diffusive motion

1.4.6.2 Translation diffusion spectral contribution

Now we consider the simple case of isotropic translational diffusion. The probability distribution $\underline{G}_s$ of the position $\underline{d}(t)$ of the particle is run by the rate equation:

$$\frac{\partial G_S}{\partial t} = D_t \nabla_d^2 G_S \tag{1.53}$$

In which:

$G_s(\underline{d},\underline{d}_0,t)$ is the probability of finding the particle at d at time t if it was at t_0 at zero time

D_t is the translational diffusion coefficient.

The solution of this equation is

$$G_s(\underline{d},\underline{d}_0,t) = (4\pi D_t t)^{-\frac{3}{2}} e^{\frac{-(\vec{d}-\vec{d}_0)^2}{4D_t t}} \tag{1.54}$$

From eq. (44) we get:

$$I_s(\underline{Q},t) = \int G_S e^{i\underline{Q}(\underline{d}(t)-\underline{d}(0)_0)} d\underline{d}d\underline{d}_0 = e^{-D_t Q^2 t} \tag{1.55}$$

And by Fourier transforming

$$S_s(\underline{Q},\omega) = \frac{1}{\pi}\frac{D_r Q^2}{\left[D_r Q^2\right]^2 + \omega^2} \tag{1.56}$$

It was noted that the scattering law (1.56) is a single Lorentzian line whose amplitude varies like Q^2 (figg.1.10-1.11-1.12). For more complex models, we get a superposition of Lorentzian (or more complicated shapes) lines whose widths and relative intensities are Q-dependent. This must be compared with the rotational case where only the amplitudes are Q-dependent.

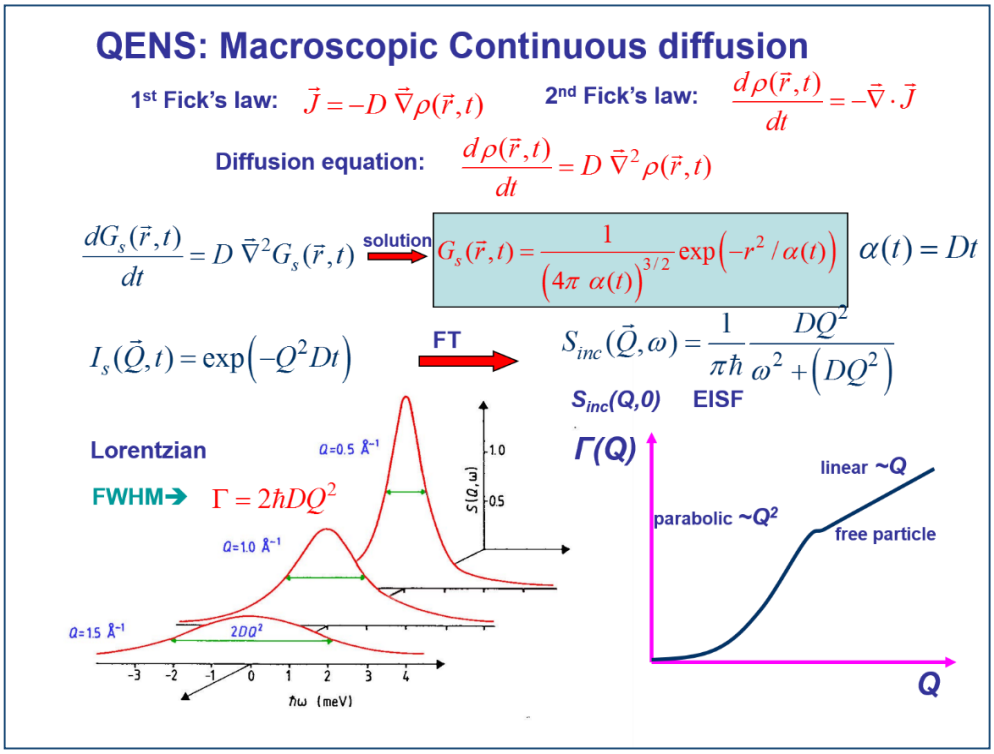

Fig. 1.10: QENS: Macroscopic continuous diffusion

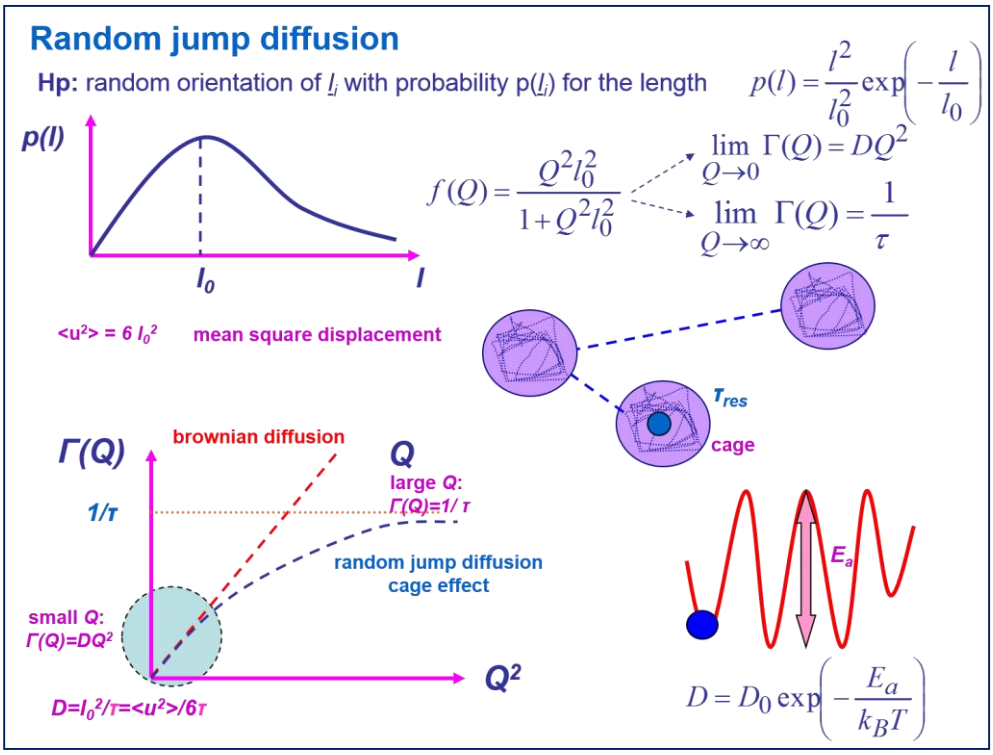

Fig. 1.11: Random jump diffusion

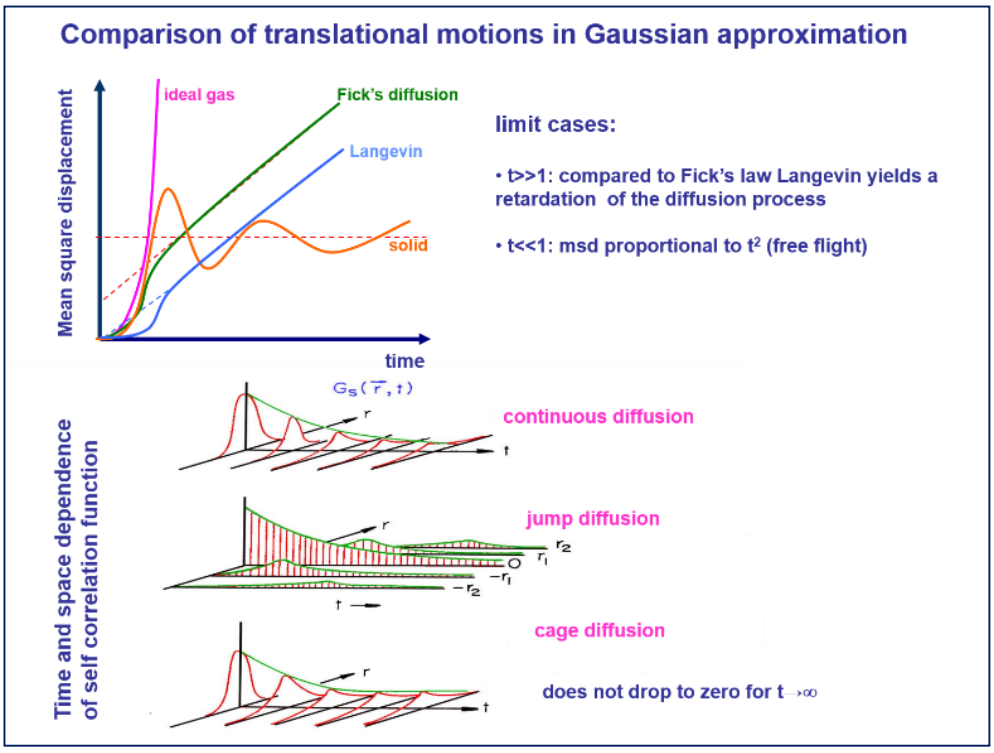

Fig. 1.12: Comparison of translational motions in Gaussian approximation.

1.4.6.3 Superposition of rotation and translation diffusion spectral contributions

The molecules are now assumed to undergo self-diffusion and reorientation. Supposing that these movements are independent, the total scattering law is the convolution of the rotational and translational scattering laws. It was noted that even if the two movements are described by simple models that we talked about, the scattering law is the sum of a number of elementary curves (Lorentzians) whose widths depend both on translational and rotational parameters and whose relative amplitudes are Q-dependent. It is therefore difficult a priori to separate the two contributions, mostly when the finite instrumental energy resolutions is regarded. Nevertheless this is now possible using the concept of the Elastic Incoherent Structure Factor (EISF) and combing measurements from various instruments, as will be seen below

1.4.6.4 Vibrational spectral contribution

Lastly, when there are vibrations, the total scattering law should be convoluted with that of vibrations, which is generally composed of sharp peaks of small intensity in the inelastic region.

In the quasi-elastic region, it can be demostrate that this affects the scattering law through a Debye-Waller factor $e^{-Q^2\langle u^2\rangle}$, where $\langle u^2\rangle$ is a mean square vibration amplitude. In this case we can write:

$$S_s^{quasi}(\underline{Q},\omega)=\left(S_s^{trans}(\underline{Q},\omega)\otimes S_s^{rot}\right)e^{-Q^2\langle u^2\rangle} \tag{1.57}$$

The Debye-Waller factor thus pictures the decrease of the total “quasi-elastic” intensity with increasing $\underline{Q}$ (i.e. the scattering angle) and povides information on the extent of the (fast) vibrational motions.

1.4.7 The Elastic Incoherent Structure Factor (EISF)

We take into account the rotational scattering law (1.52). In this law the first term is the product of a function of Q, $F(Q)$, multiplied by a $\delta(\omega)$ function. This property is

in fact general for whatever rotational model and derives from the fact that $I_s(\underline{Q},t)$ does not decay to zero where $t \to \infty$. We have:

$$F(\underline{Q}) = I_s(\underline{Q}, t=\infty) = \int G_S(\underline{r}, \underline{r}_0, \infty) e^{i\underline{Q}\underline{r}} d\underline{r} d\underline{r}_0 \tag{1.58}$$

Namely, the coefficient of the $\delta(\omega)$ function, that has the dimension of a structure factor and is called the Elastic Incoherent Structure Factor (EISF), is the spatial Fourier transform of final distribution of the rotating proton, averaged over all possible initial position.

Since $F(Q)$ pictures the "trajectory" of the moving proton, if $F(Q)$ could be extracted from spectra obtained at various $\underline{Q}$ values, one would have precious information on the nature of the rotational motion performed by the proton. The way to relate the EISF to a misurable quantity is the following: it was noted that any rotational scattering law can be written

$$S_s^{rot}\left(\underline{Q}, \omega\right) = F\left(\underline{Q}\right)\delta(\omega) + \sum_n other\ (broadened) terms \tag{1.59}$$

Furthermore, Fourier transform of eq. (1.44) and integration over ω yields:

$$\int S_S(\vec{Q}, \omega) d\omega = I_S(\vec{Q}, 0) = 1 \tag{1.60}$$

Integrating eqn. (1.59), it is evident that $F(Q)$ is the fraction of the total quasi-elastic intensity contained in the purely elastic $\delta(\omega)$ peak. If the instrumental resolution $\Delta\omega$ is (much) smaller than the reorientational rate, then the real spectra have the form sketched in fig.5, and the separation between the sharp (purely elastic) and broad components can be performed by natural extrapolation. Let $I_e(\underline{Q})$ and $I_q(\underline{Q})$ be the corresponding intensities (measured by graphical integration after subtraction of a flat background). We have:

$$\left(F(\underline{Q})\right)_{\exp} = \frac{I_e(\underline{Q})}{I_e(\underline{Q}) + I_q(\underline{Q})} \tag{1.61}$$

The analysis is a priori much more difficult and, in each case, less precise, if the two components are not well separated. Are now increasing in number the studies of purely rotational motions in molecular crystals based on these ideas. For example we mention the problem of reorientation in plastic crystals, in liquid crystals, and that of methyl group rotation in solid phases.

We have considered thus far only pure rotation but when self-diffusion is superimposed on rotation (as it is in the case in molecular liquids), one can generalize.

Practically, we find that it is necessary that we know D_t rather accurately in order to extract a reliable value for the EISF and accordingly, a reliable picture for the rotation.

The diffusion coefficient D_t can often be obtained regardless by the neutron method by working at sufficiently low Q (such that $D_t Q^2 << \tau_{rot}^{-1}$) and sufficiently high resolution (such that $\Delta\omega << D_t Q^2$). In these conditions only the translational part is seen in practice, the rotational contribution acting as a flat background. These experimental conditions can nowadays be achieved for usual liquids (D_t 10^{-7} cm^2/sec) using the backscattering technique. After determining the value of D_t, one can make experiments on a medium resolution instrument (such that $\Delta\omega \leq \tau_{rot}^{-1}$): typically $10<\Delta\omega<100$ μeV and extract the EISF from these spectra to obtain information about the rotational model.

In fig. 1.13 are shown graphs in which it is evident a time dependent pair correlation functions and of dynamical structure factors.

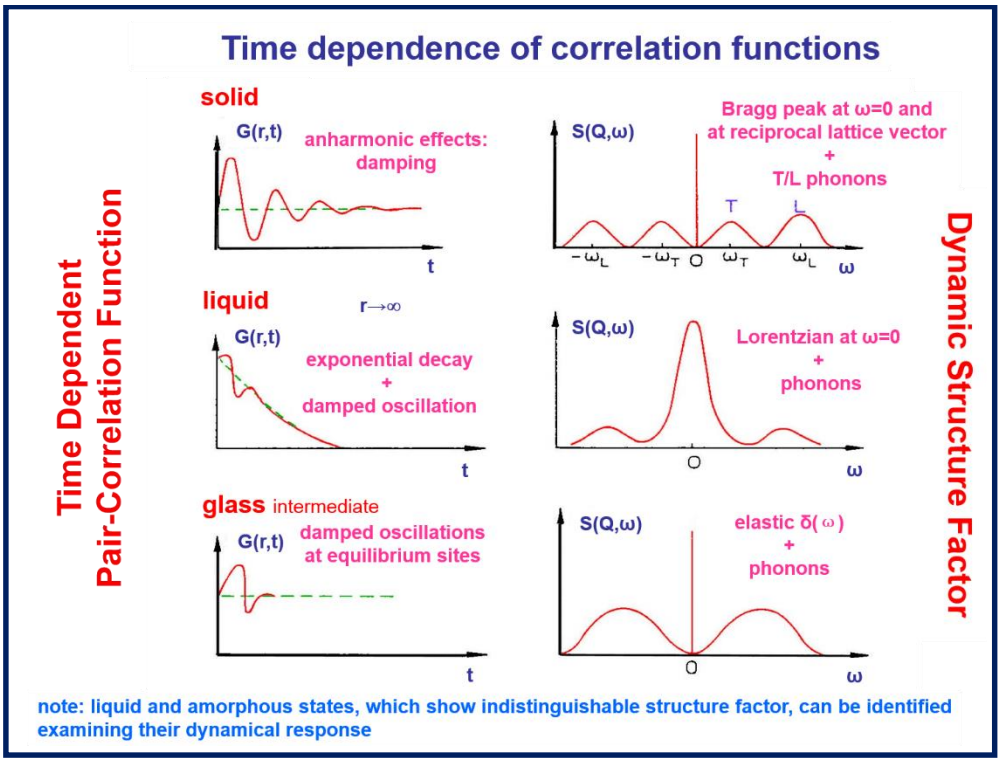

Fig 1.13: Sketch of the typical behaviour of the time dependent pair correlation functions and of the dynamic structure factor for solids, liquids and glasses

1.5 Absorption and scattering of electromagnetic waves: dielectric and infrared absorption, Raman and Rayleigh scattering

In this part, we explain how electromagnetic (e.m.) waves or photons of long wavelength (much greater than molecular dimension) can be useful to study molecular motions [1]. First and foremost we listen the properties which characterize the photon, then we focus on the principles of absorption and scattering experiments and give a few illustrative examples.

1.5.1 Electromagnetic waves and photons

The electromagnetic field is classically characterized by its electric field vector, $\underline{E}(\underline{r})$, and magnetic, $\underline{H}(\underline{r})$, field vector, and has a wave character. A plane wave is characterized by its wave vector k, its angular frequency ω_k, and moves at the velocity of light c. These quantities are related by

$$c = \frac{\omega_k}{k} \tag{1.63}$$

Furthermore, electromagnetic waves can be seen as a ultra relativistic particles, photons, moving at the velocity of light and of energy E_k given by

$$E_k = \hbar\omega_k \tag{1.64}$$

For visible light, we have $E_k \approx 2$eV and $\lambda_k \approx 6000$ Å. So is interesting put these values in comparison with the corresponding ones for neutrons, in particular the fact that the wavelength is much greater than the usual molecular dimensions. In fig. 1.14 the photon's "identity card" is reported.

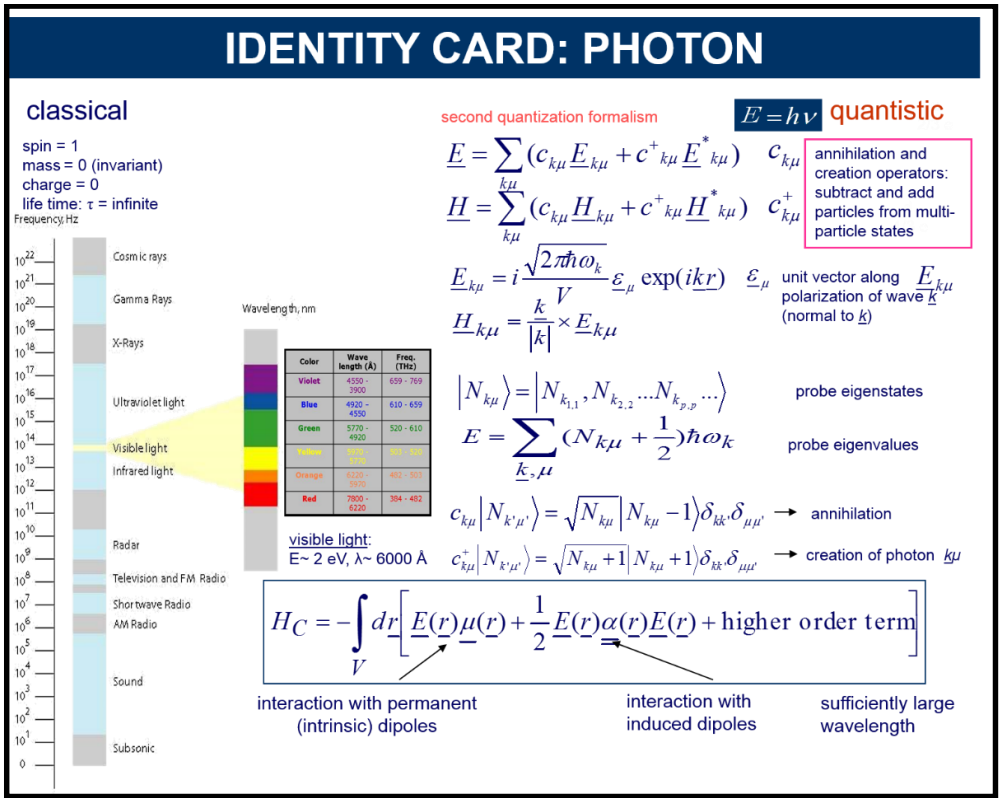

Fig. 1.14: The photon's "identity card"

Considered the electromagnetic field as a quantum object, it must be treated as an operator within the formalism of second quantization:

$$\underline{E} = \sum_{\vec{k}\mu}\left(c_{k\mu}\underline{E}_{k\mu} + c^{+}_{k\mu}\underline{E}^{*}_{k\mu}\right) \tag{1.65}$$

$$\underline{H} = \sum_{\vec{k}\mu}\left(c_{k\mu}\underline{H}_{k\mu} + c^{+}_{k\mu}\underline{H}^{*}_{k\mu}\right) \tag{1.66}$$

where $\underline{E}_{k\mu} = i\sqrt{\frac{2\pi\hbar\omega_k}{V}}\underline{\varepsilon}_{\mu}\exp(i\underline{k}\cdot\underline{r})$ (1.67)

and $\underline{H}_{k\mu} = \frac{\underline{k}}{|\underline{k}|}\wedge\underline{E}_{k\mu}$. (1.68)

$\omega_k = c_l k$ is the angular frequency

c_l the light velocity

$\underline{k}$ the wave vector

$\vec{\varepsilon}_{\mu}$ the polarization versor

V is the volume of quantization $c_{k\mu}$ and $c^{+}_{k\mu}$ the annihilation and creation operators respectively.

The eigenstates $\left|N_{k\mu}\right\rangle$ of the Hamiltonian of the field are characterized by the number $N_{k\mu}$ of photons existing in each state (k,μ)

$$\left|N_{k\mu}\right\rangle = \left|N_{k_{1,1}}, N_{k_{2,2}}, ..., N_{k_{p,p}} ...\right\rangle \tag{1.69}$$

The corresponding eigenvalues are

$$\mathrm{E}=\sum_{k,\mu}(N_{k,\mu}+\frac{1}{2})\hbar\omega_k \tag{1.70}$$

Finally, the properties of the operators $c_{k,\mu}$ and $c^{+}_{k,\mu}$ are:

$$c_{k,\mu}\left|N_{k'\mu'}\right\rangle = \sqrt{N_{k\mu}}\left|N_{k\mu}-1\right\rangle\delta_{kk'}\delta_{\mu\mu'} \text{ (annihilation of one photon } \mathbf{k}\mu) \tag{1.71}$$

$$c^{+}_{k,\mu}\left|N_{k'\mu'}\right\rangle = \sqrt{N_{k\mu}+1}\left|N_{k\mu}+1\right\rangle\delta_{kk'}\delta_{\mu\mu'} \text{ (creation of one photon } \mathbf{k}\mu) \tag{1.72}$$

1.5.2 Long wavelength e.m. waves- matter interaction

Electromagnetic waves interact with electric charges. If the medium is neutral, at each point **r**, one can define a permanent dipole moment $u(\vec{r})$, a polarizability tensor $\alpha(\vec{r})$ per unit volume. If the wavelength is enough large, it can be see that the interaction Hamiltonian can be obtained by an expansion in the electric field:

$$H_C = -\int d\underline{r}\left[\underline{E}(\underline{r})\underline{\mu}(\underline{r}) + \tfrac{1}{2}\underline{E}(\underline{r})\underline{\alpha}(\underline{r})\underline{E}(\underline{r}) + higher\ order\ terms\right] \tag{1.73}$$

The interaction with the permanent dipoles is taken into account by the first term $\underline{\mu}(\underline{r})$, and the interaction with the induced dipoles by the second term $\underline{\underline{\alpha}}(\underline{r})\underline{E}(\underline{r})$ when $\underline{\underline{\alpha}}(\underline{r})$ being the polarizability tensor.

The higher order terms include the hyperpolarizability interaction (trilinear term in the electric field), magnetic interactions, etc. For what interests us, we will restrict ourselves to these two first terms which will lead to dielectric and infrared absorption (linear term) and to Rayleigh and Raman scattering (bilinear term).

The Fig. 1.15 shows the wavevector-energy region accessible for photons.

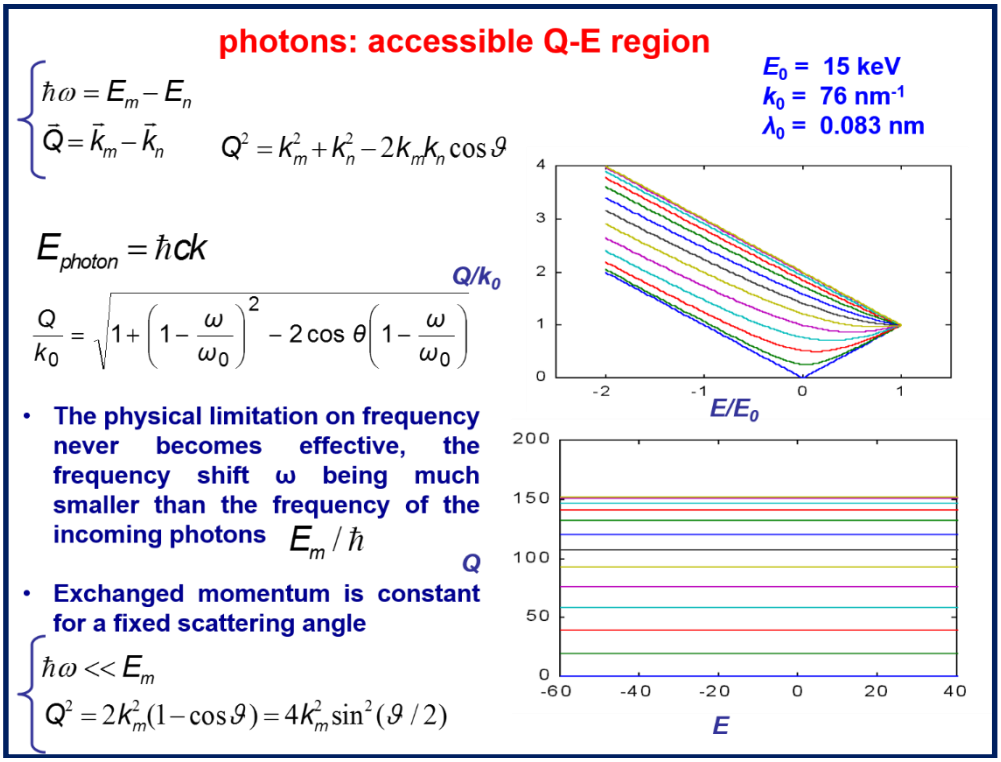

Figure 1.15: Photon accessible wavevector-energy region

1.5.3 Dielectric and infrared absorption: interaction with permanent dipoles: Introductive definitions

We must first of all say that:

the probe is the e.m. field whose eigenstates are $|N_{k\mu}\rangle$;

the reservoir is constituted by N particle which we suppose to be point-like, located at ri (long wavelength approximation) and characterized by their dipole moment μ_i. With this assumption, we can write

$$\mu(\vec{r}) = \sum_i \mu_i \delta(\vec{r} - \vec{r}_i) \tag{1.74}$$

and the present relevant interaction H_C (first term of eq.(73) is written:

$$H_C = -\Sigma \int_V \underline{E}(\underline{r})\underline{\mu}_i(\underline{r})\delta(\underline{r} - \underline{r}_i)d\underline{r} \tag{1.75}$$

using eqn. (1.67) in eq. (1.75) and performing the integration over r yields

$$H_C = -\sum_i \sum_{\underline{k},\mu} (\underline{\varepsilon}_\mu \underline{\mu}_i) i \sqrt{\frac{2\pi\hbar\omega_k}{V}} \left[c_{k\mu} e^{i\underline{k}\underline{r}_i} + c^+{}_{k\mu} e^{-i\underline{k}\underline{r}_i} \right] \tag{1.76}$$

Now we have to calculate the average value of H_C between the initial and final state of the probe, that we call $\overline{H}_C$. The initial state is $\left| N_{k_0 I} \right\rangle$, i.e. are sent on the sample photons of momentum $\mathbf{k}_0$ and polarization ε_I (a monochromatic and polarized plane wave). Now let's see what are the possible interesting final states, i.e. those for which $\overline{H}_C$ has non-zero value. They correspond, obviously, to states such that the matrix elements of $c_{k,\mu}$ or $c^+{}_{k,\mu}$ are non zero. According to eqs. (1.71) and (1.72) these are:

(i) $\left| N_{k_0 I} - 1 \right\rangle$:absorption of one photon ($\mathbf{k}_0$, $\boldsymbol{\varepsilon}_I$)

(ii) $\left| N_{k_0 I} + 1 \right\rangle$: emission of one photon ($\mathbf{k}_0$, $\boldsymbol{\varepsilon}_I$)

(iii) $\left| N_{k_0 I}, 1_{k_1 s} \right\rangle$: emission of one photon ($\mathbf{k}_1$, $\boldsymbol{\varepsilon}_s$)

The values of the matrix element are $\sqrt{N_{k_0 I}}$ $\sqrt{N_{k_0 I} + 1}$ and 1, respectively, and the corresponding probability of transition is thus proportional to $N_{k_0 I}$, $N_{k_0 I} + 1$ and 1.

If the number of incident photons is big, as always happens in practice, then $N_{k_0 I} >> 1$ and the the last case (in fact the spontaneous emission) is very weak compared to the two former ones, i.e. the induced absorption and emission. The correlation functions corresponding to these two latter cases are:

$$C^{\pm}_{\overline{H}_C \overline{H}_C}(t) = \frac{2\pi\hbar\omega_0}{V} N_{k_0 I} < \sum_{i,j} (\underline{\varepsilon}_I \underline{\mu}_i(t))(\underline{\varepsilon}_I \underline{\mu}_i(0)) e^{\pm i\underline{k}_0 [\underline{r}_i(t) - \underline{r}_i(0)]} > \tag{1.77}$$

with + for absorption and – for emission.

It was found that, a priori, the study of induced absorption and emission of e.m. waves by such a medium can provide information regarding the motions of μ_i (rotation and vibration) and on the motion of r_i (i.e. translation). Pratically, however, k_0 having a very small value (long wavelength approximation), the exponential decays much more slowly compared to the other terms and we can neglect its variation. With the conditions listed, the correlation functions for emission and absorption are the same, and we have:

$$C^{\pm}_{\bar{H}_C \bar{H}_C(t)} = \frac{2\pi\hbar\omega_0}{V} N_{k_0 I} < \sum_{i,j} (\underline{\varepsilon}_I \underline{\mu}_i(t))(\underline{\varepsilon}_I \underline{\mu}_i(0)) > \quad (1.78)$$

Eqn.(1.17) provides the corresponding probabilities of transition, one with $\omega=\omega_0$ (absorption of one photon), the other with $\omega=-\omega_0$ (emission of one photon). These two probabilities are related by eqn. (1.18) in the linear approximation and we have W^{abs} W^{emi}. As foreseen by the general considerations, the net induced phenomenon is the absorption and the corresponding probability per unit time is according to eqns. (1.16), (1.17), (1.18) and (1.78):

$$W^t = W^{obs} - W^{emi} = \frac{2\pi}{\hbar^2}\left[1 - e^{-\beta\hbar\omega}\right] C_{\bar{H}_C \bar{H}_C(t)}(\omega_0) \quad (1.79)$$

Considered a sample that is a cylinder of section S and length l (Sl=V). The problem is now to relate W^t to a measurable quantity, namely the power P_a absorbed during the experiment. Let P_0 be the incident power and $n_{k_0 I}$ the corresponding incident number of photons per cm^2 and per sec.

We have:

$$P_0 = n_{k_0 I} S \hbar\omega_0 \quad (1.80)$$

The number of incident photon in volume V is

$$N_{k_0 I} = \frac{n_{k_0 I}}{c} V \quad (1.81)$$

As the power absorbed in volume V is

$$P_a = \hbar\omega_0 W^t \quad (1.82)$$

Combining eqn. (1.78) to (1.82) we finally obtain

$$\frac{P_a}{P_0} = N \frac{(2\pi)^2}{\hbar c} \frac{\omega_0}{S} \left[1 - e^{-\beta\hbar\omega_0}\right] \bullet c_{\mu\mu}(\omega_0) \quad (1.83)$$

with

$$c_{\mu\mu}(\omega) = \frac{1}{2\pi} \int_{-\infty}^{+\infty} c_{\mu\mu}(t) e^{-i\omega t} dt \quad (1.84)$$

and

$$c_{\mu\mu}(t) = \frac{1}{N} \sum_{i,j} \underline{\varepsilon}_I \underline{\mu}_i(0) \underline{\varepsilon}_I \underline{\mu}_j(t) \quad (1.85)$$

It was found that, in the long wavelength approximation, the absorbed power is proportional to the spectral density of the fluctuation of the dipoles. Specifically, it reflects the correlation between the fluctuations of the components of the dipoles along the polarization $\underline{\varepsilon}_I$ of the field. We have an important simplification if the medium can be considered as isotropic (e.g. as in a normal liquid). Then, one can average eq. (1.85) over all possible orientations of $\underline{\varepsilon}_I$ and easily obtain:

$$c_{\mu\mu}(t) = \frac{1}{N} < \sum_{i,j} \underline{\mu}_i(0)\underline{\mu}_j(t) > \tag{1.86}$$

We highlight the fact that the electric dipole moment of a molecule is a quantity which depends on the charge distribution in the molecules and this distribution changes when the molecule vibrates. We denoted by υ the vibrational states and by q^{υ} the corresponding normal coordinates. We can write:

$$\mu = \mu_0 + \sum_{\nu} \underline{\mu}^{\nu} q^{\nu} \tag{1.87}$$

with

$$\mu^{\nu} = \left(\frac{\partial \mu}{\partial q^{\nu}} \right)_{q^{\nu}=0} \tag{1.88}$$

μ^0 is the permanent dipole

μ^{ν} is the derivative dipole corresponding to vibration ν.

According to these definitions, we have that the second member of eqn.(1.85) or (1.86) can be subdivided into various components (two for eqn. (1.86)):

$$c_{00}(t) = \frac{1}{N} < \sum_{i,j} \underline{\mu}^0{}_i(0)\underline{\mu}^0{}_j(t) > \tag{1.89}$$

and

$$c_{\nu\nu}(t) = \frac{1}{N} < \sum_{i,j,\nu,\nu'} (\underline{\mu}^{\nu}{}_i(0)\underline{\mu}^{\nu}{}_j(t))(\underline{q}^{\nu}{}_i(0)\underline{q}^{\nu}{}_j(t)) > \tag{1.90}$$

which are respectively: the relevant correlation functions for the so-called dielectric and infrared absorption in an isotropic medium. We have illustrated in detail later of these two cases.

1.5.3.1 Dielectric absorption: permanent dipoles

a) General

By eq. (1.89) we have the correlation function. If we consider identical molecules, considered $\underline{u}_i$ and $\underline{u}_j$ the unit vectors along $\underline{\mu}_i^{\,0}$ and $\underline{\mu}_j^{\,0}$, and $\theta_{i,j}$ the angle between them, eq. (1.89) the equation becomes as follows:

$$c_{00}(t) = \frac{1}{N}(\underline{\mu}^0)^2 < \sum_{i,j} \cos(\theta_{ij}(t)) > \tag{1.91}$$

This correlation function shows the fluctuations of the relative orientation of the permanent dipoles and thus reflects collective reorientational motions. A difficult problem is to relate this macroscopic function to monomolecular properties, namely to the single molecule correlation function $F_1(t)$ given by

$$F_1(t) = P_1 < \cos(\theta_{ii}(t)) > \tag{1.92}$$

where P_1 is the first order ordinary Legendre polynomial. It is possible to address the problem experimentally using a trick: should be diluted polar molecules in an inert solvent and make a study as a function of the dilution. If the dilution is sufficiently large, the active molecules can be considered sufficiently far from one another so that their correlations can be neglected i.e. that we have:

$$< \cos(\theta_{ij}(t)) > \approx 0 \qquad \text{for } i \neq j \tag{1.93}$$

In this case, Eq. (89) can be written dropping the indices ii:

$$c_{00}(t) = (\underline{\mu}^0)^2 F_1(t) \tag{1.94}$$

and by Fourier transforming

$$c_{00}(t) = (\underline{\mu}^0)^2 F_1(\omega) \tag{1.95}$$

Using the fact that

(i) in dielectric absorption $\hbar\omega_0 << k_B T$ and

(ii) N=nSl where n is the number of dipoles per unit volume,

We can write eqn. (1,83) as:

$$P_a = \alpha l P_0 \tag{1.96}$$

Where

$$\alpha = \alpha(\omega_0) = \frac{(2\pi)^2}{c}\frac{n(\mu^0)^2}{k_B T}\omega^2{}_0 F_1(\omega_0) \tag{1.97}$$

The quantity α is the absorption coefficient per unit length. Its variation with ω_0 yields the dielectric absorption spectrum.

b) Dielectric absorption spectra

We illustrate now calculations of dielectric absorption spectra. We will discuss the case of isotropic free rotation and isotropic rotational diffusion for dilute dipoles and compare the results to a real spectrum.

1) Isotropic rotational diffusion spectral contribution

The probability distribution Gs of the dipole orientation is given, in this case, by eqn.(1.50) and we have:

$$F_1(t) = \int \cos\theta G_s d\Omega = e^{-2Drt} \tag{1.98}$$

The absorption coefficient α is thus

$$\alpha(\omega_0) \propto \omega^2{}_0 F(\omega_0) \propto \frac{\omega_0^2}{(2D_r)^2 + \omega_0^2} \tag{1.99}$$

2) Classical free rotation spectral contribution

Free rotation implies that the rotational energy is conserved so, the angular velocity Ω is constant. In this case, the angle θ varies linearly with t:

$$\theta = \Omega t \tag{1.100}$$

Furthermore, given that the system is at thermal equilibrium, the distribution of angular velocities p(Ω) is Maxwellian

$$p(\Omega) = \frac{I}{k_B T}|\Omega| e^{-\frac{1}{2}\frac{I\Omega^2}{k_B T}} \tag{1.101}$$

where I is the inertial momentum of the molecule. The correlation function $F_1(t)$ can then be calculated:

$$F_1(t) = \int \cos(\Omega t)\, p(\Omega) d\Omega \tag{1.102}$$

As well as its Fourier transform. The final result is

$$\alpha(\omega_0) \propto \omega^2_0 F_1(\omega_0) \propto \left|\omega_0\right|^3 e^{-\frac{1}{2}\frac{I\Omega^2}{k_B T}} \quad (1.103)$$

Therefore we conclude that to study both collective rotational motions in pure polar liquids and individual rotational motions in dilute solutions of polar molecules in non polar solvents, dielectric absorption can be used. The ω range available in practice lies between the radiofrequencies and the far infrared via the microwaves. This, according to the range of frequencies to be studied, has resulted in a large variety of different experimental set ups. Lastly, this method is used today in the field of critical phenomena (in particular in liquids) because dielectric absorption reflects mainly collective motions.

1.5.3.2 Infrared (IR) absorption: derivative dipoles

a) General

In this case, eqn. (1.90) provides the relevant correlation. If we assume the following hypotheses:

(i) the molecules are identical,

(ii) rotations and vibrations are not coupled, and

(iii) the vibrations between the molecules and within the same molecules are not coupled, i.e.,

$$<\underline{(q^{\nu}}_i(0)\underline{q^{\nu}}_j(t))>=0 \qquad \text{for} \quad i \neq j \ , \ \nu \neq \nu' \quad (1.104)$$

$$c_w(t) = \sum_{\nu} \underline{<\mu^{\nu}}\ (0)\underline{\mu^{\nu}}\ (t) > < \underline{(q^{\nu}}\ (0)\underline{q^{\nu}}\ (t)) > \quad (1.105)$$

Moreover, if we make the assumptions that the vibrations are weakly damped, we can write

$$<\underline{(q^{\nu}}\ (0)\underline{q^{\nu}}\ (t))> = \left(q^{\nu}\right)^2 e^{-i\Omega_{\nu} t} G_{\nu}(t) \quad (1.106)$$

Where

q^{ν} is the vibrational amplitude

Ω_{ν} the frequency of vibration ν and

G_{ν} (t) a slowly decreasing function picturing the damping of the vibration (G_{ν} (t)=1 for no damping). Let θ_{ν} (t) be the angle between μ^{ν} (0) and μ^{ν} (t). We have

$$<\underline{(\mu^{\nu}}\ (0)\underline{\mu^{\nu}}\ (t))> = \left(\mu^{\nu}\right)^2 <\cos\theta^{\nu}(t)> = (\mu^{\nu})^2 F_{1\nu}(t) \quad (1.107)$$

and eq. (105) is finally written:

$$c_w(t) = \sum_\nu (\underline{\mu}^\nu \; q^\nu)^2 e^{-i\Omega_\nu t} G_\nu(t) F_{1\nu}(t) \tag{1.108}$$

and after Fourier transforming

$$c_w(\omega) = \sum_\nu (\underline{\mu}^\nu \; q^\nu)^2 G_\nu(\omega + \Omega_\nu) \otimes F_{1\nu}(\omega + \Omega_\nu) \tag{1.109}$$

This illustrates that the infrared absorption spectrum consists of a series of absorption lines centered around the vibration frequencies and that, given more or less questionable assumptions are made, each line is proportional to the convolution of the rotational and vibrational spectrum. We call this phenomenon infrared absorption since the Ωv are usually in the infrared region of the e.m. spectrum. Comparing eqns.(1.95) and (1.109), if the vibrations are not muffled $G_\nu(\omega + \Omega_\nu) = \delta(\omega + \Omega_\nu)$, it can be approximately said that for molecules in dilute solutions the infrared spectrum reproduces the dielectric spectrum around the frequencies Ωv . We said approximately because, even if the absorbed power is proportional to $\omega_0 \left[1 - e^{-\beta\hbar\omega_0}\right]$ as in the dielectric case (eqn.(1.83)), for infrared $\omega_0 \approx \left[\Omega_\nu + \omega\right] \approx \Omega_\nu$ and the absorption spectrum reproduces $c_{w\nu}(\omega)$ around Ωv. Fig.1.16 show the dependence of frequencies on atomic weight and bond energies.

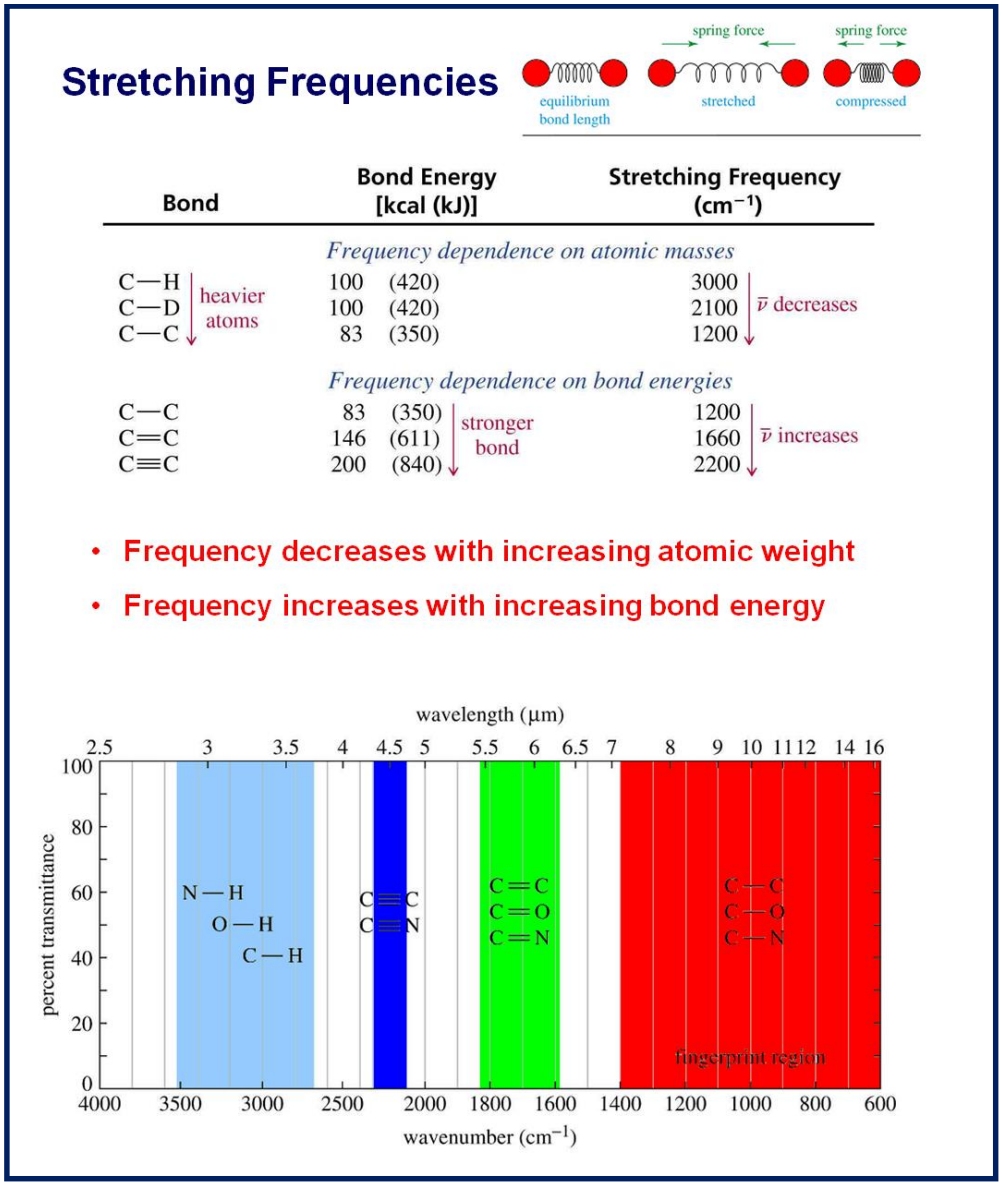

Fig. 1.16: Dependence of frequencies on atomic weight and bond energies.

b) Typical infrared spectra

We speak now of theoretical IR spectra in the same simple cases as before. We do it to illustrate this section and as for the case of dielectric absorption. Assuming no damping of the vibration.

For rotational diffusion, we have

$$F_1(\omega) \propto \frac{(2D_r)}{(2D_r)^2 + \omega^2} \tag{1.110}$$

And the corresponding infrared spectrum is sketched in Fig.1.17a: it is a single Lorentzian centered at Ωv .

For free rotation, we have

$$F_1(\omega) \propto |\omega| e^{-\frac{1}{2}\frac{I\Omega^2}{k_B T}} \qquad (1.111)$$

And the corresponding spectrum is sketched in fig.1.17b. It presents two maxima at $\Omega_\nu + \omega_m$ with $= \omega_m = \left(\frac{k_B T}{I}\right)^{1/2}$.

In fig 1.17c is shown the infrared spectrum of the polar molecule CO diluted in liquid C_2Cl_4. It clearly shows feature that recall the two borderline cases above. Specifically, the humps on each side of the spectrum suggest that the rotation is relatively free, and its general shape suggests that the numerous assumptions made are justified for this system. In particular, the additional observation that the shapes corresponding to the transition 1-0 and 2-0 are practically the same suggest that the hypothesis of weak damping of the vibration is a good one.

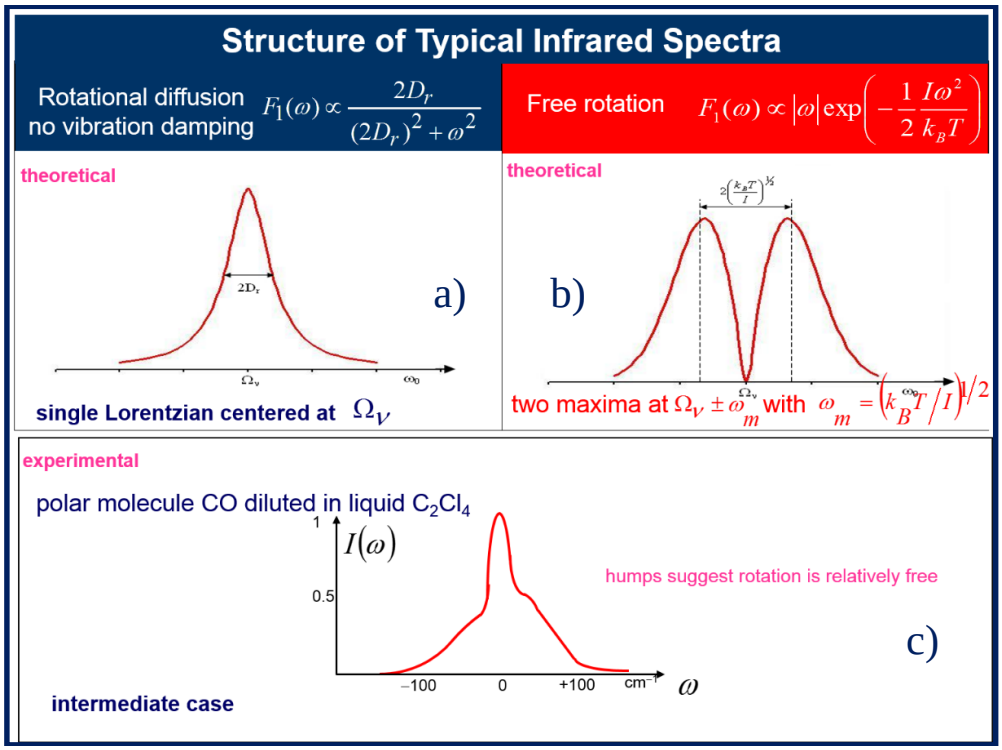

Fig 1.17: a) is a single Lorentzian centered at Ωv, b) spectrum of the single Lorentzian centered and c) infrared spectrum of the polar molecule CO diluted in liquid C_2Cl_4

We have just described a real case considering very small molecules in a diluted solution so is almost ideal. When, instead, the molecules are bigger, the vibration can be strongly damped and contribute significantly to the width of the spectra.

In which case, a trick frequently used to separate the vibrational and rotational contributions is to measure the full width of the spectra as a function of temperature, suppose that the two elementary widths are additive, and suppose that the vibrational width is temperature independent. In general, it is assumed that the relative contribution of vibration increases with the dimension of the molecule and may become the dominant one. Large molecules have a further important complication: the different vibrational levels are not sufficiently far from one another so that two or several spectra corresponding to different vibrational states overlap (inhomogeneous broadening). Finally, another important complication is the coupling between rotation and vibration.

In conclusion it seems that infrared absorption can be used to study both rotational and vibrational relaxation in liquids, but that the separation between them is difficult. Of course, additional results from other methods are needed. Comparison between dielectric and infrared absorption spectra can, in some cases, provide some information on the degree of cooperativity of the rotational motions. However, as we shall see below, Rayleigh Raman scattering of light are the most appropriate complementary methods for obtaining this kind of information as well as information about the coupling between rotation and vibration.

Finally, it should be noted that absorption of e.m. waves in liquids cannot only be produced by permanent dipoles, but also by induced dipoles (and multipoles). These multipoles are induced both by the collisions and by the probing electric field itself, which deform the molecular electronic clouds. In non-polar liquids, the absorption due to collisions generally appears in the far infrared region (50-100 cm-1) and is very wide. For describing this type of phenomenon theories are still being developed, but it is clear that they necessarily involve physical quantities such as the values of the induced multipoles, the collision frequencies and consequently contain information on the specific interaction between non-dipolar molecules. Concerning the absorption due to the probing electric field, it appears as a phenomenon which superimpose on the phenomenon of scattering.

1.6 Interaction with induced dipoles: absorption and scattering of photons

1.6.1 Introductive definitions

Again, the probe is the e.m. field whose eigenstates are $\left|N_{k\mu}\right\rangle$ [1]. The reservoir is made up of N particle which we assume to be point-like, located at r_i (long wavelength approximation) but which are now characterized by their polarizability tensor $\underline{\underline{\alpha}}_i$. With this hypothesis, we can write:

$$\underline{\underline{\alpha}}(r) = \sum_i \underline{\underline{\alpha}}_i \delta(\underline{r} - \underline{r}_i) \tag{1.112}$$

and the current relevant interaction H_C (second term of eqn. (1.73))

$$H_C = -\frac{1}{2}\sum_i \int_V d\underline{r}\,\underline{E}(\underline{r})\underline{\underline{\alpha}}_i(\underline{r})\underline{E}(\underline{r})\delta(\underline{r} - \underline{r}_i) \tag{1.113}$$

Replacing **E**(r) by its expression given by eqn. (1.67) and carrying out integration over **r** yields

$$H_C = -\frac{1}{2}\sum_{i'}\sum_{\mu\mu'}(\underline{\varepsilon}_\mu \underline{\underline{\alpha}}_i \underline{\varepsilon}_{\mu'})F_{\mu\mu'}(\underline{r}_i) \tag{1.114}$$

with

$$\begin{aligned} F_{\mu\mu'}(\underline{r}_i) = \sum_{kk'} \frac{2\pi\hbar}{V}\sqrt{\omega_k \omega_{k'}}\{\; & c_{k\mu}c^+_{k'\mu'}\exp(i(\underline{k}-\underline{k}')\underline{r}_i) + c_{k\mu}c^+_{k'\mu'}\exp(-i(\underline{k}-\underline{k}')\underline{r}_i) - \\ & - c_{k\mu}c_{k'\mu'}\exp(i(\underline{k}+\underline{k}')\underline{r}_i) - c^{+}{}_{k\mu}c^+_{k'\mu'}\exp(-i(\underline{k}+\underline{k}')\underline{r}_i) \end{aligned} \tag{1.115}$$

Now we have to calculate $\overline{H}_C$, that is the average value of H_C between the initial and final states of the probe. As for absorption experiments, the initial state is $\left|m\right\rangle = \left|N_{k_0 I}\right\rangle$

We should look for non trivial final states $\left|n\right\rangle$, i.e. final states such that H_C is non zero and such that $\left|n\right\rangle \neq \left|N_{k_0 I}\right\rangle$. The problem reduces to inspecting the matrix elements of the operator $F_{\mu\mu'}(\underline{r}_i)$ with the help of eqns. (1.71) and (1.72). From the structure of eqn. (1.115), it immediately appears that there are various possible final states among which we select the three following ones:

(i) state for which two photons ($\underline{k_0}$,$\underline{\varepsilon_I}$) are emitted or absorbed, namely $\left|N_{k_0 I} \pm 2\right\rangle$. This case corresponds to induced emission and absorption of two incident photons via the induced dipoles ($|\hbar\omega| = |2\hbar\omega_0|$), and is similar to the case described in section 4.3. The corresponding correlation functions of $\overline{H}_C$ are ($\left|N_{k_0 I}\right\rangle$>>1)

$$C^{\pm}_{\overline{H}_C \overline{H}_C}(t) = \left(\frac{\pi\hbar\omega_0}{V} N_{k_0 I}\right)^2 \left\langle \sum_{ij} \left(\underline{\varepsilon}_I \underline{\underline{\alpha}}_i(0) \underline{\varepsilon}_I\right)\left(\underline{\varepsilon}_I \underline{\underline{\alpha}}_j(t) \underline{\varepsilon}_I\right) \exp \pm 2i\underline{k}_0 \left[\underline{r}_i(t) - \underline{r}_j(0)\right] \right\rangle \tag{1.116}$$

with + for absorption and – for emission.

This equation must be compared with eq.(1.77) and an analysis similar to that of section can be made to find the probability for the net absorption and the corresponding absorption coefficient. This is a question that we will not address here, but it appears that, provided the absorption due to this phenomenon can be separated from that due to other phenomena, one can in principle obtain information on the fluctuations of the polarizability tensor (i.e. the rotations and vibrations) and on the translational motions. In practice the separation is difficult.

(ii) states for which a photon (k_0 ,ε_I) is absorbed and a different photon which we label (k_1 ,ε_s) is emitted, namely the states $\left|N_{k_0 I} - 1, I_{k_1 s}\right\rangle$. This case corresponds to the induced emission of a photon other than the initial one, and corresponds to the scattering phenomenon. The corresponding correlation function is ($\left|N_{k_0 I}\right\rangle$>>1):

$$C_{\overline{H}_C \overline{H}_C}(t) = \left(\frac{2\pi\hbar}{V}\right)^2 \omega_0 \omega_1 N_{k_0 I} \left\langle \sum_{ij} \left(\underline{\varepsilon}_S \underline{\underline{\alpha}}_i(0) \underline{\varepsilon}_I\right)\left(\underline{\varepsilon}_S \underline{\underline{\alpha}}_j(t) \underline{\varepsilon}_I\right) \exp i\underline{Q} \cdot \left[\underline{r}_i(t) - \underline{r}_j(0)\right] \right\rangle \tag{1.117}$$

where

$$\underline{Q} = \underline{k}_0 - \underline{k}_1 \tag{1.118}$$

is the exchanged momentum.

Finally states for which two photons (k_1 ,ε_1) and (k_2 ,ε_2) are emitted, namely $\left|N_{k_0 I}, 1_{k_1 s}, 1_{k_2 s}\right\rangle$ This case corresponds to spontaneous emission of two photons and as for the case of one photon , its probability is very weak (1 compared to $N_{k_0 I}$ for scattering and $N^2{}_{k_0 I}$ for absorption). In this way we will overlook this phenomenon and focus on scattering.

1.6.2 Rayleigh and Raman scattering of light

The probability per unit time W_{k1k0} that a photon is scattered into a state (k_1 ,ε_s) when $N_{k_0 I}$ photons (k_0 ,ε_I) are present in the sample is given by eqn. (1.17) where $C_{\overline{H}_C \overline{H}_C}(\omega)$ is the time Fourier transform of $C_{\overline{H}_C \overline{H}_C}(t)$ given by eqn. (1.117). We should relate this probability to a measurable quantity, namely the power P1 of photons (k_1 ,ε_s) scattered per sec. between $\underline{k}_1$ and $\underline{k}_1 + d\,\underline{k}_1$. We have:

$$P_1 = \hbar\omega_1 W_{k_1 k_0} \rho(\underline{k}_1) d\,\underline{k}_1 \tag{1.119}$$

where the number of independent states of photons of well defined polarization $\rho(\underline{k}_1)\, d\,\underline{k}_1$ is given by the same equation (25) as for neutrons.

If the sample is a cylinder of section S and lemgth l (V=Sl), the number $N_{k_0 I}$ is $\frac{P_0}{\hbar\omega_0}\frac{V}{c}$,

using the fact that $dk_1 = \frac{d\omega_1}{c}$, a simple calculation finally yields:

$$\frac{P_1}{P_0} = \frac{d^2\sigma}{d\Omega d\omega} d\Omega d\omega_1 = N k_1^4 T(\underline{Q},\omega) d\Omega d\omega_1 \tag{1.120}$$

where P_0 is again the incident power of photons (k_0 ,ε_I), $d\Omega$ is the solid angle and we have put, by analogy with neutrons (c.f. eqs. (1.38) and (1.39))

$$T(Q,\omega) = \frac{1}{2\pi}\int J(\underline{Q},t)\exp(-i\omega t)dt \tag{1.121}$$

and

$$J(\underline{Q},t) = \frac{1}{N}\left\langle \sum_{i,j} (\underline{\varepsilon}_S \underline{\underline{\alpha}}_i(0)\underline{\varepsilon}_I)(\underline{\varepsilon}_S \underline{\underline{\alpha}}_j(t)\underline{\varepsilon}_I) \exp i\underline{Q}(\underline{r}_i(t) - \underline{r}_j(0)) \right\rangle \tag{1.122}$$

Regarding neutrons, $\frac{d^2\sigma}{d\Omega d\omega}$, is the double differential cross-section and represents the normalized scattered intensity per unit solid angle and per unit energy, $J(\underline{Q},t)$ is the intermediate scattering function and $T(\underline{Q},\omega)$ is the scattering law. It is seen from eqn. (1.122) that light scattering reflects molecular motions through the fluctuations of the position (translation) and the fluctuations of the polarizability tensor (rotation and vibrations). The general situation is thus basically the same as for neutrons where all kinds of motions are also seen. There are however significant differences:

(i) for neutrons, the correlation functions corresponding to all types of movements depend on Q while for e.m. waves (in practice light), only those corresponding to translation are Q dependent (this is in fact related to the long wavelength approximation).

(ii) For neutrons, Q is usually 1 $Å^{-1}$ while for light it is usually 10^{-3} $Å^{-1}$. Because of this, the correlation function for translation decays much more slowly ($\approx 10^{-6}$ times) for light than for neutrons. We conclude therefore that for light, the hypothesis of non-coupling between the various motions seems better justified than for neutrons (at least for individual motions), and we can reasonably separate the two statistical averages in eqn. (1.122). We are now focusing on the polarizability term.

As for the dipole moment, the molecular polarizability tensoris is a physical quantity that depends on the charge distribution in the molecules, and this distribution changes when the molecules vibrate. Let ν denote all the vibrational states and with q^ν the corresponding normal coordinates. We can write, by analogy with eq. (1.87), the polarizability tensor is given by the sum of two contributions:

$$\underline{\underline{\alpha}} = \underline{\underline{\alpha}}^0 + \sum_\nu \underline{\underline{\alpha}}^\nu q^\nu \tag{1.123}$$

where $\underline{\underline{\alpha}}^0$ is the permanent polarizability tensor,

$$\underline{\underline{\alpha}}^\nu = \left(\frac{\partial \underline{\underline{\alpha}}}{\partial q^\nu} \right)_{q^\nu = 0} \tag{1.124}$$

and $\underline{\underline{\alpha}}^\nu$ are the derivative polarizability tensor corresponding to vibration ν.

With these definitions, it appears that the second member of eq. (122) can be split into various components. As a result, $J(\underline{Q},t)$ can be written as: $J(\underline{Q},t) = J_{00}(\underline{Q},t) + J_{\nu\nu}(\underline{Q},t)$ and we select the two following:

$$J_{00}(\underline{Q},t) = \frac{1}{N} \left\langle \sum_{i,j} (\underline{\varepsilon}_S \underline{\underline{\alpha}}_i^0(0) \underline{\varepsilon}_I)(\underline{\varepsilon}_S \underline{\underline{\alpha}}_j^0(t) \underline{\varepsilon}_I) \exp i\underline{Q}\left(\underline{r}_i(t) - \underline{r}_j(0) \right) \right\rangle \tag{1.125}$$

and

$$J_{\nu\nu'}\left(\underline{Q},t\right)=\frac{1}{N}\left\langle \sum_{i,\,j,\,\nu,\,\nu'}(\underline{\varepsilon}_S\underline{\underline{\alpha}}_i^{\nu}(0)\underline{\varepsilon}_I)(\underline{\varepsilon}_S\underline{\underline{\alpha}}_j^{\nu'}(t)\underline{\varepsilon}_I)q_i^{\nu}(0)q_j^{\nu'}(t)\exp i\underline{Q}\left(\underline{r}_i(t)-\underline{r}_j(0)\right)\right\rangle \qquad (1.126)$$

The former is the relevant correlation function for the so-called Rayleigh scattering; the latter is related to the Raman spectrum.

1.6.3 Raman scattering of light: derivative polarizability tensor

a) General

The corresponding correlation function is $J_{\nu\nu'}(\underline{Q},t)$. The rotations appear through $\underline{\underline{\alpha}}$, the vibrations through q and the translations through **r**. If we can assume that these three types of motions are independent, and this can be a good approximation, especially for translation compared to the other motions, then the average in eqn. (1.126) can be split into three averages. If we also suppose that the vibrations between different molecules and within the same molecules are not coupled, then eqn. (1.104) holds and eqn. (1.124) can be written:

$$J_{\nu\nu'}\left(\underline{Q},t\right)=\frac{1}{N}\sum_{i,\nu}<(\underline{\varepsilon}_S\underline{\underline{\alpha}}_i^{\nu}(0)\underline{\varepsilon}_I)(\underline{\varepsilon}_S\underline{\underline{\alpha}}_i^{\nu}(t)\underline{\varepsilon}_I)><q_i^{\nu}(0)q_i^{\nu}(t)><\exp i\underline{Q}\left(\underline{r}_i(t)-\underline{r}_i(0)\right)> \qquad (1.127)$$

We can say that, using neutrons terminology, in this case the scattering is mainly incoherent since only individual motions are seen, and that this incoherence is introduced by the vibrations. Another important and always justified approximation is to assume that the exponential is ≈1. This approximation expresses the fact that the contribution to the broadening of the spectra due to translation is always much smaller than the instrumental energy resolution (typically 10^{-3} cm^{-1} compared to 1 cm^{-1}) and that only the broadening due to rotations and vibrations is seen (typically a few cm^{-1} to a few hundred cm^{-1}). If we also assume that all the molecules are identical, then the correlation function can finally be written:

$$c_{\nu\nu'}\left(\underline{Q},t\right)=\sum_{\nu}<(\underline{\varepsilon}_S\underline{\underline{\alpha}}^{\nu}(0)\underline{\varepsilon}_I)(\underline{\varepsilon}_S\underline{\underline{\alpha}}^{\nu}(t)\underline{\varepsilon}_I)><q^{\nu}(0)q^{\nu}(t)> \qquad (1.128)$$

In addition, as for infrared absorption, we can assume that the vibrations are well separated from each other and weakly damped, in which case eq. (106) holds. If we define the function :

$$D_{SI}(t) = <(\underline{\varepsilon}_S \underline{\underline{\alpha}}^{\nu}(0)\underline{\varepsilon}_I)(\underline{\varepsilon}_S \underline{\underline{\alpha}}^{\nu}(t)\underline{\varepsilon}_I)> \tag{1.129}$$

we finally have:

$$c_{\nu\nu}(t) = \sum_{\nu}(q^{\nu})^2 \exp(-i\Omega_{\nu}t)G_{\nu}(t)D_{SI}(t) \tag{1.130}$$

$$c_{\nu\nu}(\omega) = \sum_{\nu}(q^{\nu})^2 G_{\nu}(\omega+\Omega_{\nu}) \otimes D_{SI}(\omega+\Omega_{\nu}) \tag{1.131}$$

This result shows that a Raman spectrum is composed of a series of lines centered at the vibration frequencies Ωv. It is seen that, provided some assumptions are made, each line of the Raman spectrum is the convolution of a vibrational and rotational spectrum, as for the infrared case. In fig. 1.18 polarization geometries are presented.

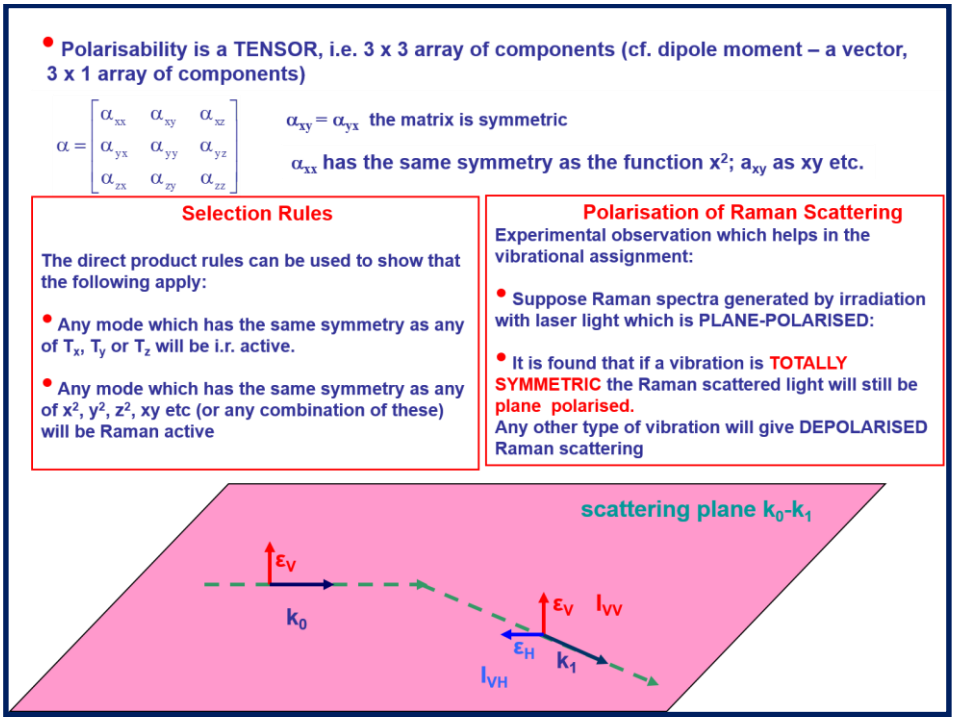

Fig.1.18: polarization geometries.

However there are two important differences:

(i) the rotational correlation function is not the same;

(ii) here we have an external parameter that we do not have in infrared, namely the relative orientation of the polarization vectors $\boldsymbol{\varepsilon}_I$ and $\boldsymbol{\varepsilon}_S$, which allows the

selection of certain components of the polarizability tensor and which is usually divided into its isotropic part $\bar{\alpha}\underline{\underline{I}}$ and its anisotropic part $\underline{\underline{\beta}}$:

$$\underline{\underline{\alpha}}^{\nu} = \overline{\alpha}^{\nu}\,\underline{\underline{I}} + \underline{\underline{\beta}}^{\nu} \tag{1.132}$$

with

$$\bar{\alpha} = \frac{1}{3}Tr(\underline{\underline{\alpha}}) \tag{1.133}$$

and

$$\underline{\underline{\beta}} = \underline{\underline{\alpha}} - \frac{1}{3}Tr(\underline{\underline{\alpha}}) \bullet \underline{\underline{I}} \tag{1.134}$$

$\underline{\underline{I}}$ being the unit tensor.

According to the geometry of the experiment, different combinations of isotropic and anisotropic parts can be chosen and corresponding spectra will reflect different aspects of the (same). In this sense, Raman scattering is comparable to neutron scattering, the external parameter being the momentum transfer Q is this latter case. In the following, we discuss the calculations in a simple case, for two typical geometrical configurations called VH and VV configurations.

b) The case of a linear molecule

We proceed to consider a linear molecule, whose orientation is characterized by its unit vector $\underline{u}$ and we only considerthe vibration q^{ν} along $\underline{u}$. Due to the cylindrical symmetry, the polarizability tensor is diagonal in the molecular frame and contains two independent components α_A and α_B:

$$\underline{\underline{\alpha}}^{\nu} = \begin{pmatrix} \alpha_A & 0 & 0 \\ 0 & \alpha_B & 0 \\ 0 & 0 & \alpha_B \end{pmatrix} \tag{1.135}$$

Let u_r(r=x,y,z) be the components of $\underline{u}$ with laboratory frame. Simple algebra yields:

$$\underline{\underline{\alpha}}_{rs}{}^{\nu} = \overline{\alpha}^{\nu}\delta_{rs} + (\alpha_A - \alpha_B)(u_r u_s - \frac{1}{3}\delta_{rs}) \tag{1.136}$$

(i) **VH configuration: depolarised spectrum**.

In this configuration, we choose a scattering angle of 90°. The beam comes along Oy with $\underline{\varepsilon}_I$ along Oz and is scattered along Ox with $\underline{\varepsilon}_S$ along Oy. In this case we have

$$\underline{\varepsilon}_S \underline{\underline{\alpha}} \underline{\varepsilon}_I = \alpha_{yz} = (\alpha_A - \alpha_B)(u_y u_z) \tag{1.137}$$

and

$$D_{yz}(t) = (\alpha_A - \alpha_B)^2 < u_y(0) u_z(0) u_y(t) u_z(t) > \tag{1.138}$$

Let us suppose that the medium is isotropic. Then we can average Dyz over all possible orientations of $\underline{u}(0)$ or equivalently, take $\underline{O}z$ along $\underline{u}(0)$. Calling θ(t) and Φ(t) the polar coordinates of $\underline{u}(t)$, we have:

$$D_{yz}(t) = (\alpha_A - \alpha_B)^2 < \sin\theta(t)\cos\theta(t)\sin\Phi(t) > \tag{1.139}$$

The function in brackets is an associated Legendre polynomial of order 2, P_2^m. Since in an isotropic medium its average is independent of m, putting $F_2(t)=<P_2\cos(\theta(t))>$ where P_2 is the ordinary Legendre polynomial of order 2, we finally have :

$$C_{\nu\nu}^{VH}(t) = (q^\nu)^2 (\alpha_A - \alpha_B)^2 G_\nu(\omega + \Omega_\nu) \otimes F_2(\omega + \Omega_\nu) \tag{1.140}$$

This equation should be compared with eqn.(1.109). The comparison between infrared and Raman spectra can provide valuable information on the details of the rotational model. It appears here that the depolarised Raman spectrum reflects the same motion as the infrared absorption spectrum: vibration and rotations, except that the first order Legendre polynomial is replaced by the second order one.

(ii) **VV configuration: polarized spectrum**.

In this configuration, the experimental geometry is the same as for VH except that $\underline{\varepsilon}_S$ is also along $\underline{O}z$. In this case, we have

$$\underline{\varepsilon}_S \underline{\underline{\alpha}} \underline{\varepsilon}_I = \alpha_{zz} = \overline{\alpha}^\nu \delta_{rs} + (\alpha_A - \alpha_B)(u^2{}_z - \frac{1}{3}) \tag{1.141}$$

With the same previous hypotheses, applying a bit of math, we get:

$$C_{\nu\nu}^{VV}(\omega) = (q^\nu)^2 G_\nu(\omega + \Omega_\nu) \otimes \left[\left(\overline{\alpha}^\nu \right)^2 + \frac{4}{45}(\alpha_A - \alpha_B) F_2(\omega + \Omega_\nu) \right] \tag{1.142}$$

What we have obtained shows that the polarized Raman spectrum is the sum of:

- a purely vibrational proportional term proportional to $\left(\overline{\alpha}^{\nu}\right)^2$
- a term identical to that obtained in the depolarized case.

This is a very important result because, from a comparison of the two types of spectra, one can immediately say something about the time scale of the various motions. If the VH spectrum or the infrared spectrum is broad and the VV spectrum presents a central narrow component, then we can assign with certainty this narrow component to the purely vibrational term and the broader one to rotations, and reasonably conclude that vibrations and rotations are weakly coupled. If, on the contrary, both spectra havewidth of the same order, this last result is certainly not true. Its width is about 1.5 cm^{-1}, to be compared with about 100cm^{-1} for the infrared spectrum. An example of the latter situation is found fo HCl in CO2 where the width of the infrared spectrum is about 61 cm^{-1}, compared with about 48 cm^{-1} for the VV+VH Raman spectrum. In fig.1.19 a sketch of classical interpretation of Raman effect is reported.

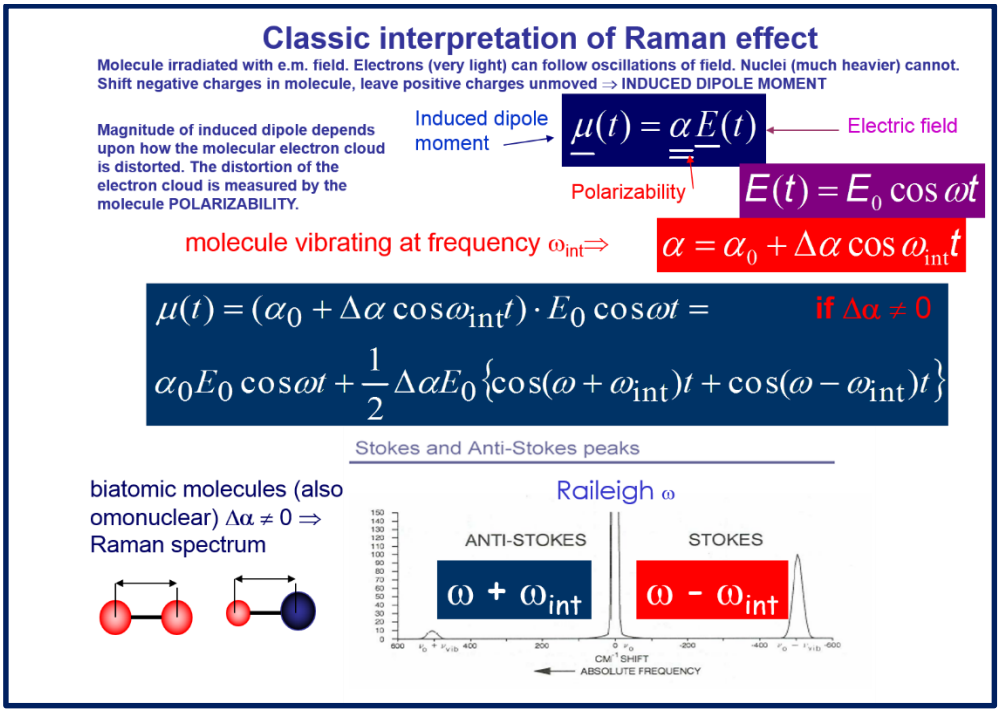

Fig.1.19: Sketch of the Raman classical interpretation

We conclude, therefore, that Raman scattering of light may be a powerful method for studying vibrational and rotational movements in liquids. Because of the incoherence introduced by vibrations, only individual movements are seen in practice, even in pure liquids. Precious information about nature, time scale, and degree of coupling between

different movements can be provided by comparing spectra obtained in different configurations and infrared absorption. Although the amount of Raman data in liquids is increasing the precise theoretical description of the Raman line shapes is difficult, especially due to the great number of possible vibrational relaxation processes. Moverover as in the infrared case, on the experimental side the problem also becomes very difficult with large molecules, due to possible overlap of the various vibrational band (inhomogeneous broadening). Concerning the instrumental energy resolution, with the best monochromators one can reach $\Delta\omega$ about 0.2 cm^{-1} about 20 μeV, i.e. the same order of magnitude as with ILL neutrons. This corresponds to a time scale of 10^{-11} sec., which means that in any case only fast motions can be seen by this method. So far, we have considered experiments using continuous waves. It should be noticed that an alternative manner of conducting Raman experiments is to use picosecond pulsed techniques which can yield additional information on the nature of the relaxation processes.

1.6.4 Rayleigh scattering of light: permanent polarizability tensor

a) General

In this case the relevant correlation function is given by eq. (1.125), where as opposed to the raman case, the vibrations do not appear. For which there is no mechanism to decouple the relative motions and the scattering is coherent in the sense that it mainly reflects the collective motions. If the translations and rotations appear on a different time scale, here also it is reasonable to separate the two averages in eq. (1.125), and we have:

$$J_{00}(\underline{Q},t) = \frac{1}{N}\sum_{i,j} < (\underline{\varepsilon}_S \underline{\underline{\alpha}}^0_i \underline{\varepsilon}_I)(\underline{\varepsilon}_S \underline{\underline{\alpha}}^0_j \underline{\varepsilon}_I) > < \exp i\underline{Q}(\underline{r}_i(t) - \underline{r}_j(0)) > \qquad (1.143)$$

The fourier transform shows that the Rayleigh spectra are centered around the incident photon energy. As for the case of the derivative tensor, the permanent tensor can be split into an isotropic part α^0_I and an anisotropic part β^0 . So even in this case also, by choosing the relative orientation $\underline{\varepsilon}_S$ and ε_I, one can pick out different aspects of the motion. Let us consider the same two configuration.

b) VH spectrum: depolarised spectrum

Like the Raman case, the relevant tensor component, in th laboratory frame, is β_{yz} and the corresponding correlation function is

$$J_{00}^{VH}(\underline{Q},t) = \frac{1}{N}\sum_{i,j} < \beta_{i,yz}^{0}(0)\beta_{j,yz}^{0}(t) >< \exp i\underline{Q}\left(\underline{r}_i(t) - \underline{r}_j(0)\right) > \tag{1.144}$$

If the rotation are much faster than the translations, the spectrum corresponding to the correlation function of β is much broader than that corresponding to the exponential (i.e. we can take the exponential about 1) and the depolarised Rayleigh spectrum only reflects the(collective) rotational motions. In this case, the comparison between the two results can provide valuable information on the degree of cooperativity of the rotational motions since, among other things, depolarized Raman spectrum reflects individual rotational (and vibrational) motions. In practice, the Rayleigh spectrum of a pure liquid is generally found to benarrower than the corresponding raman spectrum, showing that the collective motions are slower than the individual ones, as expected from general consideratios.

c) VV spectrum: polarized Rayleigh scattering

The corresponding correlation function, as for the Raman case, contains two kinds of the terms: terms related to the isotropic part of the permanent polarizbility tensor and terms related to the anisotropic part. Let us consider these terms separately.

(i) The term related to $\bar{\alpha}^{0}$

$$J_{00}^{VV}(\underline{Q},t) = \frac{1}{N}\sum_{i,j} \overline{\alpha_i^0}\,\overline{\alpha_j^0} < \exp i\underline{Q}\left(\underline{r}_i(t) - \underline{r}_j(0)\right) > \tag{1.145}$$

It is seen that this function is formally identical to the neutron intermediate pair correlation function Ip(Q,t) for a monoatomic liquid (eq.(41)). This means that VV Rayleigh light scattering and coherent neutron scattering contain a priori the same kind of information about the collective translational motions, the only difference being the very different momentum transfer range which can be reached (about 10^{-3} $\mathring{A}^{-1}$ compared to 1 $\mathring{A}^{-1}$).

Since the space scale, and also the time scale due to a better energy resolution, are much larger with light than with neutrons, light scattering is more suitable than neutrons to test slow, large-scale phenomena such as those predicted by hydrodynamic and critical

phenomena theories. In particular, hydrodynamics predicts that the spectrum contains three components, a central component called the Rayleigh line, whose with is proportional to the thermal diffusivity timesQ^2, and two side lines, centered at $\omega = \pm v_s Q$ where v_s is the velocity of sound, whose width is also proportional toQ^2, and which is called the Brillouin doublet.

In same special cases, a fourth central component may appear, called the Mountain line, the characteristics of which are linked to the shear viscosity properties. With neutrons, since Q is much larger, all the lines are much broader. However, neutrons are unique for testing the validity of these theories in the limits of short distances and times.

(ii) The term related to $\underline{\underline{\beta}}^0$ is

$$J_{00}^{VV}(\underline{Q},t) = \frac{1}{N}\sum_{i,j} < \beta_{i,zz}^0(0)\beta_{j,zz}^0(t) >< \exp i\underline{Q}\left(\underline{r}_i(t) - \underline{r}_j(0)\right) > \qquad (1.146)$$

This term is comparable to the corresponding one in the VH geometry. It generally corresponds to a broader band which mainly reflects the collective rotational motions.

The total VV scattering being the sum of these two contributions, a polarized Rayleigh spectrum should appear as the sum of three or four sharp components superimposed on a broad band. In practice the feature will depend on the actual energy resolution.

We can conclude that Rayleigh scattering of light appears to be a powerful method for studying collective and rotary collateral movements in liquids. It is suitable for studying long space and time scale phenomena and testing hydrodynamic theories.

A very high energy resolution, many orders of magnitude better than that which can be achieved with neutrons are due to advances in laser technology. Figure 1-20 shows an example of active CO2 bands. Progress in the technology of laser techniques has made it possible to obtain very high energy resolution, many orders of magnitude better In fig.1.20 an example of active bands for CO_2 is reported.

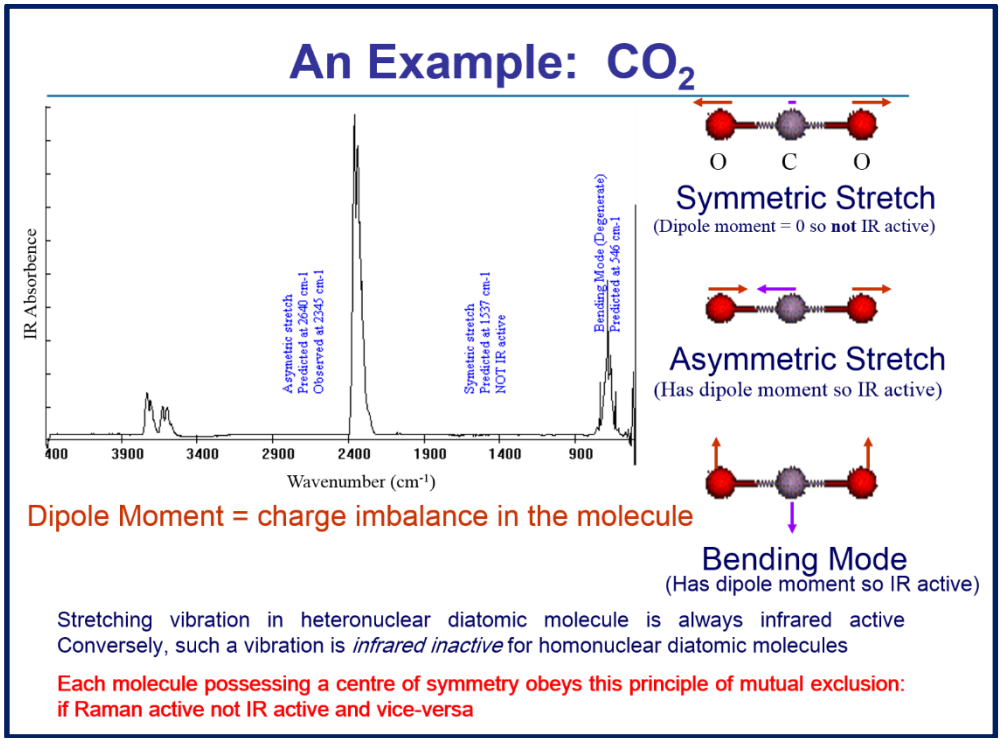

Fig.1.20: Example of active bands for CO_2.

In table 1.2, a comparison among different techniques is reported

TECHNIQUE	COUPLING	CORRELATION FUNCTION	TIME SCALE
Elastic light Scattering	EM-permanent polarized tensor $\underline{\underline{\alpha}}_i^0$	$\underline{\underline{\alpha}}_i^0 \underline{\underline{\alpha}}_j^0 \exp\left\{i\underline{Q}\cdot\left[\underline{r}_i(t)-\underline{r}_j(0)\right]\right\}$	10^{-15}s
Photon correlation	EM-permanent polarized tensor $\underline{\underline{\alpha}}_i^0$	$\underline{\underline{\alpha}}_i^0(0)\underline{\underline{\alpha}}_j^0(t)\exp\left\{i\underline{Q}\cdot\left[\underline{r}_i(t)-\underline{r}_j(0)\right]\right\}$	$10^{-6}\div 10$s
Brillouin scattering	EM-permanent polarized tensor $\underline{\underline{\alpha}}_i^0$	$\underline{\underline{\alpha}}_i^0(0)\underline{\underline{\alpha}}_j^0(t)\exp\left\{i\underline{Q}\cdot\left[\underline{r}_i(t)-\underline{r}_j(0)\right]\right\}$	$10^{-11}\div 10^{-8}$s
Raman Scattering	EM-perm. polar. tensor derivative $\left(\partial\underline{\underline{\alpha}}/\partial q^\nu\right)_{q^\nu=0}=\underline{\underline{\alpha}}^\nu$	$\underline{\underline{\alpha}}_i^\nu(0)\underline{\underline{\alpha}}_j^{\nu'}(t)q_i^\nu(0)q_j^{\nu'}(t)\exp\left\{i\underline{Q}\cdot\left[\underline{r}_i(t)-\underline{r}_j(0)\right]\right\}$	$10^{-15}\div 10^{-11}$s
Infrared absorption	EM-dipole moment derivative $\left(\partial\vec{\mu}/\partial q^\nu\right)=\vec{\mu}^\nu$	$\underline{\mu}_i^\nu(0)\underline{\mu}_j^{\nu'}(t)q_i^\nu(0)q_j^{\nu'}(t)$	$10^{-15}\div 10^{-12}$s
X-Ray diffraction	EM-electron charge density β	$\beta_i\beta_j\exp\left\{i\underline{Q}\cdot\left[\underline{r}_i-\underline{r}_j\right]\right\}$	$10^{-19}\div 10^{-17}$s
Neutron scattering	Neutron-nucleus	$b_i b_j\exp\left\{i\underline{Q}\cdot\left[\underline{r}_i(t)-\underline{r}_j(0)\right]\right\}$	$10^{-14}\div 10^{-8}$s
Ultrasound	Ultrasound-mass density ρ	$\rho_i(0)\rho_j(t)\exp\left\{i\underline{Q}\cdot\left[\underline{r}_i(t)-\underline{r}_j(0)\right]\right\}$	$10^{-6}\div 10^{-1}$s

Table 1.2: Comparison among different techiniques

In table 1.3 a comparison of neutron, infrared and Raman spectroscopies is presented.

	NEUTRON	INFRARED	RAMAN
Wavelength	λ~1.8 Å interatomic spacings $\hbar\omega \sim 26meV$ tras. Energy in s.c.m.	$\lambda = 10^7 \div 7800Å$	$\lambda = 3900 \div 7800Å$
Scatt. Centre	Nucleus	Electron	Electron
Coupling	$H: \sigma = 81.67\ 10^{-28} m^2$ relatively small perturbation: system responds linearly	$\sigma_R \approx 10^{-22}\ m^2/molec$	2nd order in E (weaker) $\sigma_{Raman} \approx 10^{-32}\ m^2/molec$
Selection rules	No -H pseudo-selection rule -longitudinal/transverse pseudo selection rule through polarization vector	Yes, at least one over 3 (isolated molecules, crystals: group theory)	Yes, at least one over 6 High % of optically inactive modes in highly symmetric molecules; e.g. C_{60}>70% -polarization vector analysis
Probe	$\omega = \hbar k^2/2m$ (non relativistic)	$\omega = ck$	$\omega = ck$
Dispersion law	Phonon dispersion law from B.N. Brockhouse (1955): typically the first Brillouin zone in a solid: $k = \pi/a = 10nm^{-1}$ (a =crystal constant) $\hbar\omega = 25.85meV$; $k = 35.2nm^{-1}(E_{inc}, \theta)$	$\lvert K\rvert = 0$ phonon dispersion	$\lvert K\rvert = 0$ phonon dispersion $\lambda = 5145Å$ ($\hbar\omega = 2.41eV$); $k = 1.22\ 10^{-2} nm^{-1}$ (X-ray: $\hbar\omega > 1keV$- $k = 10nm^{-1}$)
Spectral intensities	Direct relation with vibrational eigenvectors (oscillation amplitude): harmonic oscillator vibrational spectrum (n=0 elastic, n=1 fundamental, n>1 overtone)	Intensity depends on number of scatterers and on electronic structure of molecular systems electric anharmonicity distorces spectra	Polarizability increases with electronic number Z: light elements masked in presence of heavy element
Band activity	Can be easily calculated	Difficult to calculate	Difficult to calculate

Table 1.3 Comparison of techniques

Chapter 2

Recent Development on Elastic Incoherent Neutron Scattering (EINS) and Resolution Elastic Neutron Scattering (RENS)

2.1 Introduction

An excellent probe to characterize thermal molecular motions and conformational changes in biological systems is represented by neutrons as they have a wavelength of 1 Å and an energy close to 1 kcal / mol [4-10]. In particular, they provide information on mean-square fluctuations in a given timescale by Elastic Incoherent Neutron Scattering (EINS) [11], on correlation times of diffusion motions by QENS [12], and on vibrational modes by INS [13].

It is also known that, compared with QENS, EINS requires a relatively small amount of material, due to the fact that elastic contribution is often a factor of 100 ÷ 1000 higher than the almost elastic low-energy transfer;

It is also well known that, in comparison with QENS, EINS due to the fact that the elastic contribution is often a factor 100÷1000 higher than the quasi-elastic one at low energy transfer, requires a relatively small amount of material; this point allows the investigation of a relevant number of interesting systems, such as for example those of interest in the biophysical field. Furthermore when dealing with QENS one of the main drawbacks is constituted by a relatively high number of fitting parameters. In this frame EINS, through the so called “elastic-window-method”, introduced by Alefeld and Kollmar [53], is one of the most effective approach for evaluating atomic MSD in hydrogenous systems and it is often preferred to the QENS technique. The MSDs obtained by an analysis as a function of Q are dominated by hydrogen motions due to its large incoherent cross-section value [14-15].

2.2 Fourier Transform (FT)

In the first part of the 19th century, Joseph Fourier, a French mathematician and physicist, showed that any periodic function can be decomposed in a series of simple oscillating functions, namely sines and cosines (or complex exponentials). The generalization to the non-periodic signals has come only a century later, and took the name of Fourier Transform (FT), a tribute brought to the original idea. The FT decomposes a signal in complex exponential functions at different frequencies. The equations used in the decomposition and reconstruction part are the following:

$$X(\omega) = \int_{-\infty}^{+\infty} x(t)e^{-j\omega t}dt \tag{2.1}$$

$$x(t) = \frac{1}{2\pi}\int_{-\infty}^{+\infty} X(\omega)e^{j\omega t}d\omega \tag{2.2}$$

In the above equations, *t* stands for time, $\omega = 2\pi f$ for frequency, x denotes the signal in the time domain and X denotes the signal in the frequency domain (also known as the spectrum of the original signal). The computation of the FT is done over all times, making no distinction between signals' stationary parts and transient ones (whether the frequency component 'ω' appears at time t_1 or, t_2 it will have the same effect at the output of the integration). The scaling property of the FT states that if we have a scaled version of the original

$$x_s(t) = x(st) \tag{2.3}$$

then, its corresponding FT will be $X_s(\omega)$

$$X_s(t) = \frac{1}{|s|}X\left(\frac{\omega}{s}\right) \tag{2.4}$$

From the last two equations we can see that if we reduce the time spread of x by s (if s>1) than the FT is dilated by s, meaning that if what we have gained in time localization, we have lost in frequency localization. Projecting the signal on complex exponentials leads to good frequency analysis, but no time localization. The poor time localization is the main disadvantage of the Fourier transform, making is not suitable for all kind of applications. To see how the frequency content of a signal changes over time, we can cut the signal into blocks and compute the spectrum of each block. This is the base concept of the Short Time Fourier Transform (STFT) introduced in 1946 by Gabor [2], and again in 1977 by J.B. Allen [3], the latter giving it a filterbank interpretation. For computing STFT we simply multiply the original signal by a window function, which is non-zero for only a short period of time, and

then we compute the Fourier Transform of the obtained signal. The result is a two-dimensional representation of the signal, that can be mathematically written as:

$$STFT\{x(t)\} \equiv X(\tau, \omega) = \int_{-\infty}^{+\infty} x(t)\omega(t-\tau)e^{-j\omega t}dt, \quad (2.5)$$

where $\omega(t)$ is the window function, commonly a Hann window or a Gaussian centered around zero, and $x(t)$ is the signal to be analyzed. This equation can be interpreted as an analysis of the signal by a sliding window in time or by a sliding bandpass filter in frequency. A particularity of this transform is the fact that the window is of constant length throughout the whole analysis process, meaning that the transform has a fixed resolution in time and frequency.

Time and frequency energy concentrations are restricted by the Heisenberg uncertainty principle. If we consider a finite energy function, $f \epsilon L^2(\mathbb{R})$ ($\int |f(t)|^2\, dt < \infty$) and we consider it centered around zero in time and its Fourier transform $F(\omega)$ centered around zero in frequency, then the temporal variance, σ_t^2(given in eq. 2.6) and the frequency variance, σ_ω^2 (given in eq. 2.7) of the wave function satisfy the condition (2.8):

$$\sigma_t^2 = \frac{1}{\|f\|^2}\int_{-\infty}^{+\infty} t^2\, |f(t)|^2 dt, \quad (2.6)$$

$$\sigma_\omega^2 = \frac{1}{8\pi^3\|f\|^2}\int_{-\infty}^{+\infty} \omega^2\, |F(\omega)|^2 d\omega, \quad (2.7)$$

$$\sigma_t^2\sigma_\omega^2 \geq \frac{\pi}{2}. \quad (2.8)$$

$\|f\|$ denotes the norm of the function f, computed as: $\sqrt{\int_{-\infty}^{+\infty}|f(t)|^2 dt}$.

Depending on the time localization that is more suitable for our application, we can choose the width of the analysis window, namely a short window for a good time but poor frequency localization (suitable for signals with a high frequency content) or a wide window for good frequency localization with the price of poorer time localization.

2.3 Definition and relations existing between the functions $G(\vec{r},t)$, $I(\vec{Q},t)$, $S(\vec{Q},\omega)$ and $D(\vec{r},\omega)$

Considering a particle system as an ensemble of n_{tot}particles j, sited in $\vec{r}_j(t)$at time t, following Van Hove[5], one can introduce the system time dependent pair correlation function *G(r⃗,t)* [16], defined as:

$$G(\vec{r},t) = \frac{1}{n_{tot}}\langle\sum_{i,j}^{N}\int d\vec{r}'\cdot\delta(\vec{r}+\vec{r}_i(0)-\vec{r}')\delta(\vec{r}'-\vec{r}_j(t))\rangle \quad (2.9)$$

Where *r'* refers to an integration variable and the angle brackets <> denote an ensemble average. $G(\vec{r},t)$ can be interpreted as the probability to find a particle j at time t at the place r if this or another particle i was at time $t=0$ at the origin $r=0$, sodescribing how the correlation between the particle positions evolve with time. The one dimensional spatial Fourier Transform,FT_r, of the time dependent pair correlation function is called the intermediate scattering function $I(\vec{Q},t)$[5]:

$$FT_r[G(\vec{r},t)] = I(\vec{Q},t) \quad (2.10)$$

By introducing the two dimensional space-time Fourier Transform, $FT_{r,t}$, one can introduce the system scattering law $S(\vec{Q},\omega)$:

$$FT_{r,t}[G(\vec{r},t)] = S(\vec{Q},\omega) \quad (2.11)$$

$$S(\vec{Q},\omega) = \int_{-\infty}^{+\infty}\int_{-\infty}^{+\infty} G(\vec{r},t)e^{-2\pi i(\vec{Q}r+\omega t)}drdt \quad (2.12)$$

In the case of systems which can be regarded as composed of distinguishable particles (Boltzmann statistics) the $G(\vec{r},t)$function splits in two parts:

$$G(\vec{r},t) = G_s(\vec{r},t) + G_d(\vec{r},t) \quad (2.13)$$

$G_s(\vec{r},t)$,where the subscript *s* stands for "self", describes the correlation between positions of one and the same particles at different times, while $G_{dist}(\vec{r},t)$, where the subscript *d* stands for "distinct", refers to pairs of distinct particles. More precisely, they are defined as follows:

$$G_s(\vec{r},t) = \frac{1}{n_{tot}}\langle\sum_{j=1}^{n_{tot}}\int d\vec{r}'\cdot\delta(\vec{r}+\vec{r}_j(0)-\vec{r}')\delta(\vec{r}'-\vec{r}_j(t))\rangle \quad (2.14)$$

$$G_d(\vec{r},t) = \frac{1}{n_{tot}}\langle\sum_{j\neq i=1}^{n_{tot}}\int d\vec{r}'\cdot\delta(\vec{r}+\vec{r}_i(0)-\vec{r}')\delta(\vec{r}'-\vec{r}_j(t))\rangle \quad (2.15)$$

In other terms, $G_s(\vec{r},t)$can be interpreted as the probability to find one particle at time t at place $\vec{r}$ if the same particle was at time $t=0$ at $r=0$. $G_d(\vec{r},t)$ can be interpreted as the probability to find at time t at place r one particle distinct from the one that was at the

origin at time 0. More precisely, for short times, the self correlation function $G_s(\vec{r},t)$ approximates to a δ-function, while the distinct correlation function $G_d(\vec{r},t)$ is approximately the radial distribution function. For large times, as $t \to \infty$, $G_d(\vec{r},\infty) \approx \rho$, which is the density of system, given by $\frac{n_{tot}}{V}$, where V is the volume. Similarly, for the $G_s(\vec{r},\infty) = \frac{1}{V}$, that tends to zero when V tends to ∞. In other, words, $G_s(\vec{r},t) \to 0$ and $G_d(\vec{r},t) \to \rho$. These qualitative behavior of $G_s(\vec{r},t)$ and $G_d(\vec{r},t)$ for isotropic systems, i.e. $\vec{r} = r$ are reported in Fig.2.1.

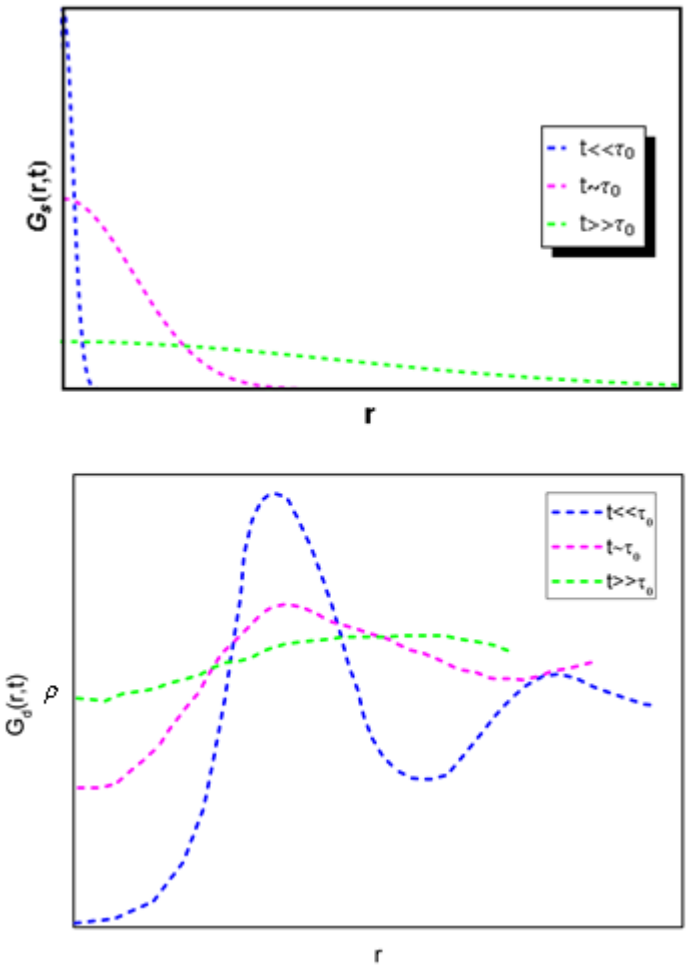

Fig. 2.1 Qualitative behavior of $G_s(r,t)$, i.e. the self term, and $G_d(r,t)$, i.e. the distinct term, for severalvalue of t. In the top(a) $G_s(r,t)$is shown, in the bottom (b) $G_d(r,t)$; τ_0 is the system relaxation time.

It results:

$$FT_r[G_s(\vec{r},t)] = I_s(\vec{Q},t) \tag{2.16}$$

$$FT_r[G_d(\vec{r},t)] = I_d(\vec{Q},t) \tag{2.17}$$

The one dimensional time FT, FT_t, of the intermediate scattering function is the scattering function $S(\vec{Q},\omega)$:

$$FT_t\left[I(\vec{Q},t)\right] = S(\vec{Q},\omega) \tag{2.18}$$

It results:

$$FT_t\left[I_s(\vec{Q},t)\right] = S_s(\vec{Q},\omega) \tag{2.19}$$

$$FT_t\left[I_d(\vec{Q},t)\right] = S_d(\vec{Q},\omega) \tag{2.20}$$

By introducing the two dimensional space-time FT, $FT_{r,t}$, one can write:

$$FT_{r,t}[G(\vec{r},t)] = S(\vec{Q},\omega) \tag{2.21}$$

The quantity:

$$D(\vec{r},\omega) = FT_t[G(\vec{r},t)] = FT_r\left[S(\vec{Q},\omega)\right] = FT_{r,t}\left[I(\vec{Q},t)\right] \tag{2.22}$$

is called *dynamic correlation function*.

Figure 2.2 summarizes the space and time FT relations existing between the introduced functions, i.e. $G(\vec{r},t), I(\vec{Q},t), S(\vec{Q},\omega)$ and $D(\vec{r},\omega)$:

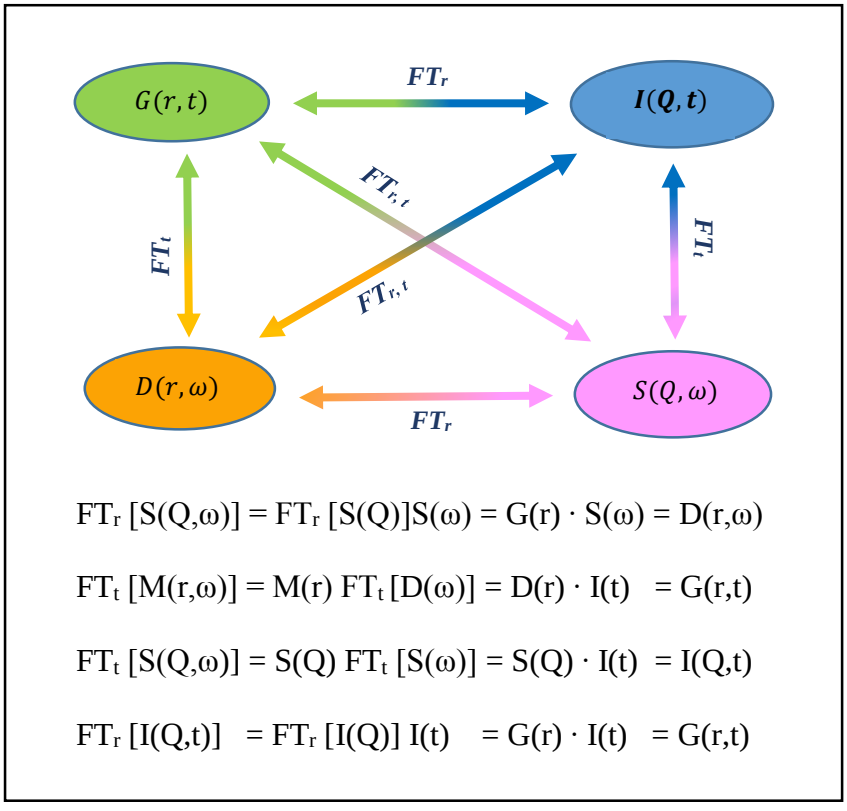

Fig. 2.2 Sketch of the one and two dimensional space-time Fourier transform connections among system quantities.

2.4 Theoretical approach on elastic neutron scattering (EINS)

As already mentioned the scattering law $S(Q,\omega)$ and the intermediate scattering function $I(Q,t)$ are connected by a time Fourier transform [16-21]:

$$S(Q,\omega) = \frac{1}{\sqrt{2\pi}}\int_{-\infty}^{+\infty} I(Q,t)e^{-i\omega t}dt \tag{2.23}$$

$$I(Q,t) = \frac{1}{\sqrt{2\pi}}\int_{-\infty}^{+\infty} S(Q,\omega)e^{i\omega t}d\omega \tag{2.24}$$

If the introduced functions of two independent variables are separable then they can be expressed as a product of two functions each of them depending on only one variable, i.e.:

$$\mathrm{S(Q,\omega) = S(Q)S(\omega)} \tag{2.25}$$

$$\mathrm{R(Q,\omega) = R(Q)R(\omega)} \tag{2.26}$$

On the other hand, as far as the system cross section is concerned, indicating with k_0 and k_1 the incoming and outcoming neutron wavevectors, b_α and b_β the scattering lengths of atom α and β respectively, $\left|\bar{b}\right|^2 = \langle b_\alpha^* b_\beta\rangle$, $\overline{|b|^2} = \langle b_\alpha^* b_\alpha\rangle$, $\sigma_{coh} = 4\pi\left|\bar{b}\right|^2$ and $\sigma_{inc} = 4\pi\left(\left|\bar{b}\right|^2 - \overline{|b|^2}\right)$ where σ_{coh} takes into account interference effects among waves produced by the scattering of a single neutron from all the nuclei whereas σ_{inc} refers to single particle properties, the neutron scattering double differential cross section can be written as:

$$\frac{d^2\sigma}{d\Omega d\omega} = \frac{k_1}{k_0}\frac{1}{2\pi}\int_{-\infty}^{+\infty} dt\, e^{-i\omega t}\frac{1}{N}\sum_{\alpha=1}^{N}\sum_{\beta=1}^{N}\langle b_\alpha^* b_\beta e^{-i\mathbf{Q}\cdot\boldsymbol{R}_\alpha(0)}e^{-i\mathbf{Q}\cdot\boldsymbol{R}_\beta(t)}\rangle =$$

$$= \frac{k_1}{k_0}\frac{1}{2\pi}\int_{-\infty}^{+\infty} dt e^{-i\omega t}\frac{1}{N}\left[\left|\bar{b}\right|^2\sum_{\alpha}\sum_{\alpha\neq\beta}\langle e^{-i\mathbf{Q}\cdot\boldsymbol{R}_\alpha(0)}e^{-i\mathbf{Q}\cdot\boldsymbol{R}_\beta(t)}\rangle\right.$$

$$\left. + \overline{|b|^2}\sum_{\alpha}\langle e^{-i\mathbf{Q}\cdot\boldsymbol{R}_\alpha(0)}e^{-i\mathbf{Q}\cdot\boldsymbol{R}_\alpha(t)}\rangle\right] =$$

$$\frac{k_1}{k_0}\left|\bar{b}\right|^2 S_{coh}(\mathrm{Q},\omega) + \frac{k_1}{k_0}\overline{|b|^2}S_{inc}(\mathrm{Q},\omega) + \frac{k_1}{k_0}\left(\left|\bar{b}\right|^2 - \overline{|b|^2}\right)S_{inc}(\mathrm{Q},\omega) =$$

$$\frac{k_1}{k_0}\left|\bar{b}\right|^2 S_{coh}(\mathrm{Q},\omega) + \frac{k_1}{k_0}\left(\left|\bar{b}\right|^2 - \overline{|b|^2}\right)S_{inc}(\mathrm{Q},\omega) =$$

$$= \frac{k_1}{k_0}\frac{\sigma_{coh}}{4\pi}S_{coh}(\mathrm{Q},\omega) + \frac{k_1}{k_2}\frac{\sigma_{inc}}{4\pi}S_{inc}(\mathrm{Q},\omega) =$$
$$\frac{\mathrm{k_1}}{\mathrm{k_0}}\left[\frac{\sigma_{\mathrm{coh}}}{4\pi}S_{coh}(\mathrm{Q},\omega) + \frac{\sigma_{\mathrm{inc}}}{4\pi}S_{inc}(\mathrm{Q},\omega)\right] \quad (2.27)$$

In our case, due to the high percentage of hydrogen atoms in the investigated systems (H: $\sigma_{\mathrm{coh}} = 1{,}76$; $\sigma_{\mathrm{inc}} = 80{,}26$) only this latter contribution is relevant:

$$\frac{\mathrm{d}^2\sigma}{\mathrm{d}\Omega\mathrm{d}\omega} \cong \frac{\mathrm{k_1}}{\mathrm{k_0}}\left[\frac{\sigma_{\mathrm{inc}}}{4\pi}\mathrm{S_{inc}}(\mathrm{Q},\omega)\right] \quad (2.28)$$

These functions make reference to the system properties and not to measured quantities; in fact, it should be taken into account that, for example, when the experimental technique gives access to the scattering law one should take into account the less straightforward connection with the measured scattering function, which is the convolution of the scattering law with the instrumental resolution function.

Since, as noted above, these functions refer to system properties, and not to the measured quantities, the instrumental resolution function R(Q,ω) can be introduced in the ω space which is connected to the corresponding time instrumental resolution function by the following Fourier transform:

$$\mathrm{R}(\mathrm{Q},\mathrm{t}) = \frac{1}{2\pi}\int_{-\infty}^{+\infty}\mathrm{R}(\mathrm{Q},\omega)\mathrm{e}^{\mathrm{i}\omega\mathrm{t}}\mathrm{d}\omega \quad (2.29)$$

As a consequence the measured scattering law corresponds to the convolution of the scattering law with the resolution function, i.e.:

$$\mathrm{S_R}(\mathrm{Q},\omega) = \mathrm{S}(\mathrm{Q},\omega) \otimes \mathrm{R}(\mathrm{Q},\omega) \quad (2.30)$$

So, from a formal point of view, the convolution of the two function $S(Q,\omega)$ and $R(Q,\omega)$ produces a third function $S_R(Q,\omega)$ which can be viewed as modified version of the original function, that is, the $S(Q,\omega)$ and the ω-inverted $R(Q,\omega)$ functions when this latter is translated. As a consequence for instrumental function $R(Q,\omega)$ symmetric in ω, the convolution coincides with the cross-correlation between $S(Q,\omega)$ and $R(Q,\omega)$.

By the convolution theorem can be written as:

$$S_R(Q,\omega) = S(Q,\omega) \otimes R(Q,\omega) =$$

$$= \frac{1}{\sqrt{2\pi}}\int_{-\infty}^{+\infty} I(Q,t)\cdot R(Q,t)e^{-i\omega t}dt \quad (2.31)$$

Since we are dealing with incoherent scattering, I(Q,t) is an even function of t, as well as R(Q,t); therefore their product too. This circumstance allows one to consider the cosine Fourier transform, i.e.:

$$S_R(Q,\omega) = S(Q,\omega) \otimes R(Q,\omega) =$$

$$\frac{1}{\sqrt{2\pi}} \int_{-\infty}^{+\infty} I(Q,t) \cdot R(Q,t) cos\omega t dt = \tag{2.32}$$

$$FT_{resolution\ windowed}[I(Q,t)] =$$

$$Gabor\ Transform\ [I(Q,t)]$$

In the following the sub-index R indicates that the relative function is affected by the instrumental resolution, whereas the absence of this sub-index indicates that the relative function is connected only to the sample.

In the ideal case of purely elastic scattering in which the resolution function is a delta in the ω-space and, hence, a constant in the t-space,

$$R(Q,\omega) = \delta(\omega) \equiv R(Q,t) = const$$

we obtain from Eq. (2.32) that the measured scattering law coincides with the scattering law:

$$S_R(Q,\omega) = \frac{1}{\sqrt{2\pi}} \int_{-\infty}^{+\infty} I(Q,t) \cdot R(Q,t) cos\omega t dt =$$

$$= \frac{const.}{\sqrt{2\pi}} \int_{-\infty}^{+\infty} I(Q,t) cos\omega t dt = S(Q,\omega) \cdot const \tag{2.33}$$

so, by the final value theorem, that say that the signal at the origin in the frequency domain equals the signal area in the time domain, we have:

$$S_R(Q,\omega=0) = \frac{1}{\sqrt{2\pi}} \int_{-\infty}^{+\infty} I(Q,t) \cdot R(Q,t) e^{-i\omega t} dt = \frac{1}{\sqrt{2\pi}} \int_{-\infty}^{+\infty} I(Q,t) \cdot R(t) dt \tag{2.34}$$

the measured scattering law $S_R(Q,\omega)$ reduces to a time average of the intermediate scattering function $I(Q,t)$. This value corresponds to the green dot in figure 2.3.

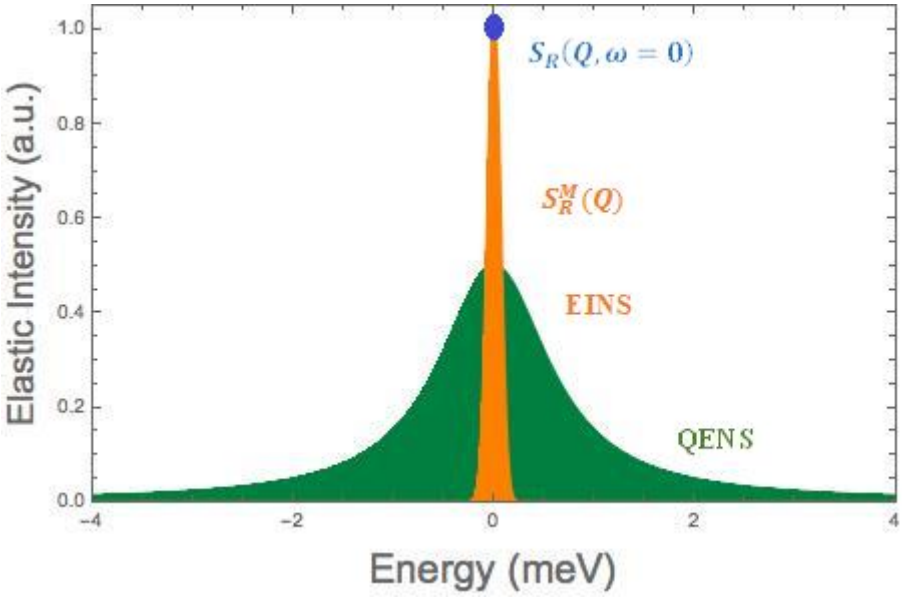

Fig. 2.3 . S_R^M as a function of the logarithm of the instrumental resolution

A part from this idea case, in the more general condition in which the resolution function in the ω-space has a nonegligible width, the experimentally measured elastic scattering law, due to the finite energy instrumental resolution Δω, $S_R^M(Q)$ is

$$S_R^M(Q) = \int_{-\frac{\Delta\omega_{RES}}{2}}^{+\frac{\Delta\omega_{RES}}{2}} S_R(Q,\omega)d\omega \tag{2.35}$$

And hence,

$$S_R^M(Q) = \int_{-\frac{\Delta\omega_{RES}}{2}}^{+\frac{\Delta\omega_{RES}}{2}} S(Q,\omega) \otimes R(Q,\omega)d\omega = \int_{-\frac{\Delta\omega_{RES}}{2}}^{+\frac{\Delta\omega_{RES}}{2}} \left[\frac{1}{\sqrt{2\pi}}\int_{-\infty}^{+\infty}\big(I(Q,t)\cdot R(Q,t)\big)e^{-i\omega t}dt\right]d\omega \tag{2.36}$$

In order to show the operation approach of RENS as well as the expected experimental output we numerically test the behavior of the measured elastic scattering function versus the instrumental energy resolution.

For the general case evaluation, assuming for example a Gaussian function for the resolution in the ω-space, characterized by a resolution time τ_{RES} and a Gaussian or Lorentzian behaviour with a characteristic relaxation time τ for the intermediate scattering function, we operate in the frequency space and evaluate $S_R^M(Q)$ as a function of the

energy instrumental resolution $\Delta\omega$. In particular, in order to numerically get the RENS output we consider an increasing instrumental resolution function linewidth $\Delta\omega$ and apply (2.36) for determining the value of the definite integral as a function of $\Delta\omega$.

Figure 2.3 shows the result of such a calculation: there is an increasing sigmoid trend whose inflection point occurs when the linewidth of the resolution function approaches the linewidth of the system scattering law; in other words, in such a semilogarithmic plot the inflection point occurs when the instrumental resolution time crosses the system relaxation time. Such a result shows the operating way of the RENS approach: from the inflection point of EINS profiles versus the logarithm of the energy resolution one can extract the system relaxation time. It should be noticed that, in a complementary way, for a given fixed instrumental energy resolution function from EINS, starting by (2.36):

$$S_R^M(Q) = \int_{-\frac{\Delta\omega_{RES}}{2}}^{+\frac{\Delta\omega_{RES}}{2}} \left[\frac{1}{\sqrt{2\pi}}\int_{-\infty}^{+\infty}\big(I(Q,t)\cdot R(Q,t)\big)cos\omega dt\right] d\omega \approx\ S_R(Q,\omega=0)\cdot\Delta\omega_{RES} \tag{2.37}$$

In order to show how the cosine transform acts on the integral function, fig. 2.4 shows the $\cos\omega t$ as a function of t in a time interval corresponding to the characteristic time τ of the integral function $I_{inc}(Q,t)\cdot R(Q,t)$, at three different values: $\omega t = 2\pi\cdot 0.1$, $\omega t = 2\pi$, $\omega t = 2\pi\cdot 10$. At $\omega t = 2\pi\cdot 0.1$, the expansion of the cosine contribution $\cos\omega t \cong 1-\frac{\omega^2 t^2}{2} \cong e^{\left(\frac{-\omega^2 t^2}{2}\right)}$ furnishes a Gaussian behaviour; at $\omega t = 2\pi$ the cosine contribution drastically deviates from the constant behavior; and finally at $\omega t = 2\pi\cdot 10$ it quickly oscillates giving rise to a negligible value for the integral.

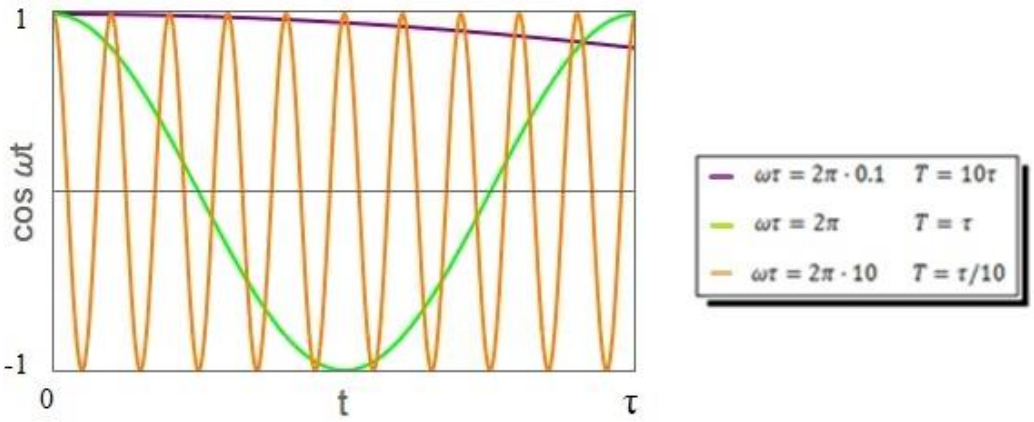

Fig. 2.4: $\cos\omega t$ at three different values: $\omega t = 2\pi\cdot 0.1$, $\omega t = 2\pi$, $\omega t = 2\pi\cdot 10$. At $\omega t = 2\pi\cdot 0.1$, the expansion of the cosine contribution $\cos\omega t \cong 1-\frac{\omega^2 t^2}{2} \cong e^{\left(\frac{-\omega^2 t^2}{2}\right)}$ furnishes a Gaussian behaviour; at $\omega t = 2\pi$ the cosine contribution drastically deviates from the constant behavior; and finally at $\omega t = 2\pi\cdot 10$ it quickly oscillates giving rise to a negligible value for the integral.

More precisely, by considering a fixed intermediate scattering function $I_{inc}(Q,t)$ (with a fixed relaxation time), and a fixed resolution function $R(Q,t)$ (with a fixed resolution time), fig. 2.5 shows in magenta the integral function, given by the product of the previous functions i.e. $I_{inc}(Q,t) \cdot R(Q,t)$; in orange the $\cos \omega t$ function at three different values: $\omega t = 2\pi \cdot 0.1$, $\omega t = 2\pi$, $\omega t = 2\pi \cdot 10$ is reported; in blue the obtained $I_{inc}(Q,t) \cdot R(Q,t)\ cos\omega t$ function; and finally the light blue areas furnish the measured elastic contribution.

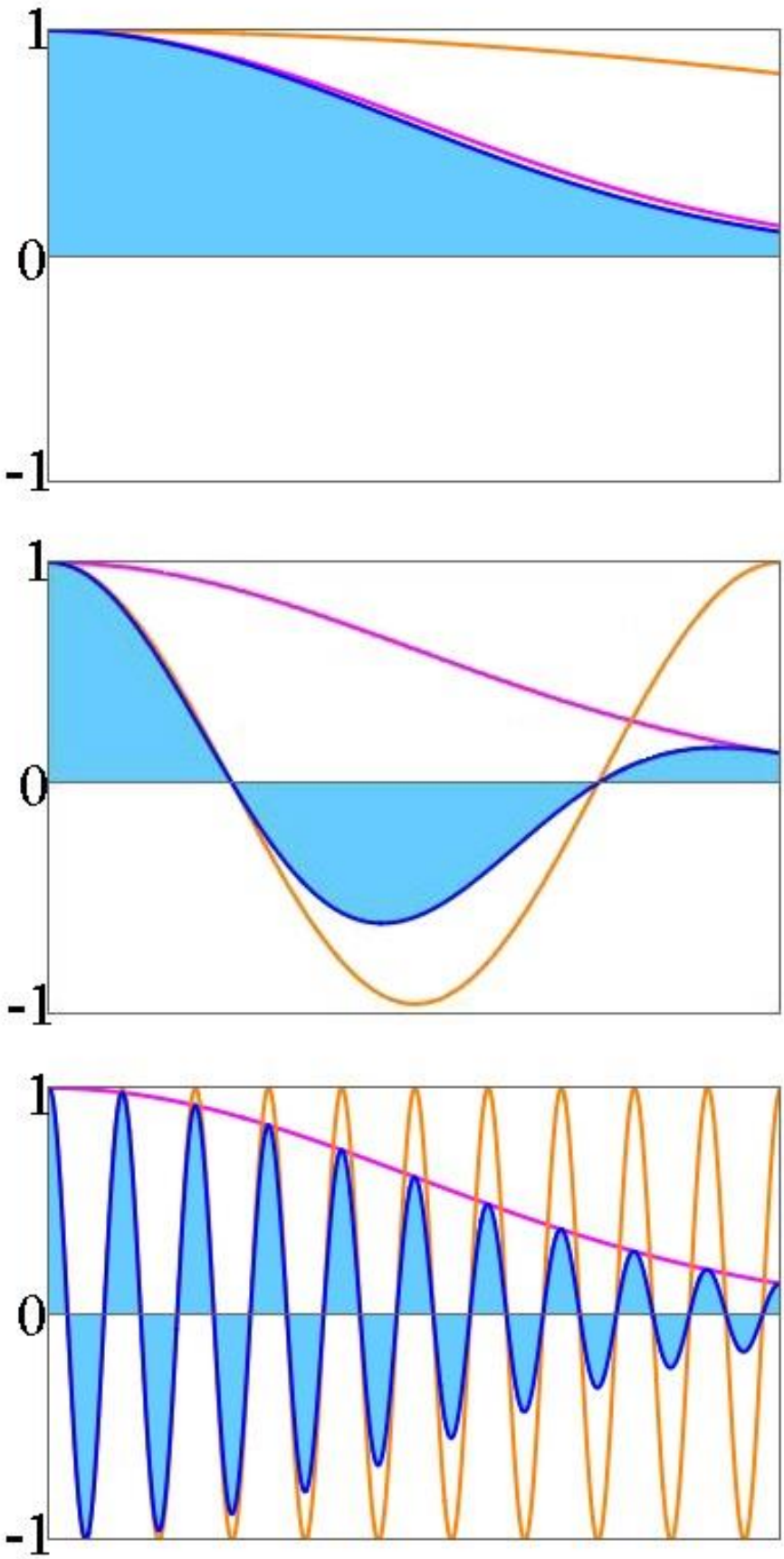

Fig. 2.5. The elastic incoherent neutron scattering evaluated through eqn. 2.36, considering the product of a fixed intermediate scattering function $I_{inc}(Q,t)$, a fixed resolution function $R(Q,t)$ at three different values of the $\cos \omega t$: $\omega t = 2\pi \cdot 0.1$, $\omega t = 2\pi$, $\omega t = 2\pi \cdot 10$.

2.5 RENS

In order to evaluate the behaviour of EINS vs temperature and of RENS vs instrumental energy resolution, we have numerically performed the expected experimental outputs, namely the measured elastic scattering function as a function of temperature and as a function of the instrumental energy resolution. On this purpose we have evaluated $S_R{}^M(Q)$ in the case in which the scattering law $S_{inc}(Q,\omega)$ is a Lorentzian curve, as for example it occurs for a simple Brownian translational diffusion process, and consequently the intermediate scattering function $I_{inc}(Q,t)$ is an exponential function with a fixed linewidth (see dashed-dotted green curve in fig. 2.6) for three values of the resolution function linewidth (see the dashed blue curve in fig 2.6). In the same figure in magenta the $I_{inc}(Q,t)\cdot R(Q,t)$ product is reported. In particular, in order to numerically evaluate the RENS response function we have taken into account an increasing instrumental resolution function linewidth $\Delta\omega_{RES}$ and then we have applied eqn. 2.37 for determining the value of the definite integral as a function of $\Delta\omega_{RES}$.

Figure 2.7 shows the result of such a calculation, i.e. $S_R{}^M$ as a function of temperature and of logarithm of the instrumental resolution. As it can be seen it shows in both the case a sigmoid trend. In the case of RENS the elastically scattered intensity is an increasing as a function of the logarithm of $\Delta\omega_{RES}$ with an inflection point which occurs when the linewidth of the resolution function approaches the linewidth of the system scattering law; in other words the inflection point occurs when the instrumental resolution time crosses the system relaxation time. Such results show the operating way of the EINS versus temperature and RENS versus instrumental energy resolution approach: from the inflection point of EINS profiles versus temperature and versus the logarithm of the energy resolution one can extract the system relaxation time. In fact, in a complementary way, for a given fixed instrumental energy resolution function, from EINS profiles versus temperature one is able to obtain, from the inflection point, the temperature value for which the system relaxation time equals the resolution time.

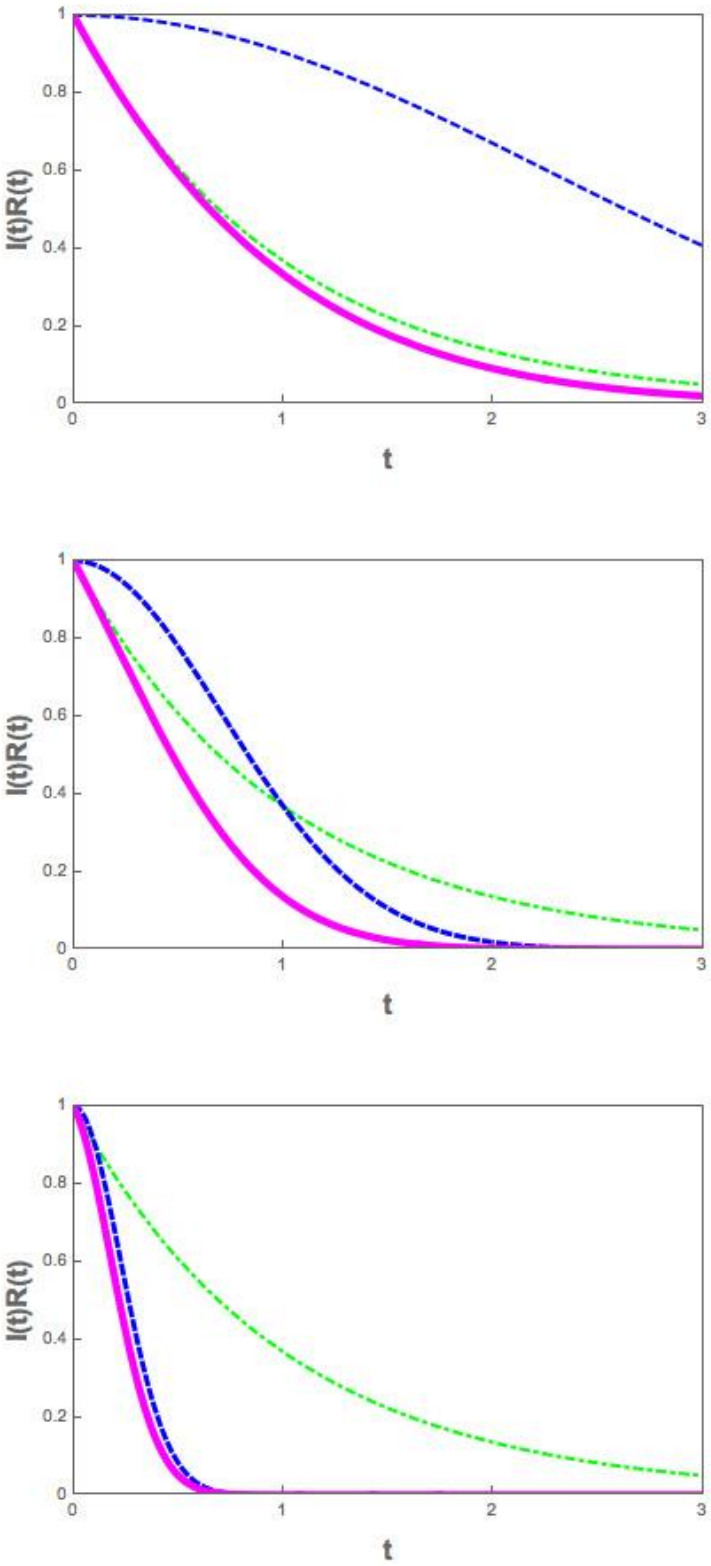

Fig 2.6: $S_R{}^M(Q)$ evaluated in the case in which the intermediate scattering function $I_{inc}(Q,t)$ is an exponential with a fixed linewidth for three linewidths of a Gaussian resolution function.

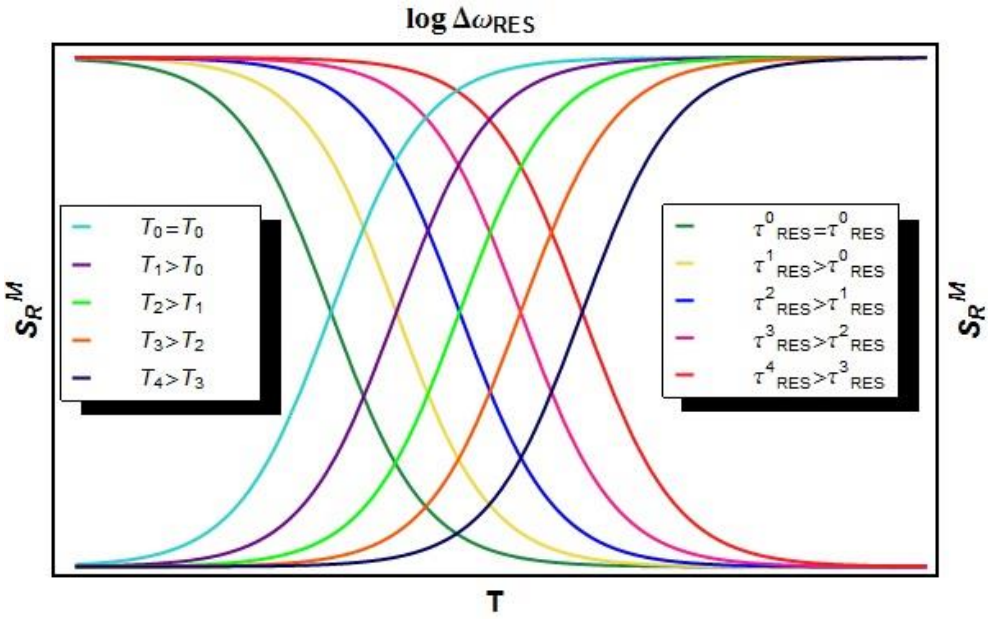

Fig 2.7. Measured elastic scattering law $S_R{}^M(T, \omega = 0, \Delta\omega_{RES})$ vs. log $\Delta\omega_{RES}$ for different temperature values (left side); an inflection point occurs at the instrumental energy resolution value which corresponds to the system relaxation time. Measured elastic scattering law $S_R{}^M$ vs. T for different instrumental energy resolution values (right side); an inflection point occurs at a temperature value for which $\tau=\tau_{RES}$

In table 2.1 the values of incoming wavelength, instrumental energy resolution value for the elastic peak and geometry for different spectrometers of different neutron scattering international large scale facilities are reported.

Spectrometer	Instrumental energy resolution (μeV)	Incoming wavelength (Å)	Geometry
IN6@ILL	1	6.30	Backscattering
IN13@ILL	8	2.23	Backscattering
IN10@ILL	1	6.30	Backscattering
IN6@ILL	170 120 70 50	4.1 4.6 5.1 5.9	Time of Flight
IN5@ILL	≈10 ÷ 6000 100	1.8 ÷ 20 (e.g. 5 with 8500 rpm)	Time of Flight
HFBS@NIST	0.9	6.2	Backscattering
DSC@NIST	≈ 10 ÷ 1000 50	2.3 ÷ 10 (e.g. 5 with 20000 rpm)	Time of Flight
IRIS@ISIS	1 11 17.5 54.4	Mica 002 Mica 006 PG 002 PG 004	Backscattering
SPHERES@JCNS	0.66	6.2	Backscattering
TOFTOF@JCNS	5 ÷ 5000	1.5 ÷ 16	Time of Flight
MARS@PSI	1		Backscattering
FOCUS@PSI	≈ 7 ÷ 1000 26	≈ 2 ÷ 16 (e.g. 11)	Time of Flight

Table 2.1: Instrumental energy resolution values, incoming wavelengths and instrument geometries for different spectrometers at different neutron large scale facilities.

Chapter 3

Mean Square Displacement (MSD)

3.1 Brownian motion

Brownian motion is stochastic motion of small particles suspended in a solution. The molecules (for example water molecules) constituting the fluid constantly hit the immersed objects which results in chaotic and non-directed motions. Atomic displacement does not follow a simple trajectory: "collisions" with other atoms render atomic trajectories quite complex shaped in space.

The trajectory followed by an atom in a liquid resembles that of a pedestrian random walk. Mathematically this represents a sequence of steps done one after another where each step follows a random direction which does not depend on the one of the previous step (Markov's chain of events).

In the case of a one-dimensional system (straight line) the displacement of the atom will therefore be either a forward step (+) or a backward step (-). Furthermore it will be impossible to predict one or the other direction (forward or backward) since they have an equal probability to occur [26].

One can conclude that the distance an atom may travel is close to zero. Nevertheless if we choose not to sum the displacements themselves (+/-) but the square of these displacements then we will end up with a non-zero, positive quantity of the total squared distance traveled.

Consequently this allows to obtain a better evaluation of the real (square) distance traveled by an atom.

These movements can be measured by the mean square displacement (MSD) and the lag time Δt and is characterized by the diffusion coefficient D which is a measure of the speed of diffusion. For three-dimensional brownian motions these terms can be put into an equation as follows

$$\langle r^2 \rangle = 6 \cdot D \cdot \Delta t \tag{3.1}$$

This is only true for isotropic and unrestricted translational diffusion. Brownian motion is actually observed for many different dynamical phenomena. Here we concentrate on isotropic translational displacements (random walk) but brownian motion can be also of rotational, undulating etc. nature. Translational diffusion or random walk in three dimensions can mathematically be described by a differential equation:

$$\frac{\partial \rho \vec{r}}{\partial t} = D \cdot \Delta \rho \vec{r} \tag{3.2}$$

Where $\rho \vec{r}$ is the particle location distribution and Δ is the Laplace-Operator which is a second order differential operator.

In 1905, Einstein published a paper that predicted a relationship between the mean squared magnitude of Brownian excursions and the size of molecules [27-28]. Now all that remained was to do the experiment. Jean Perrin won the Nobel Prize in 1926 for his work confirming Einstein's hypothesis. Since then, a thorough understanding of Brownian motion has become essential for diverse fields are ranging from polymer physics to biophysics, aerodynamics to statistical mechanics, and even stock option pricing.

Albert Einstein has calculated the diffusion coefficient to for a spherical particle

$$D = \frac{k_B T}{3 \cdot \pi \cdot \eta \cdot d} \tag{3.3}$$

where k_B is the Boltzmann constant, *T* the temperature, η the viscosity of the medium and *d* the diameter of the diffusing particle. The given relation among diffusion coefficient, temperature, viscosity and particle size is only true for isotropic, non-hindered diffusion of a spherical particle. The diffusion coefficient therefore gives us information about the temperature and viscosity of the system and size and shape of the diffusing particle.

For two and one dimensions the time dependence of mean square displacements for isotropic diffusion differs only in the numerical factor:

2D space: $\langle r^2 \rangle = 4 \cdot D \cdot \Delta t$

1D space: $\langle r^2 \rangle = 2 \cdot D \cdot \Delta t$

The diffusion coefficient does not depend on the dimensions in which the diffusion takes place. Hindered or restricted diffusion is, for example, the case where the particle has to

diffuse in a porous or structured environment as in cells. Anisotropic diffusion takes place in cases when the particle itself has an asymmetric shape. Then the diffusion coefficient is no simple scalar like in eq.3.3 anymore but becomes a complex tensor.

Consequently this allows to obtain a better evaluation of the real (square) distance traveled by an atom.

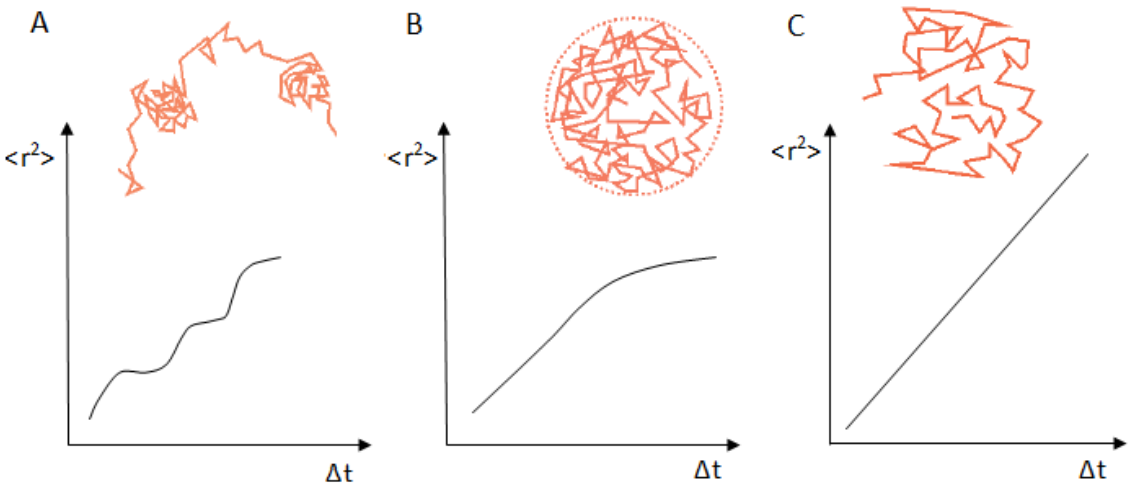

Fig 3.1. Different types of random walk and their corresponding MSD plot. From left to right: (A) partially confined random walk (hopping); (B) confined random walk; (C) isotropic random walk.

3.2 Definition

We can define the **M**ean **S**quare **D**isplacement as follow:

$$\text{MSD}\ (t) = \langle r^2(t) \rangle = \langle |r_i(t) - r_i(0)|^2 \rangle \tag{3.4}$$

where $r_i(t)$ is the position of the atom *i* at the time *t*, and the $\langle\ \rangle$ represent an average on the time steps and/or the particles [29].

However, during the analysis of the results of molecular dynamics simulations it is important to subtract the drift of the center of mass of the simulation box:

$$\text{MSD}\ (t) = \langle r^2(t) \rangle = \langle |r_i(t) - r_i(0) - [r_{cm}(t) - r_{cm}(0)]|^2 \rangle \tag{3.5}$$

where $r_{cm}(t)$ represents the position of the center of mass of the system at the time *t*.

3.3 Self-Distribution Function Procedure

The SDF procedure allows the evaluation of both the total and the partial MSDs through the total and the partial SDFs. In particular, it has been shown that the MSD is not the simple sum of the different partial displacement contributions, but it is the weighed sum of the partial MSDs in which the weights are obtained by a fitting procedure of measured EINS intensity data.[31,37] The results of such a procedure have been compared with other approaches, relative to a spatial analysis, reported in the literature.[54-56] Starting from the fact that in the ω-space the experimentally accessible quantity, the measured scattering law $S_R(Q,\omega)$, is the convolution of the scattering law with the instrumental resolution function, it is important to clarify how the measured intensity depends on the instrumental resolution.[31-37]

Several contributions reported in the literature [57-60] deal with the effects of the instrumental energy resolution on the measured MSD obtained by EINS data. In particular, Gabel and Bellissent-Funel [57] have realized a dynamical analysis on C-PhycoCyanin (CPC) in the presence of trehalose starting from the EINS intensity profiles collected with different energy resolutions. In their approach, the analysis of the effects of the instrumental resolution is performed on elastic scattering data and shows the presence of a quasi elastic contribution in the elastic measured spectra related to non-Gaussian hydration water motions at temperatures higher than 235 K.

Moreover, Kneller and Calandrini [58] have estimated the influence of the finite instrumental resolution on the elastic intensity for a protein system starting from the assumption that, as far as the internal protein dynamics is concerned, the single particle motions can be described by fractional Ornstein-Uhlenbeck processes. This study has allowed the evaluation of the missing part of the quasi elastic intensity profile, which is not accessible because of the finite instrumental resolution. The authors also furnished an estimation of the attenuation factor for the observed atomic position fluctuations both assuming a Gaussian and a triangular resolution function; as a result, when the quasi elastic neutron scattering (QENS) half width at halfmaximum increases to a relatively high value, in the lowfrequency region, the measured spectrum differs more and more in respect to the ideal one. Finally, Becker and Smith [15] have investigated the effects of the energy resolution and of dynamical heterogeneities on EINS spectra for some

molecular systems. They considered the convolution of a given QENS scattering law with the instrumental resolution function (a rectangular function). The MSD has then been calculated by evaluating the second derivative of the measured scattering function; this latter consists of two contributions: the first one is connected both to the vibrational and to the elastic incoherent structure factor contributions, while the second one is connected with resolution effects.

The SDF procedure is essentially based on the determination of the self-distribution function and on its use in the evaluation of the average statistical values of the physical quantity of interest ⟨A⟩ defines as follows [30-36]:

$$\langle A \rangle = \int_{-\infty}^{\infty} A(\vec{\mathrm{r}}) G^{self}(\vec{\mathrm{r}}) d\vec{\mathrm{r}} \tag{3.6}$$

in which the spatial self-distribution function, as a probability density, may be normalized to unit

$$\int_{-\infty}^{\infty} G^{self}(\vec{\mathrm{r}}) d\vec{\mathrm{r}} = 1 \tag{3.7}$$

In the specific case of the MSD evaluation, the dynamic observable *A* corresponds to the second power of the displacement, $\vec{\mathrm{r}}^2$

$$\langle \vec{\mathrm{r}}^2 \rangle = \int_{-\infty}^{\infty} \vec{\mathrm{r}}^2 G^{self}(\vec{\mathrm{r}}) d\vec{\mathrm{r}} \tag{3.8}$$

In the case in which the system can be considered isotropic, the volume integral becomes dependent only on the scalar *r*. In such a case, the normalization condition and the MSD become

$$\int_{-\infty}^{\infty} 4\pi r^2 G^{self}(r) dr = 1 \tag{3.9}$$

$$\langle \vec{r}^2 \rangle = \int_{-\infty}^{\infty} r^2 [4\pi r^2 G^{self}(r)] dr \tag{3.10}$$

Considering that the self-distribution function can be written as a sum of Gaussian functions [31,32], the normalization condition gives the following result [37,38]:

$$G^{self}(r) = \sum_n A_n \, G^{self}(r) = \sum_n \frac{A_n}{16(\pi a_n)^{3/2}} exp(-r^2/4a_n) \tag{3.11}$$

in which $\sum_n A_n = 1$;
in addition, the MSD results:

$$\langle \vec{r}^2 \rangle = 6 \sum_n A_n \, a_n = \sum_n A_n \langle \vec{r}^2 \rangle_n \tag{3.12}$$

in which are present the partial MSDs. This formula highlights that the MSD corresponds to a weighted sum of the different displacement contributions present in the system.
$\langle \vec{r}^2 \rangle$ represents the MSD in 3D space; if $\langle r^2 \rangle$ represents the MSD in 1D space, for isotropic systems, we have that

$$\langle r^2 \rangle = 1/3 \, \langle \vec{r}^2 \rangle \tag{3.13}$$

This implies that eq 3.12 in 1D yields

$$\langle r^2 \rangle = 2 \sum_n A_n \, a_n = \sum_n A_n \langle r^2 \rangle_n \tag{3.14}$$

The same result for the MSD in 1D space can be obtained considering directly the scalar expression of eq 3.8, that is, the scalar expression of the average statistical values of the displacement, $\vec{r}^2$

$$\langle r^2 \rangle = \int_{-\infty}^{\infty} r^2 G^{self}(r) dr \tag{3.15}$$

In this case, the normalization condition changes and gives the following result:

$$\int_{-\infty}^{\infty} G^{self}(r)dr = 1 \tag{3.16}$$

$$G^{self}(r) = \sum_n A_n\, G^{self}(r) = \sum_n \frac{A_n}{2(\pi a_n)^{1/2}} exp(-r^2/4a_n) \tag{3.17}$$

in which $\sum_n A_n = 1$. The MSD results

$$\langle r^2 \rangle = 2\sum_n A_n\, a_n = \sum_n A_n \langle r^2 \rangle_n \tag{3.18}$$

This result is the same as that of eq 3.14, which was obtained from eqs 3.12 and 3.13.
To adapt the previous definition of the MSD to the case of the EINS experiments, it is necessary to consider that the instrumental energy resolution influences the physical observables; therefore, eq 3.15 can be rewritten as follows:

$$\langle r^2 \rangle_R = \int_{-\infty}^{\infty} r^2 G^{self}(r)dr \tag{3.19}$$

Starting from this relation in the following, we shall analyze the instrumental energy resolution effects on the MSD in the frame of an EINS experiment.

It is possible now to obtain the partial MSD values:

$$\langle r^2 \rangle_n = \int_{-\infty}^{\infty} r^2 G_n^{self}(r)dr = 2a_n \tag{3.20}$$

the exponent of each Gaussian being the MSD relative to a particular r-domain and the weight An being interpretable as the relative percentage weight. Therefore this procedure allows to obtain the autocorrelation function $G^{self}(r,t)$ versus r, together with its different partial contributions, as well to determine the partial MSDs, their weights and the total MSD.

3.4 MSD in translational motions

We shall consider two types of MSD:
1) the "system MSD" (i.e., $\langle\langle \vec{r}^2 \rangle(t)\rangle$)

2) the "measured MSD" (i.e., $\langle \vec{r}^2 \rangle_R$).

The first one is a function of time whereas the second one is the MSD value as obtained by EINS that is a pure number and not a function of time.

Infact, remembering eq. 3.19, we can consider two procedures for MSD evaluation.

- the first one is based on the following equation:

$$= \int_{-\infty}^{\infty} FT_r\{I_R(Q,t)\} r^2 dr \tag{3.21}$$

Starting from the equation:

$$S_R(Q,\omega) = S(Q,\omega) \otimes R(\omega) = \int_{-\infty}^{\infty} S(Q,\omega-\omega')R(\omega')d\omega' \tag{3.22}$$

that, taking into account eq. 2.1, yields:

$$S_R(Q,\omega) = \left[\frac{1}{\sqrt{2\pi}}\int_{-\infty}^{\infty} I(Q,t)e^{-i\omega t}dt\right] \otimes R(\omega) =$$
$$= \frac{1}{\sqrt{2\pi}}\int_{-\infty}^{\infty} I(Q,t)e^{-i(\omega-\omega')t}dt\, R(\omega')d\omega' =$$
$$= \int_{-\infty}^{\infty} I(Q,t)e^{-i\omega t}dt\left[\frac{1}{\sqrt{2\pi}}\int_{-\infty}^{\infty} e^{i\omega' t}\, R(\omega')d\omega'\right] =$$
$$= \int_{-\infty}^{\infty} I(Q,t)R(t)e^{-i\omega t}dt \tag{3.23}$$

Considering that:

$$S_R(Q,\omega) = \int_{-\infty}^{\infty} I(Q,t)R(t)e^{-i\omega t}dt = FT_t\left\{\sqrt{2\pi} I(Q,t)R(t)\right\}$$
$$\frac{1}{\sqrt{2\pi}} FT_t\{\, S_R(Q,\omega)\} = I(Q,t)R(t)$$
$$\tfrac{1}{\sqrt{2\pi}} I_R(Q,t) = I(Q,t)R(t) \tag{3.24}$$

Now, eq. 3.21 becomes:

$$\langle \vec{r}^2 \rangle_R = \int_{-\infty}^{\infty} FT_r\{I_R(Q,t)\} r^2 dr =$$
$$= \sqrt{2\pi}\int_{-\infty}^{\infty} FT_r\{I(Q,t)R(t)\} r^2 dr =$$
$$= \sqrt{2\pi}\int_{-\infty}^{\infty} G^{self}(r,t)R(t) r^2 dr =$$
$$= \sqrt{2\pi} R(t)\langle r^2 \rangle(t) \tag{3.25}$$

so leads to the following conclusion:

$$\langle \vec{r}^2 \rangle_R(t) = \sqrt{2\pi} R(t) \langle r^2 \rangle(t) \tag{3.26}$$

The MSD obtained by this procedure is a function of time.

- The second one is based on the following method:

$$\mathrm{F_r}\{\mathrm{S_R}(\mathrm{Q}, \omega = 0)\} = \int_{-\infty}^{\infty} \mathrm{G(r,t)R(t)dt} \tag{3.27}$$

by referring to the MSD definition:

$$\langle \mathrm{r}^2 \rangle(\mathrm{t}) = \int_{-\infty}^{\infty} \mathrm{G(r,t)r^2 dr} \tag{3.28}$$

in eq. 3.27 apply the integral and multiply by r^2 both terms, we have:

$$\int_{-\infty}^{\infty} FT_r\{S_R(Q, \omega = 0)\} r^2 dr = \int_{-\infty}^{\infty} r^2 dr \int_{-\infty}^{\infty} G(r,t) R(t) dt =$$

$$= \int_{-\infty}^{\infty} R(t) dt \int_{-\infty}^{\infty} G(r,t) r^2 dr = \int_{-\infty}^{\infty} R(t) dt \langle \vec{r}^2(t) \rangle = \langle \vec{\boldsymbol{r}}^{\boldsymbol{2}} \rangle_R \tag{3.29}$$

So we conclude:

$$\langle \vec{r}^2 \rangle_R = \int_{-\infty}^{\infty} \langle \vec{r}^2 \rangle(t) R(t) dt \tag{3.30}$$

The MSD obtained by this procedure is a number. From this equation the measured MSD corresponds to the integration in the time domain of the product of the system MSD times the resolution function.

The connection between the two MSD is:

$$\langle \vec{r}^2 \rangle_R = \frac{1}{\sqrt{2\pi}} \int_{-\infty}^{\infty} \langle \vec{r}^2 \rangle_R(t) dt \tag{3.31}$$

Moreover, it depends on the employed instrumental resolution so, if its measurement is carried out with instruments having different instrumental resolution, in order to compare the data obtained their proper normalization is required.

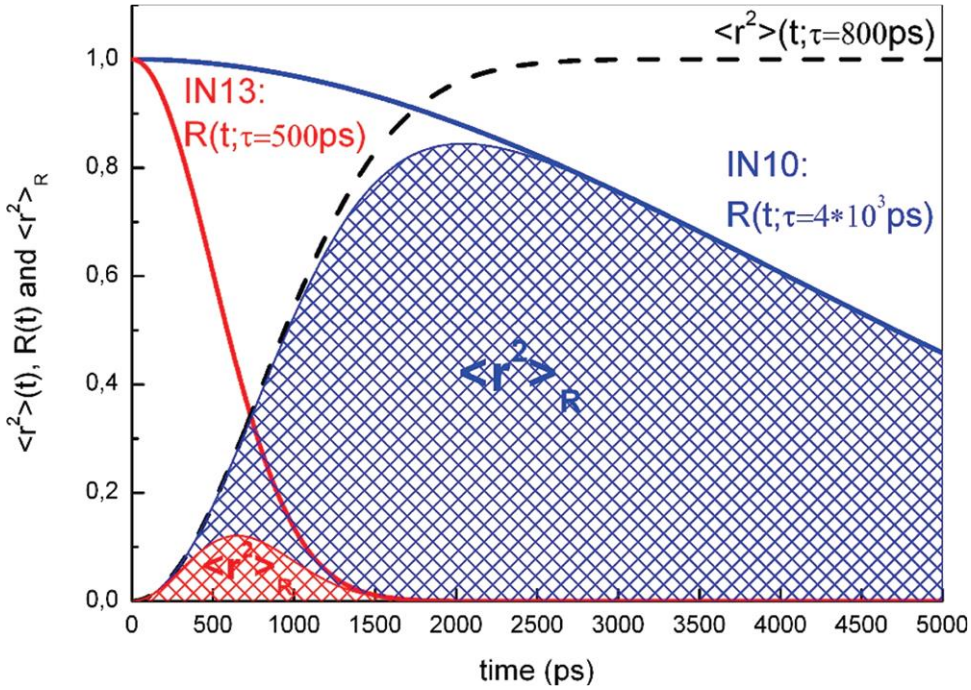

Fig 3.2. Normalized time behavior of the system MSD at a fixed τ value, $\langle \vec{r}^2 \rangle(t;\tau)$ (in black); resolution function for different τ_{RES} values, $R(t;\tau_{IN13})$ (in red) and $R(t;\tau_{IN10})$ (in blue); measured MSD $\langle r^2 \rangle_R$ evaluated by eq 3.30.

Figure 3.2 shows the effect on the measured MSD because of employing the resolution function; as it can be seen, at the same system MSD, because of the different employed energy resolutions, different measured MSDs correspond.

Chapter 4

Investigated systems and methods

4.1 Proteins and their structures

Proteins are the largest and most varied class of biological molecules, and they show the greatest variety of structures. The function of proteins depends on their structure, and defining the structure of individual proteins is a large part of modern Biochemistry and Molecular Biology.

To make a protein, amino acids are connected together by a type of amide bond called a "peptide bond". This bond is formed between the alpha amino group of one amino acid and the carboxyl group of another in a condensation reaction. When two amino acids join, the result is called a dipeptide, three gives a tripeptide, etc. Multiple amino acids result in a polypeptide (often shortened to "peptide"). Because water is lost in the course of creating the peptide bond, individual amino acids are referred to as "amino acid residues" once they are incorporated. Another property of peptides is polarity: the two ends are different. One end has a free amino group (called the "N-terminal") and the other has a free carboxyl group ("C-terminal") [43,45].

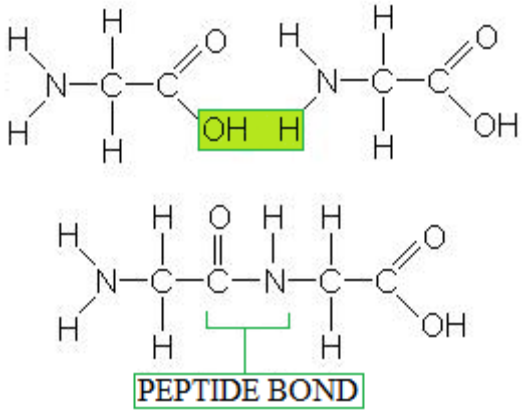

Fig 4.1 A molecule of water is removed from two glycine amido acids to form a peptide bond

In the natural course of making a protein, polypeptides are elongated by the addition of amino acids to the C-terminal end of the growing chain. Conventionally, peptides are written N-terminal first; therefore gly-ser is not the same as ser-gly or GS is not the same as SG. The connection gives rise to a repeating pattern of "NCC-NCC-NCC…" atoms along the length

of the molecule [48]. This is referred to as the "backbone" of the peptide. If stretched out, the side chains of the individual residues project outwards from this backbone.

Below we will describe the protein structure in terms of four levels (primary to quaternary) of increasing complexity.

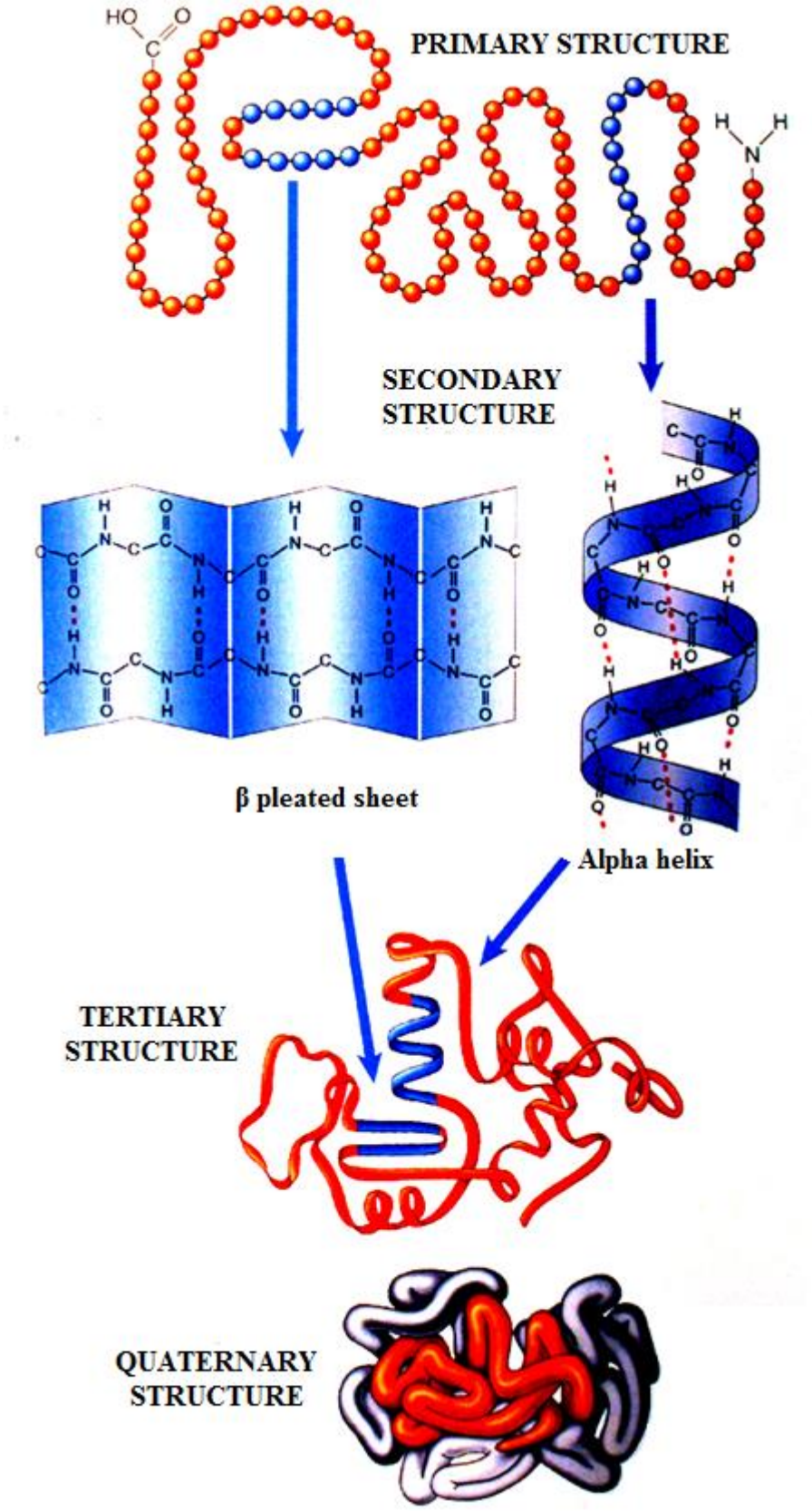

Fig 4.2. Protein structure, from primary to quaternary.

4.1.1 Primary Structure of Proteins

Primary structure is simply the sequence of residues making up the protein [43-47]. Thus primary structure involves only the covalent bonds linking residues together.

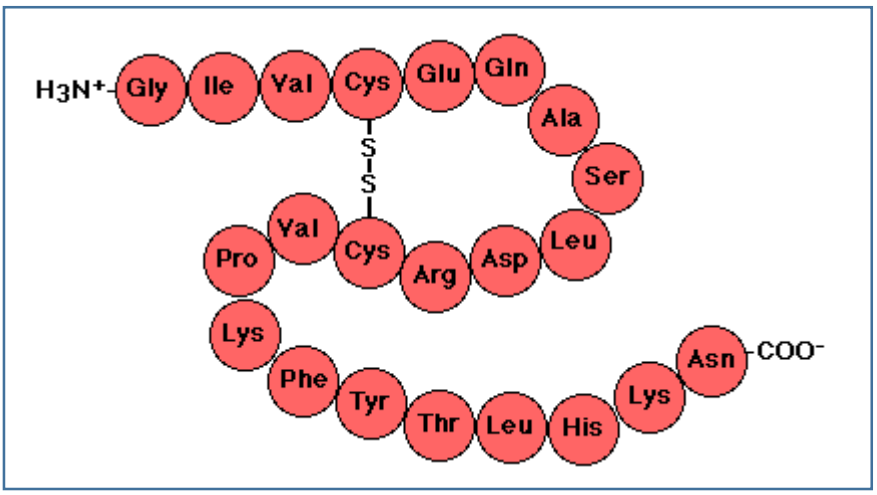

Fig 4.3 Primary structure of proteins

The minimum size of a protein is defined as about 50 residues; smaller chains are referred to simply as peptides. So the primary structure of a small protein would consist of a sequence of 50 or so residues. Even such small proteins contain hundreds of atoms and have molecular weights of over 5000 Daltons (Da).

4.1.2 Secondary Structure

This level of structure describes the local folding pattern of the polypeptide backbone and is stabilized by hydrogen bonds between N-H and C=O groups. Various types of secondary structure have been discovered, but by far the most common are the orderly repeating forms known as the a helix and the b sheet [43].

An a helix, as the name implies, is a helical arrangement of a single polypeptide chain, like a coiled spring. In this conformation, the carbonyl and N-H groups are oriented parallel to the axis. Each carbonyl is linked by a hydrogen bond to the N-H of a residue located 4 residues further on in the sequence within the same chain. All C=O and N-H groups are involved in hydrogen bonds, making a fairly rigid cylinder. The alpha helix has precise dimensions: 3.6 residues per turn, 0.54 nm per turn. The side chains project outward and contact any solvent, producing a structure something like a bottle brush or a round hair brush [44-47].

The structure of a b sheet is very different from the structure of an a helix. In a b sheet, the polypeptide chain folds back on itself so that polypeptide strands like side by side, and are held together by hydrogen bonds, forming a very rigid structure. Again, the polypeptide N-H and C=O groups form hydrogen bonds to stabilize the structure, but unlike the a helix, these bonds are formed between neighbouring polypeptide (b) strands. Generally the primary structure folds back on itself in either a parallel or antiparallel arrangement, producing a parallel or antiparallel b sheet. In this arrangement, side chains project alternately upward and downward from the sheet. The major constituent of silk (silk fibroin) consists mainly of layers of b sheet stacked on top of each another[45].

4.1.3 Tertiary Structure

This level of structure describes how regions of secondary structure fold together – that is, the 3D arrangement of a polypeptide chain, including a helices, b sheets, and any other loops and folds. Tertiary structure results from interactions between side chains, or between side chains and the polypeptide backbone, which are often distant in sequence. Every protein has a particular pattern of folding and these can be quite complex.

Whereas secondary structure is stabilized by H-bonding, all four "weak" forces contribute to tertiary structure. Usually, the most important force is hydrophobic interaction (or hydrophobic bonds) [44-47].

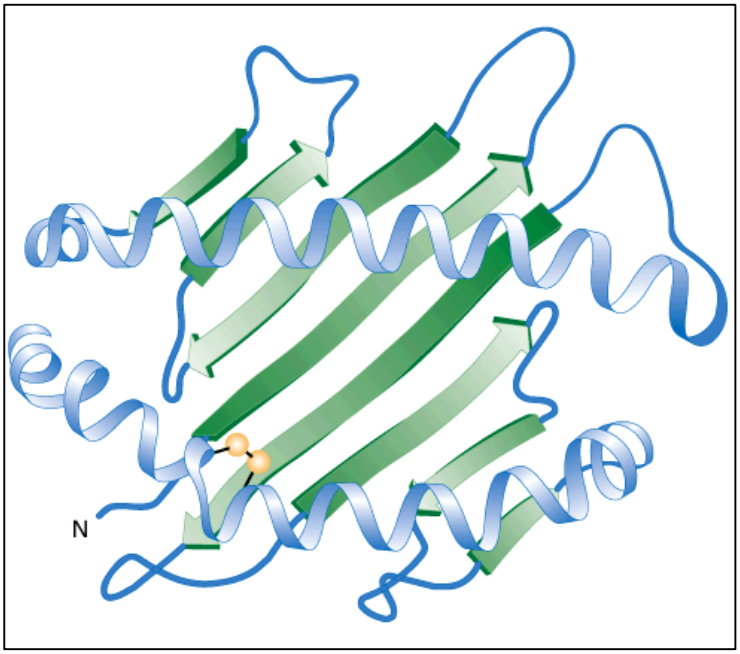

Fig 4.4. Tertiary structure of proteins

Other forces that contribute to tertiary structure are ionic bonds between side chains, hydrogen bonds, and van der Waals forces. These bonds are far weaker than covalent bonds, and it takes multiple interactions to stabilize a structure.

There is one covalent bond that is also involved in tertiary structure, and that is the disulfide bond that can form between cysteine residues. This bond is important only in non-cytoplasmic proteins since there are enzyme systems present in the cytoplasm to remove disulfide bonds.

4.2.4 Quaternary Structure

Some proteins are composed of more than one polypeptide chain. In such proteins, quaternary structure refers to the number and arrangement of the individual polypeptide chains. Each polypeptide is referred to as a subunit of the protein [48]. The same forces and bonds that create tertiary structure also hold subunits together in a stable complex to form the complete protein.

Individual chains may be identical, somewhat similar, or totally different. As examples, CAP protein is a dimer with two identical subunits, whereas hemoglobin is a tetramer containing two pairs of non-identical (but similar) subunits. It has 2 a subunits and 2 b subunits. Secreted proteins often have subunits that are held together by disulfide bonds. Examples include tetrameric antibody molecules that commonly have two larger subunits and two smaller subunits ("heavy chains" and "light chains") connected by disulfide bonds and noncovalent forces [54,57].

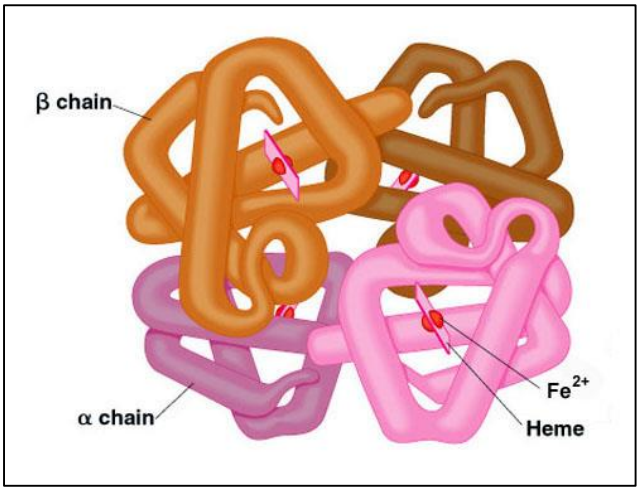

Fig 4.5 Quaternary structure of proteins

4.2 Lysozyme

The protein we have studied is Lysozyme.

Lysozyme is part of the innate immune systema possesses bacteriolytic able to hydrolyze peptidoglycan in the cell wall of the bacteria [41]. It is a natural enzyme, found in human tears, saliva, and other body fluids, secreted by epithelial cells, macrophages, astrocytes and microglia. In high concentration, about 3% from all proteins, Lysozyme is present in chicken egg-white[42].

In viruses (or bacteriophages), Lysozyme is used as an agent to break into the host bacterial cell. Lysozyme from the tail of the virus (or bacteriophage) destroys the peptidoglycan bacterial cell wall and then virus can injects its DNA. After multiplication in bacteria, many Lysozyme molecules are created to lyse the bacterial cell wall and release new viruses.

Lysozyme catalyzes the breakdown of certain carbohydrates found in the cell walls of certain bacteria (e.g., cocci). It thus functions, in the case of lacrimal fluid, to protect the cornea of the eye from infection [48].

Lysozyme retains both anti-oxidant and anti-inflammatory properties, and the level of lysozyme has been reported to be increased in Cerebrospinal fluid during inflammation.[40]

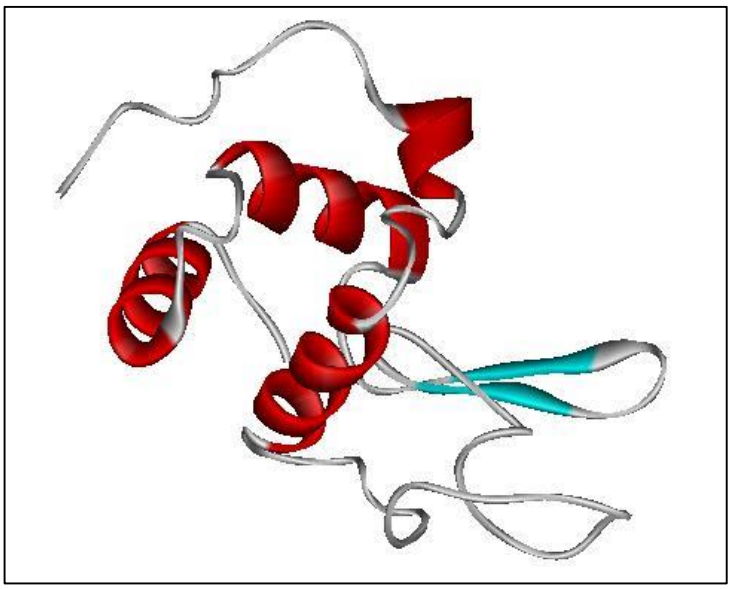

Fig 4.6 The main chain of lysozyme structure is represented in schematic view - solid ribbon representation. Alpha-helices are shown by red colour; beta-strands are coloured blue and irregular loops are shown by grey rope.

Historically, Lysozyme was discovered in 1922 by Alexander Fleming (Fleming A. (1922) On a remarkable becteriolytic element found in tissues and secretion. Proc Roy Soc Ser B, 93, 306-317.). This enzyme was discovered by accident, which was happen in the Fleming's lab. The nasal drippings were accidentally occurring in the petre dish with bacterial culture and these cells were lysed. This phenomenon was carefully investigated and the main acting enzyme was identified as Lysozyme.

Lysozyme is 129 aminoacid residues enzyme, hydrolase which catalyzes hydrolysis of 1,4-beta-linkages between N-acetylmuramic acid and N-acetyl-D-glucosamine residues in peptidoglycan and between N-acetyl-D-glucosamine residues in chitodextrins. Molecular weight of Lysozyme is an approximately 14.7 kDa. Alternative name for Lysozyme are 1,4-N-acetylmuramidase, L-7001, N,O-diacetylmuramidase, PR1-Lysozyme, Globulin G1, Globulin G, Lysozyme G, Mucopeptide N-acetylmuramoylhydrolase, Mucopeptide glucohydrolase and Muramidase[48].

In 1965 the structure of Lysozyme was solved by X-Ray analysis with 2 angstrom resolution by David Chilton Phillips. For many years Lysozyme was the best object for X-Ray analysis due to many unique properties of this enzyme. First of all Lysozyme is easy to purify from egg-white. Secondly, this protein is very easy to crystallize, which is not the case for most of the other proteins. This feature of Lysozyme is widely used for it purification. And finally, crystals of Lysozyme diffract X-Ray beam to a very high resolution, currently the highest resolution structure, presented in Protein Data Bank, was solved at resolution 0.94 Angstrom.

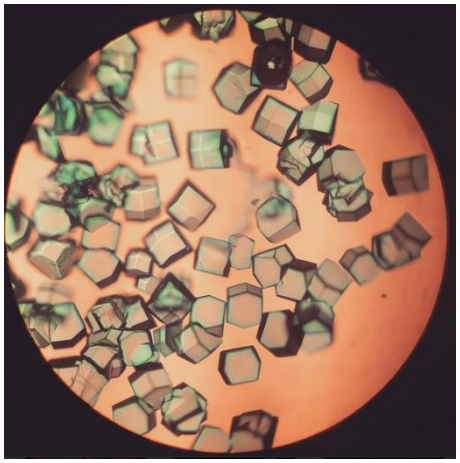

Fig. 4.7 Lysozyme crystals

Lysozyme belongs to the hydrolases enzymatic class. The hydrolases catalyze the hydrolysis or hydrolytic cleavage of a chemical bond by reaction:

A – B + H2O → A – OH + B – H.

This class of enzymes is usually classified by nature of the hydrolysed bond, then by chemical nature of the substrate, and finally by the enzyme. Despite systematic name for hydrolases always include hydrolase, the recommended name is formed by the name of the substrate with the suffix -ase.

Within the class of hydrolases, Lysozyme belongs to the Glycosylases family. Lysozyme reaction is the hydrolysis of the beta glycosidic bond between N-acetylglucosamine sugar (NAG) and N-acetylmuramic acid sugar (NAM) and therefore it is possible classify it as Glycosidases, i.e. enzymes hydrolyzing O- and S-glycosyl with number 17 in this group [49,50].

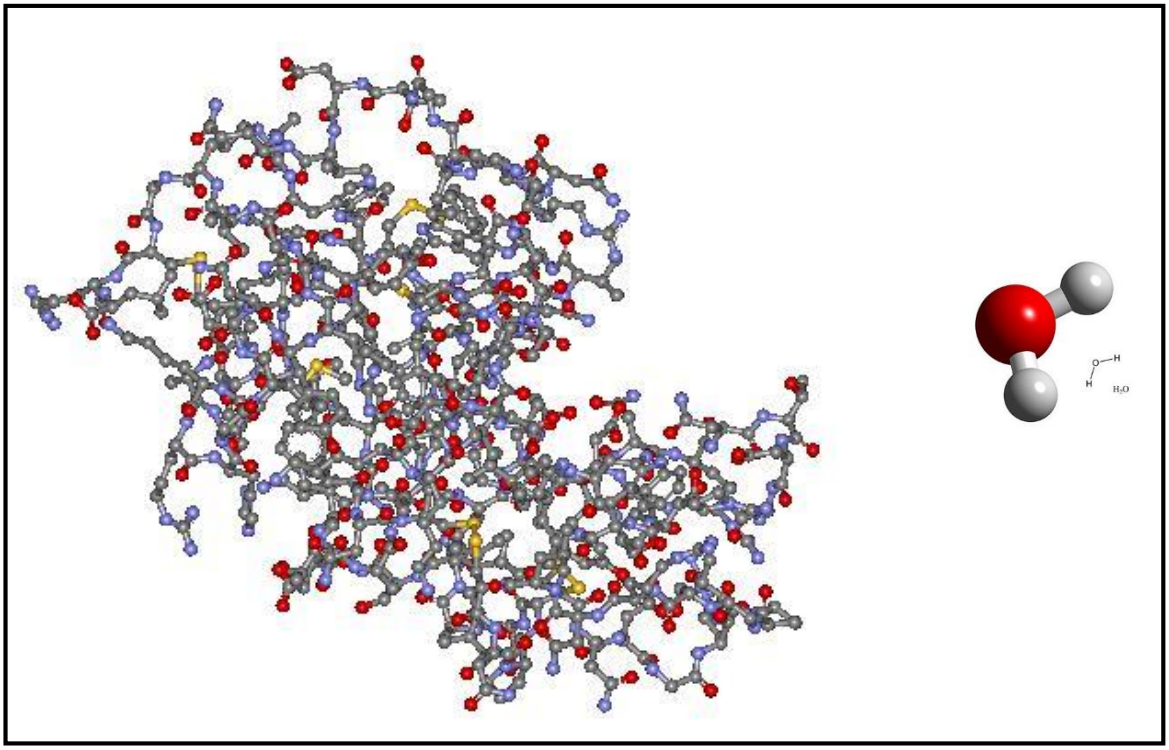

Fig. 4.8 Ball-and-stick representation of the lysozyme and a water molecule structure. In this view all protein atoms are shown as balls and bonds between atoms are shown as a stick. Carbon; nitrogen; oxygen and sulphur atoms are coloured grey; blue; red and yellow respectively.

We use lysozyme, a relatively small globular protein whose structure and function are well studied, so that we can focus on studying its dynamics and hydration effects.

The incoherent neutron scattering experiments are layers conducted on a dry lysozyme sample and on a lysozyme hydrate both in H_2O and in D_2O.

In experiments on a D_2O hydrate sample can provide information on protein dynamics since neutrons scattered by atomic nuclei are more sensitive to hydrogen atoms than deuterium and other atoms in proteins and hydrogen atoms reflect the motions of the side chains and backbone to which they are bound. In addition, we measured both H_2O hydrated sample and D_2O hydrated sample and took their difference to obtain the signal contributed solely from hydration water.

4.3 CHARACTERISTIC OF THE USED SPECTROMETERS

4.3.1 IN10

The **IN10** backscattering spectrometer is designed for inelastic or quasielastic scattering experiments requiring very high energy resolution and moderate momentum transfer resolution. IN10 owes its high energy resolution to the use of nearly perfect backscattering both at the monochromator and at the analyser crystals[51].

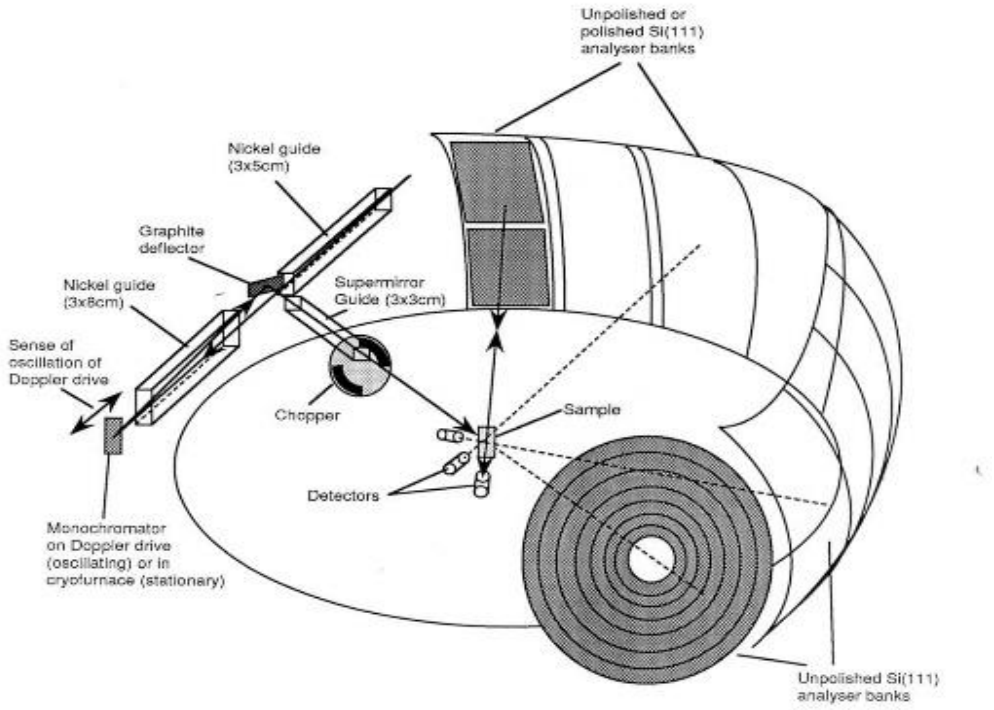

Fig. 4.9 ILL Spectrometer IN10 scheme

Is situated at the end of the curved nickel coated neutron guide H15 which views the vertical cold source of the ILL [2.24]. The cold neutron beam has a total flux of about 2.109 neutrons/cm2s with a spectral distribution around 6 Å. The width of the neutron guide is 3 cm, the height 20 cm. Only the upper 5 cm of the beam is used for IN10. The beam travels along a straight neutron guide section with 3 x 5 cm2cross-section and 10 meters length. It is followed by a further section with the same width, but 8 cm high and 6.3 meters long. The neutrons are backscattered from the monochromator which is mounted on the piston of a crank shaft velocity drive. The Bragg angle is 89.8°.

About 40% of the backscattered monochromatic beam is deflected off a (002) oriented graphite crystal (situated just above the incoming primary beam) into a third neutron guide (branching-off tube) of 3 x 3 cm2 and 4.25 m length. This guide has a supermirror coating in order to reduce transmission losses due to the increased divergency of the beam after the deflector. The deflector has an anisotropic mosaic distribution, i.e. ηvertical = 0.4°, ηhorizontal = 1.2°.

The neutrons then pass a chopper and a monitor, enter the analyser container and hit the sample. The scattered neutrons are analyzed for momentum and energy changes by analyser crystals. The analysers consist of single crystal wafers that are glued in the (111) or (311) orientation to the surface of spherically curved aluminum plates. These spherical segments have a radius of curvature of 1.5 m and are aligned so that neutrons backreflected from each one are focussed onto a 3He-detector located near the sample. Initially the analyser spheres where covered by small hexagonal single crystals of 1 cm diameter and 0.7 mm thickness (see Figures below). All analysers of IN10 were a few years ago changed by adopting a new technique to deform large Si-crystals which had been developed on IN16. Today the analysers consist of hexagonal silicon single crystal slices of 0.5 mm thickness and a diameter of 6 cm. Spectra with up to 8 different momentum transfers can be measured simultaneously. An additional set of seven circular analyzers centered around the forward transmitted beam covers the small angle region ($0.07 < Q < 0.3$ Å-1). The chopper has a duty cycle of 50% and provides the trigger signal for the electronic gate. Neutrons, scattered into the detector directly from the sample, are not counted.

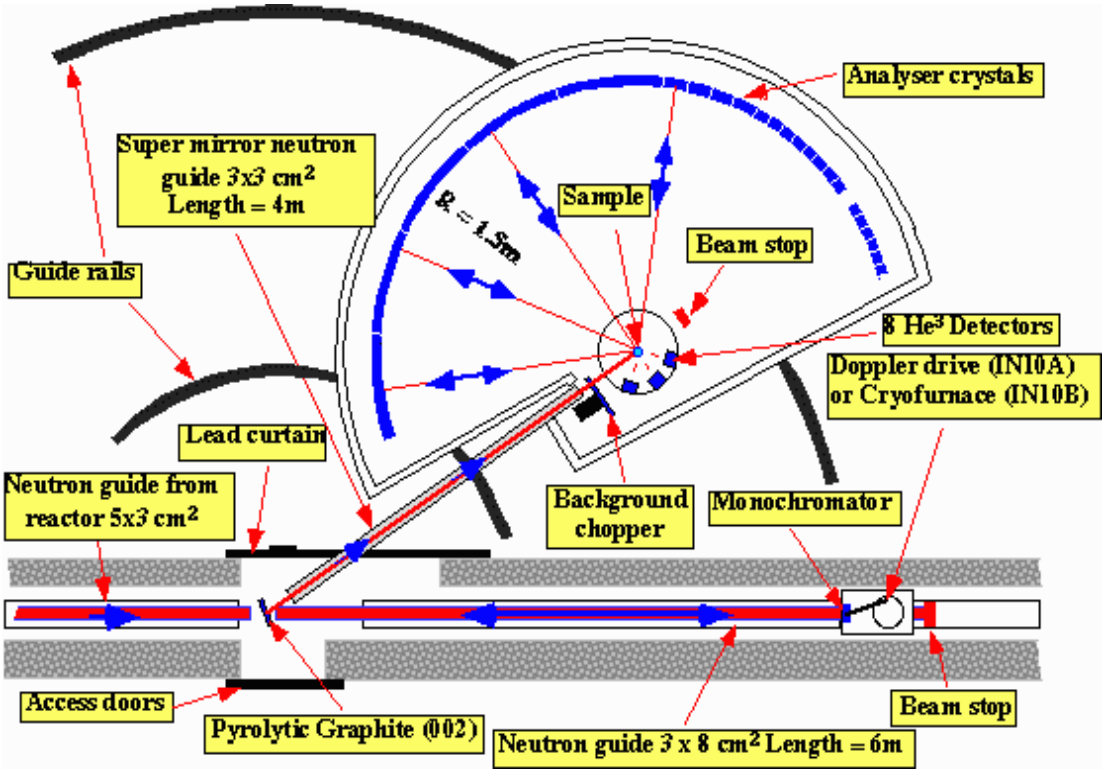

Fig. 4.10 Schematic drawing of the backscattering spectrometer IN10 for thermal neutrons at the HFR of the ILL in Grenoble.

The graphite crystal, the branching-off-guide and the analyser container with the chopper can be rotated around a vertical axis, defined by the crossover of the mid line of the main guide and the branching-off-guide, when the wavelength is changed.

The Doppler velocity of the monochromator is measured with an induction coil and a magnetic core, which is rigidly connected to the monochromator. It provides a voltage signal directly proportional to the velocity of the monochromator. The output voltage is amplified and digitalised. Together with the detector code it defines the channel number of the core storage into which the neutrons are sorted. (more information on data acquisition here)

The analyser container can be filled with Argon gas to reduce neutron losses and the background.

The flux at the sample position was 2*10**4 neutrons/s cm**2 with the unpolished monochromator. Beam size: 3*3 cm**2.

The instrument was commissioned in 1974. Subsequently, it became very popular and could until recently be considered as the first work horse in neutron backscattering

spectroscopy. The majority of publications until about 1995 (see references to chapter 4) is based on experiments performed on this machine [51].

Cold neutron backscattering has one drawback: the limitation in momentum transfer: $Q < 2Å^{-1}$ for 6 Å neutrons. Therefore the IN10 spectrometer has an additional set of Si(311) monochromator and analyzers crystals which permit to access Q values up to 3.8 $Å^{-1}$. This setup has been used with success to measure the elastic incoherent structure factor of adamantane [4.47]. The problem with this setup is however the low intensity. Therefore a dedicated backscattering spectrometer for *thermal* neutrons, IN13, was developed at the ILL and commissioned in 1980.

4.3.2 IN13

IN13 is installed at the thermal neutron guide H24 of the ILL with a total flux of 5.10^8 neutrons/cm^{2}s

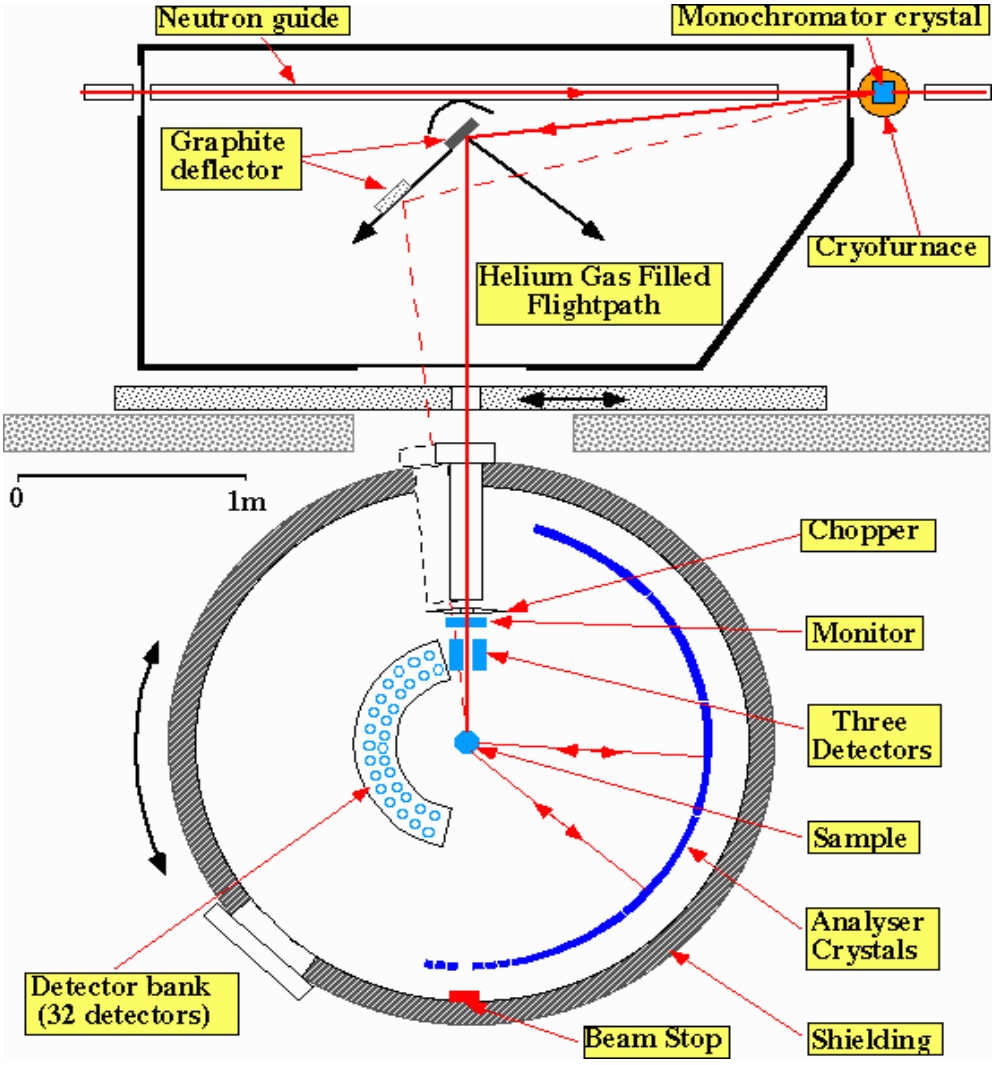

Fig. 4.11 Schematic drawing of the backscattering spectrometer IN13 for thermal neutrons at the HFR of the ILL in Grenoble.

CaF_2 crystals with orientation are used for the monochromator and analyzers yielding a final energy of 16.45 meV (λ = 2.23 Å) in backscattering [52]. The incident energy is scanned via thermal expansion of the monochromator crystals (13.5 cm high, 5 cm wide and 1 cm thick) which are mounted in a cryofurnace operating with liquid N_2 as coolant. The temperature of the monochromator can be scanned from 80 K to 720 K continuously

with a stability of 0.5 K yielding an energy transfer range from -125 μeV to 300 μeV. The analyser crystals are held at room temperature. The monochromator Bragg angle can be varied between 89° and 81° with a corresponding energy resolution of the spectrometer between 8 μeV and 24 μeV (FWHM). A vertically curved composite graphite crystal (9 lamella of 5 x 1.5 x 0.4 cm^3, mosaic spread 0.4°) focuses the beam onto the sample. The scattered neutrons are analyzed for energy and momentum transfer by a set of seven spherically curved composite crystal analyzers (60 cm high, 30 cm wide, radius of curvature 1 meter) with individual flat crystals of CaF_2 of 2 x 2 x 0.15 cm^3.

An additional set of three circular analyzers centered around the forward transmitted beam covers the small angle region ($0.15 < Q < 0.5$ $Å^{-1}$). A disk chopper with 4 windows and a duty cycle of 33% between the deflector and the sample is used to suppress the background of directly scattered neutrons and higher order contaminations [52]. The neutrons are counted with a cylindrically shaped polydetector consisting of 32 vertical ^3He detectors in two staggered rows and three end window individual 3He counters for the small angle analyzers.

Chapter 5

Result and discussion

5.1 Theoretical results

5.1.1 Gaussian Approximation for MSD evaluation

In the literature there are several works in which MSD is evaluated. However, the calculation is often carried out considering different ranges in Q (ie spatial) and different values of energy resolution (ie different resolution times). Furthermore, the data are often normalized so as not to make direct or even possible to compare the values obtained with different instruments or in different experimental conditions. So is important to examine the various possible procedures to perform data normalization and see which does not involve a change in the calculation of the mean square displacement [39].

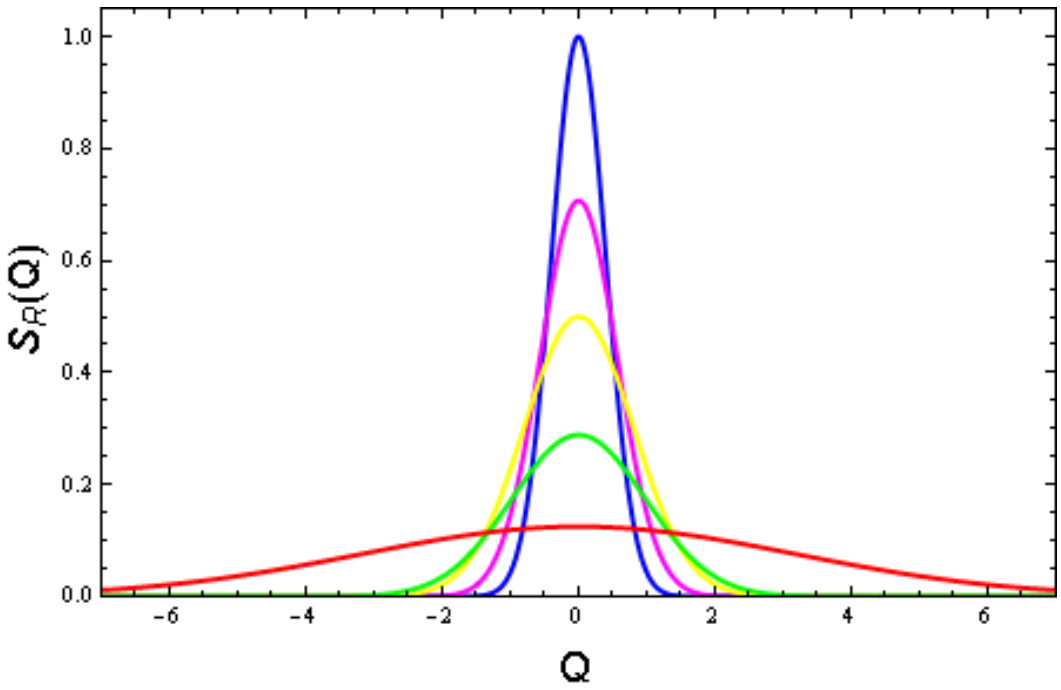

Fig. 5.1 Gaussian approximation of EINS data

We consider the function:

$$S_R = Ae^{-Q^2\langle r^2\rangle}$$

where A = 1 and $\langle r^2\rangle = 0.02$

Let's take into account how the different normalization procedures applied on S_R registered intensity affects the MSD evaluation.

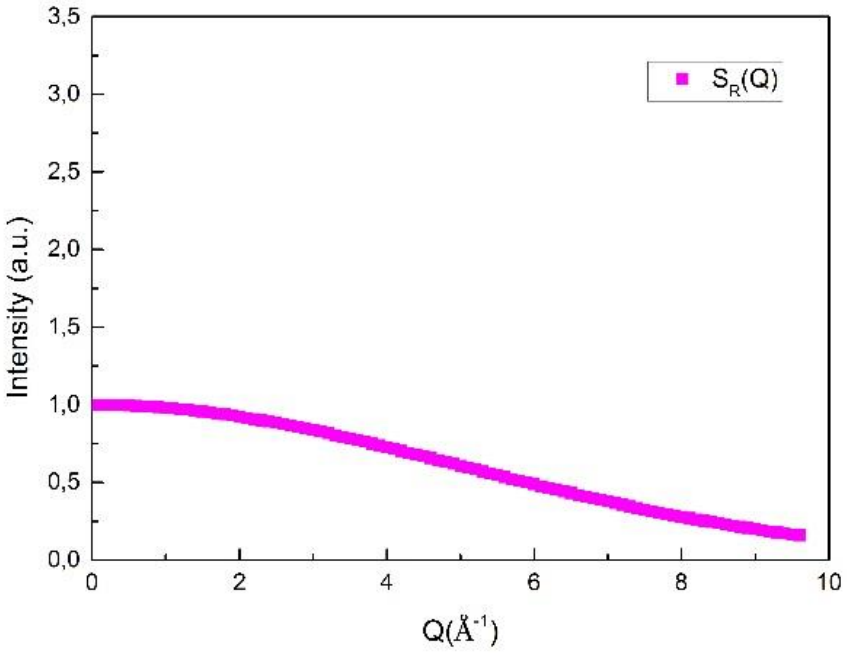

Fig. 5.2 Representation of the function S_R as a function of Q in a linear-linear plot

5.1.2 Data Normalization criteria

We show two different ways of dealing with the problem of data normalization: the first analyzing the Gaussian function and the second analyzing its logarithm

5.1.2.1 Normalization performed on the Gaussian function

5.1.2.1.1 Normalization by multiplication

For the MSD calculation, representing the function S_R as a function of Q in a linear-linear plot and performing a normalization multiplying it by the value n, one gets:

$$nS_R = ne^{-Q^2\langle u^2\rangle}$$
$$\langle r^2\rangle'_R = \langle r^2\rangle_R \qquad (5.1)$$

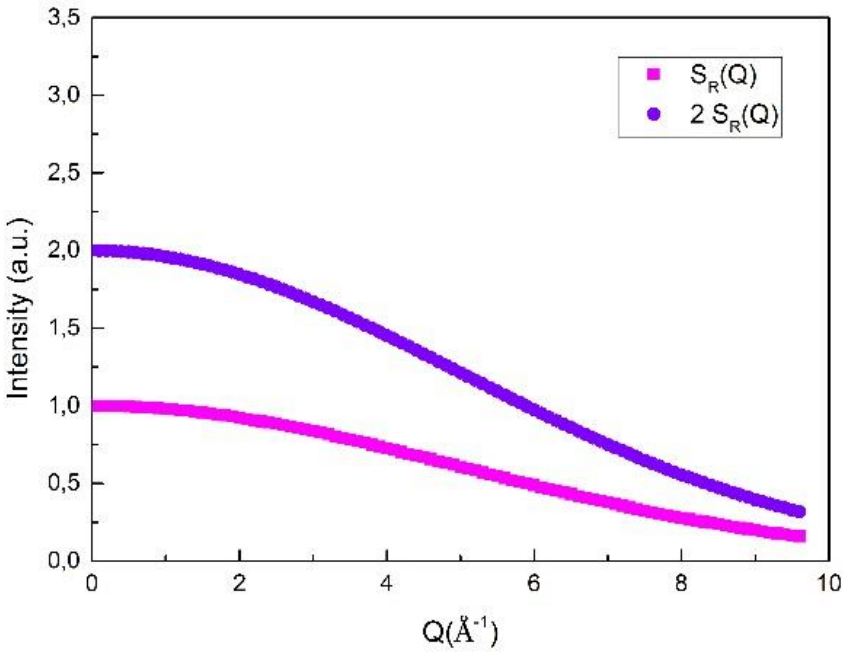

Fig. 5.3 In magenta representation of the function S_R as a function of Q; in violet representation of the function nS_R as a function of Q in a linear-linear plot

This transformation, therefore, can be used to achieve the same intensity value when, for example, spectra are collected with a different integration times and does not produce any change in the evaluation of the MSD

5.1.2.1.2 Normalization by sum

For the MSD calculation, representing the function S_R as a function of Q in a linear-linear plot and adding to it the value n_i, one gets:

$$S_R + n_i = e^{-Q^2\langle u^2\rangle} + n_i \tag{5.2}$$

$$\langle r^2\rangle'_R \approx \frac{\langle r^2\rangle_R}{1+2n}$$

This type of transformation involves, therefore, a change in the value of the MSD and, therefore, the procedure is not correct.

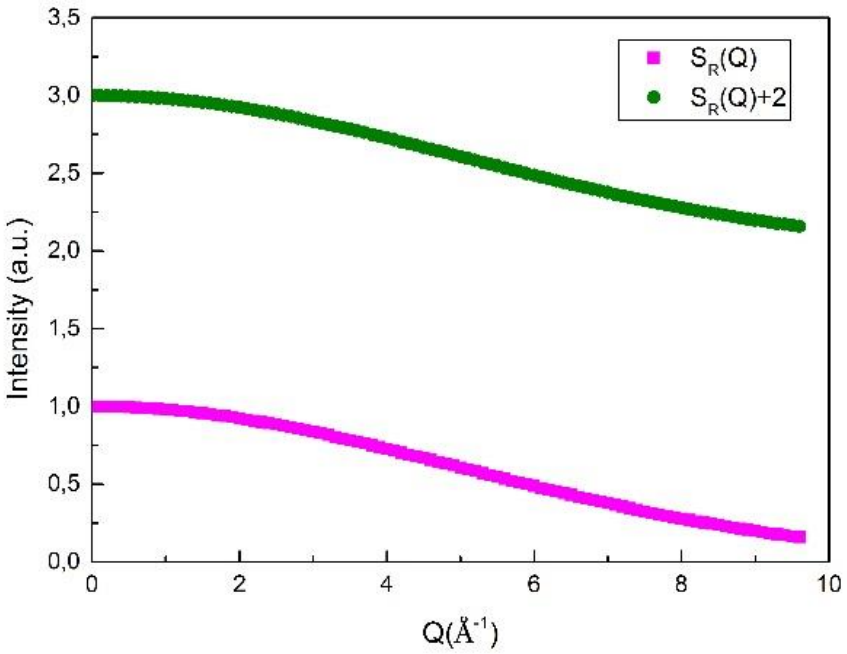

Fig. 5.4 In magenta representation of the function S_R as a function of Q; in green representation of the function $S_R + n$ as a function of Q in a linear-linear plot

5.1.2.1.3 Normalization considering two different temperatures

Representing the function Intensity as a function of Q in a linear-linear plot for values obtained, respectively, at two different temperatures (T_0 <T); the value of MSD calculated for $S_R(T)/S_R(T_0)$ is:

$$\langle r^2 \rangle'_R(T) = \langle r^2 \rangle_R(T) - \langle r^2 \rangle_R(T_0) \tag{5.3}$$

since:

$$\frac{S_R(T)}{S_R(T_0)} = \frac{e^{-Q^2\langle r^2 \rangle_R(T)}}{e^{-Q^2\langle r^2 \rangle_R(T_0)}} = e^{-Q^2[\langle r^2 \rangle_R(T) - \langle r^2 \rangle_R(T_0)]} \tag{5.4}$$

This procedure, therefore, would lead to a change in the MSD.

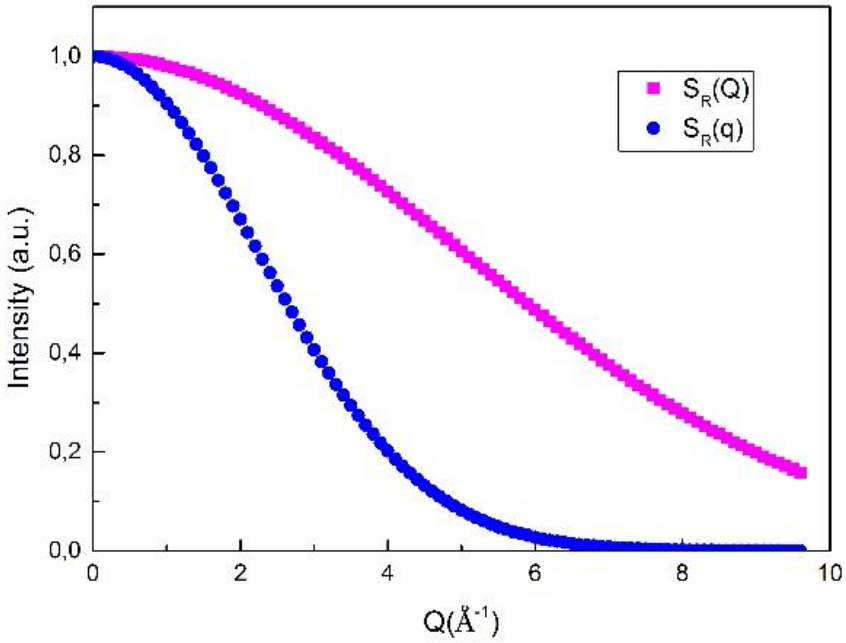

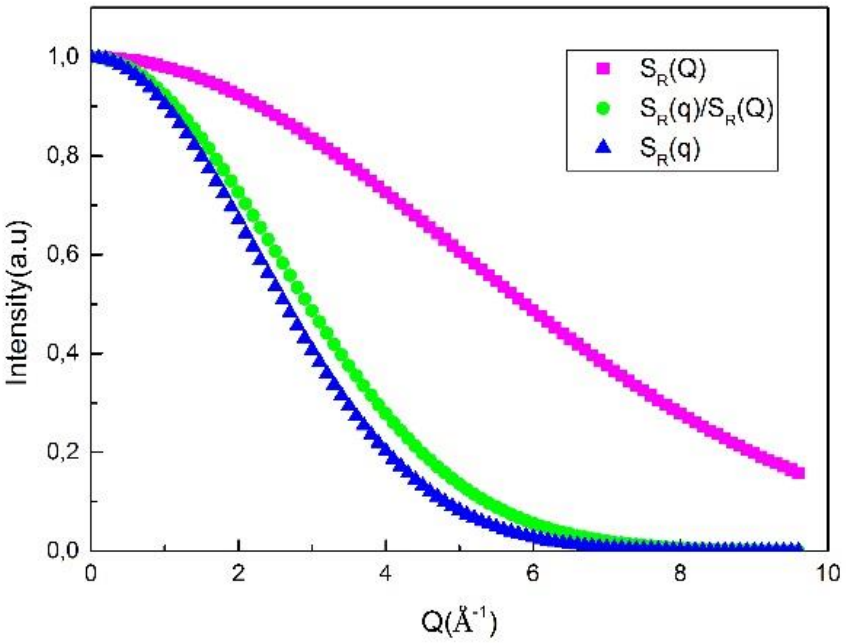

Fig. 5.5 In magenta representation of the function $S_R(T)$ as a function of Q; in blue representation of the function $S_R(T_0)$ as a function of Q; in green representation of the function $S_R(T)/S_R(T_0)$ as a function of Q in a linear-linear plot

5.1.2.2 Normalization performed on the logarithm of the Gaussian function

As far as the the application of logarithm is concerned, one has:

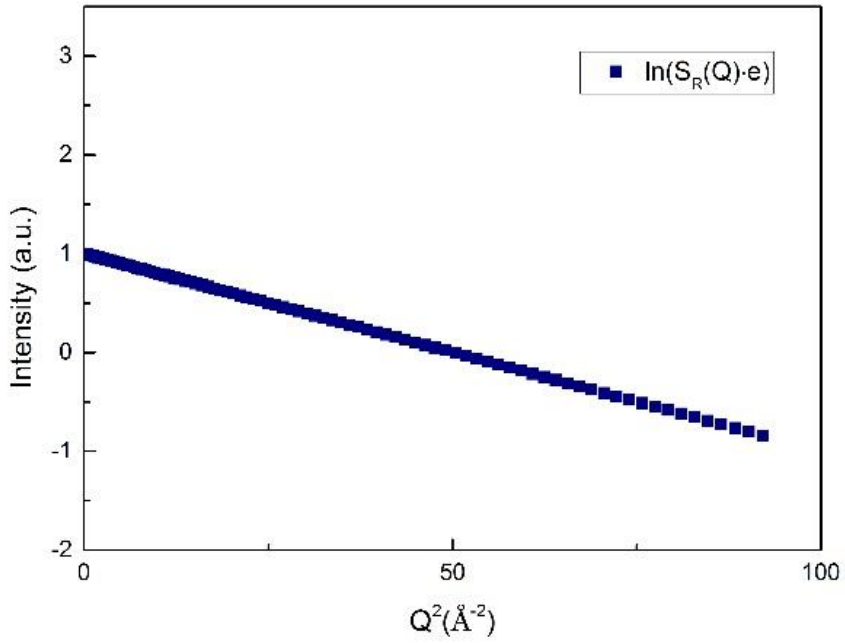

Fig. 5.6 Representation of the function $ln(S_R)$ as a function of Q^2 in a log-lin plot

5.1.2.2.1 Normalization by multiplication

The normalization for a multiplicative factor n, if applied to the logarithm of the function S_R, turns out to be a tricky procedure since it leads to an incorrect value of the MSD. Infact, the normalization of the logarithm according this procedure, implies an elevation in the power that comes from a known property of logarithms:

$$n\ ln(S_R) = ln(S_R)^n \tag{5.5}$$

so:

$$\langle r^2 \rangle'_R = n\langle r^2 \rangle_R$$

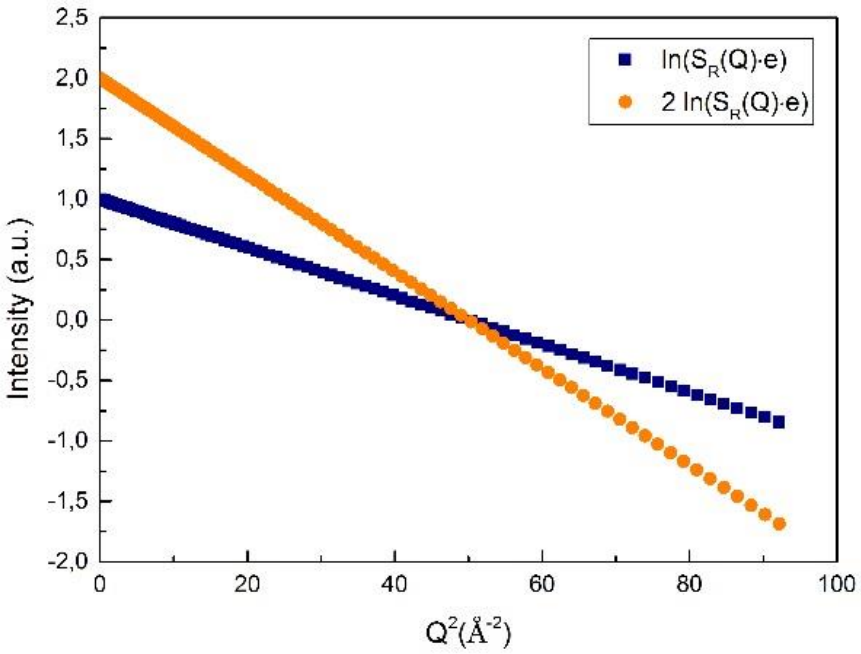

Fig. 5.7 In navy representation of the function $\ln(S_R)$ as a function of Q^2; in orange representation of the function $n \cdot \ln(S_R)$ as a function of Q^2 in a logarithmic-linear plot

5.1.2.2.2 Normalization by the sum of the logarithm

Adding to the logarithm of the function a value, implies from the graphical point of view to obtain a straight line parallel to the previous one; therefore, a translation of the function in the plot and therefore the operation is the correct normalization to be performed. This is due to the fact that:

$$ln(S_R) + ln(n) = \ln(nS_R)$$

Based on the properties just stated, also multiplying the argument of the logarithm for a factor n, furnishes graphically a straight line parallel to the preceding one and, thus, also this procedure is to be considered correct.

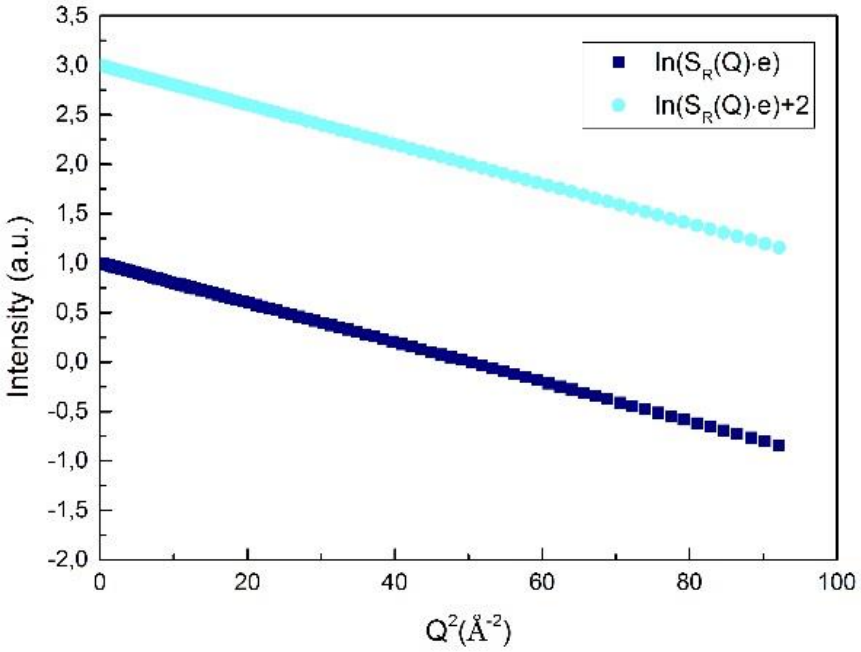

Fig. 5.8 In navy representation of the function $ln(S_R)$ as a function of Q^2; in light blue representation of the function $ln(S_R \cdot n)$ as a function of Q^2 in a logarithmic-linear plot log-lin plot

5.1.2.2.3 Normalization by the sum of logarithm argument

Adding up to the argument of the logarithm a constant term, one notes that the graphic representation is no longer a straight line but a curve. Therefore, the normalization performed by following this protocol is not a proper procedure.

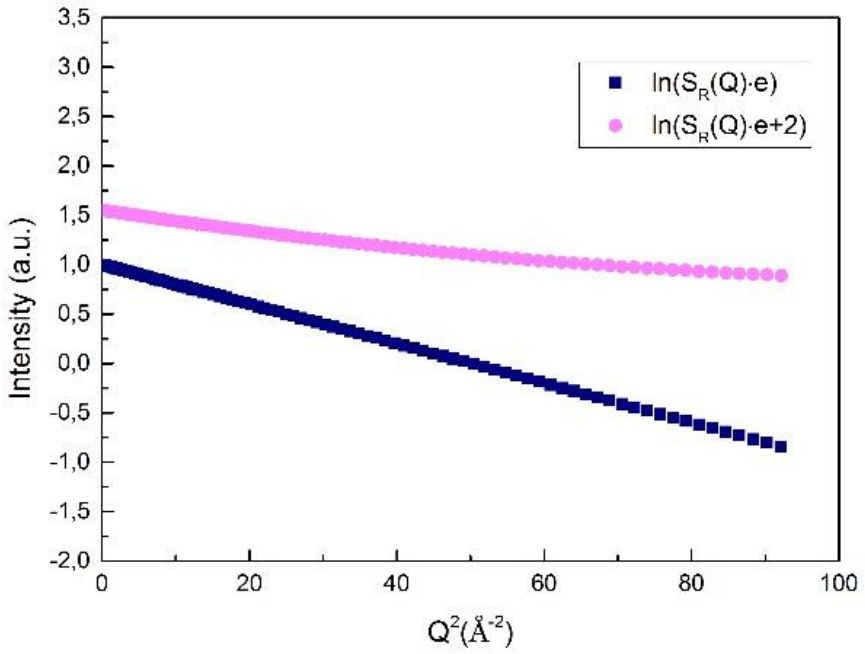

Fig. 5.9 In navy representation of the function $ln(S_R)$ as a function of Q^2; in lilac representation of the function $ln(S_R + n)$ as a function of Q^2 in a logarithmic-linear plot

Therefore we conclude that, in a linear-linear plot, the only normalization procedure does not vary the value of MSD is obtained multiplying the function by the value n and also, in a logarithmic-linear plot, adding to the logarithm of the function a value, the normalization procedure does not vary the value of MSD and so also multiplying the argument of the logarithm for a factor n

5.2 Experimental results and comparison with developed theory

5.2.1 Characteristics of IN10 and IN13 spectrometers for lysozyme experiments

Experimental data were collected at the Institute Laue Langevin (Grenoble, France) by the IN13 and IN10 spectrometers. These spectrometers are characterized by a relatively

high energy of the incident neutrons (16 meV) and allow to span a quite wide range of momentum transfer with two different energy resolutions [51,52]. More specifically, for the IN13 spectrometer, the incident wavelength was 2.23 Å, the *Q*-range was 0.28 ÷ 4.27 Å-1, and the elastic energy resolution was 8 μeV, which corresponds to an elastic time resolution of 516 ps; for the IN10 spectrometer, the incident wavelength was 6.27 Å, the *Q*-range was 0.30 ÷ 2.00 Å-1, and the elastic energy resolution (fwhm) was 1 μeV, which corresponds to an elastic time resolution of 4136 ps [25]. Thus, scattering particles which move in a time scale much slower than the characteristic time corresponding to the energy resolution are seen as elastic scatterers, whereas a decrease of the elastic intensity is observed for scattering particles which move faster. This implies that a scattering particle which moves in a time scale between the resolution time of IN13 and IN10 contributes as an elastic process in the IN13 spectra and as a nonelastic process in the IN10 spectra.

Partially deuterated lysozymes in dry, in D2O, and in H2O environments at a hydration value of *h* =0.4 (*h* = water/protein weight fraction) have been employed. The considered hydration value has been chosen because the activity of proteins depends crucially on the presence of at least a minimum amount of solvent water.[22,23] It is believed that 0.3 g of water per gram of protein is sufficient to cover most of the protein surface with one single layer of water molecules and to fully activate the protein functionality. In particular, for lysozyme, this hydration level was chosen to have a monolayer of water covering the protein surface.[24]

SPECTROMETER	Incident wavelength	*Q*-range	Instrumental energy resolution (FWHM)	Instrumental time resolution
IN10	6.27 Å	0.30 ÷ 2.00 $Å^{-1}$	1 μeV	4136 ps
IN13	2.23 Å	0.28 ÷4.27 $Å^{-1}$	8 μeV	516 ps

Table 5.1 Instrumental characteristics

A scattering particle which moves in a time scale between there solution time of IN13 and IN10 contributes as an elastic process in the IN13 spectra and as a non elastic process

in the IN10 spectra. So because a decrease of the elastic intensity is observed for scattering particles which move faster whereas the scattering particles which move in a time scale much slower than the characteristic time corresponding to the energy resolution are seen as elastic scatterers.

5.2.2 Data obtained through the spectrometers IN10 and IN13 on the analyzed samples

The following figures show the EINS data collected by IN10 and IN13 spectrometers. In particular in Fig. 5.10, the scattered intensity profile of dry lysozyme mixtures as a function of exchanged wavevector Q is shown at different temperature values. Subsequently in Fig. 5.11, the scattered intensity profile of hydrated lysozyme (H_2O) mixtures as a function of exchanged wavevector Q is reported at different temperature values. Lastly in Fig. 5.12, the scattered intensity profile of hydrated lysozyme (D_2O) mixtures as a function of exchanged wavevector Q is shown at different temperature values.

As it can be seen in all three cases, by increasing temperature, the scattered intensity at the higher temperature values, generally drops in Q fulfilling a decaying behavior.

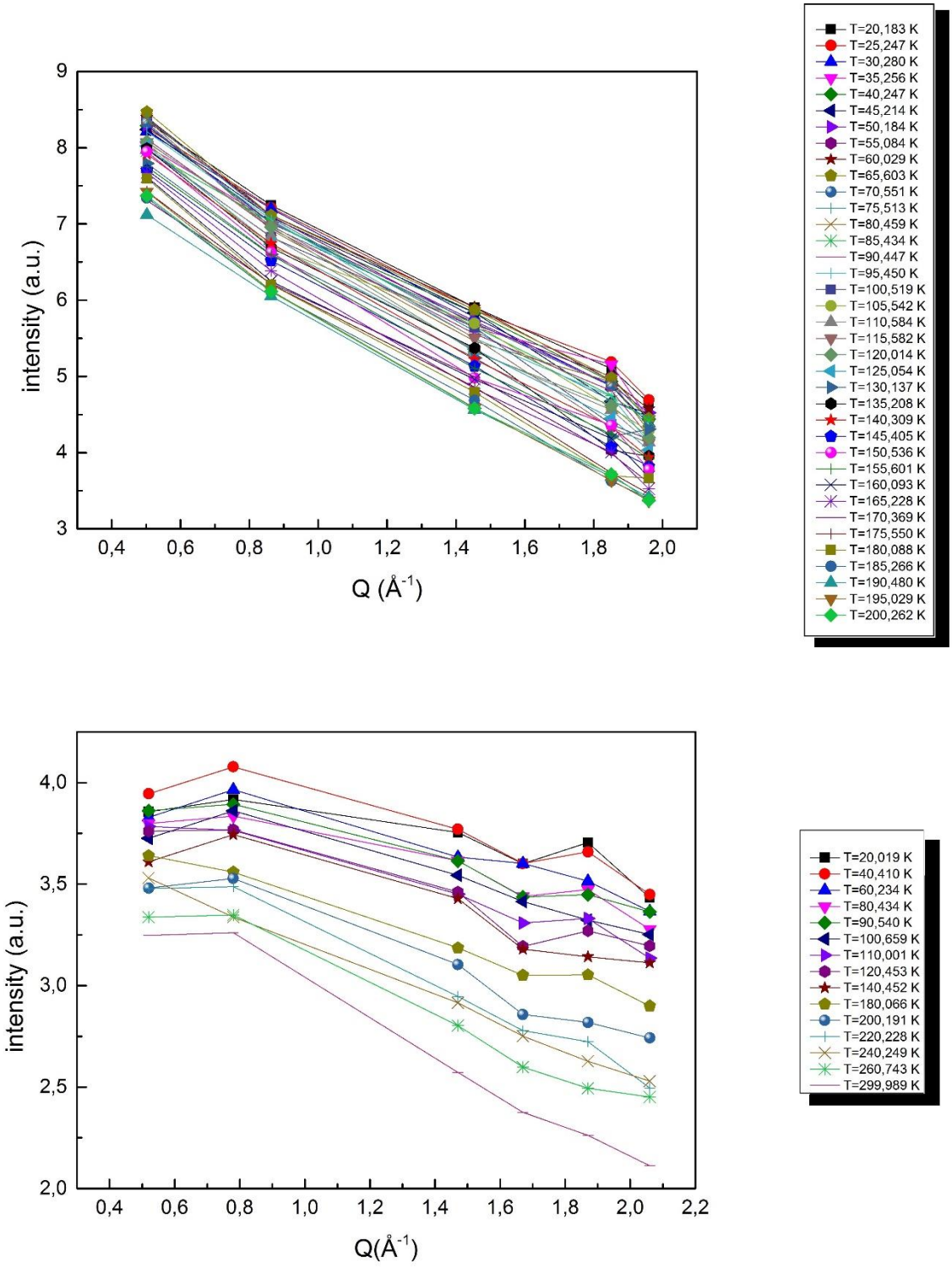

Fig. 5.10: Elastically scattered intensity profile of dry lysozyme sample as a function of the exchanged wavevector Q, in the range between 0.50 and 1,96 $Å^{-1}$, and at temperature values in the range from 19 K to 200 K, for IN10 and in the range between 0.52 and 2,06 $Å^{-1}$, and at temperature values in the range from 19 K to 300 K, for IN13. As it can be seen in all two cases, by increasing temperature, the scattered intensity at the higher temperature values, generally drops in Q fulfilling a decaying behavior.

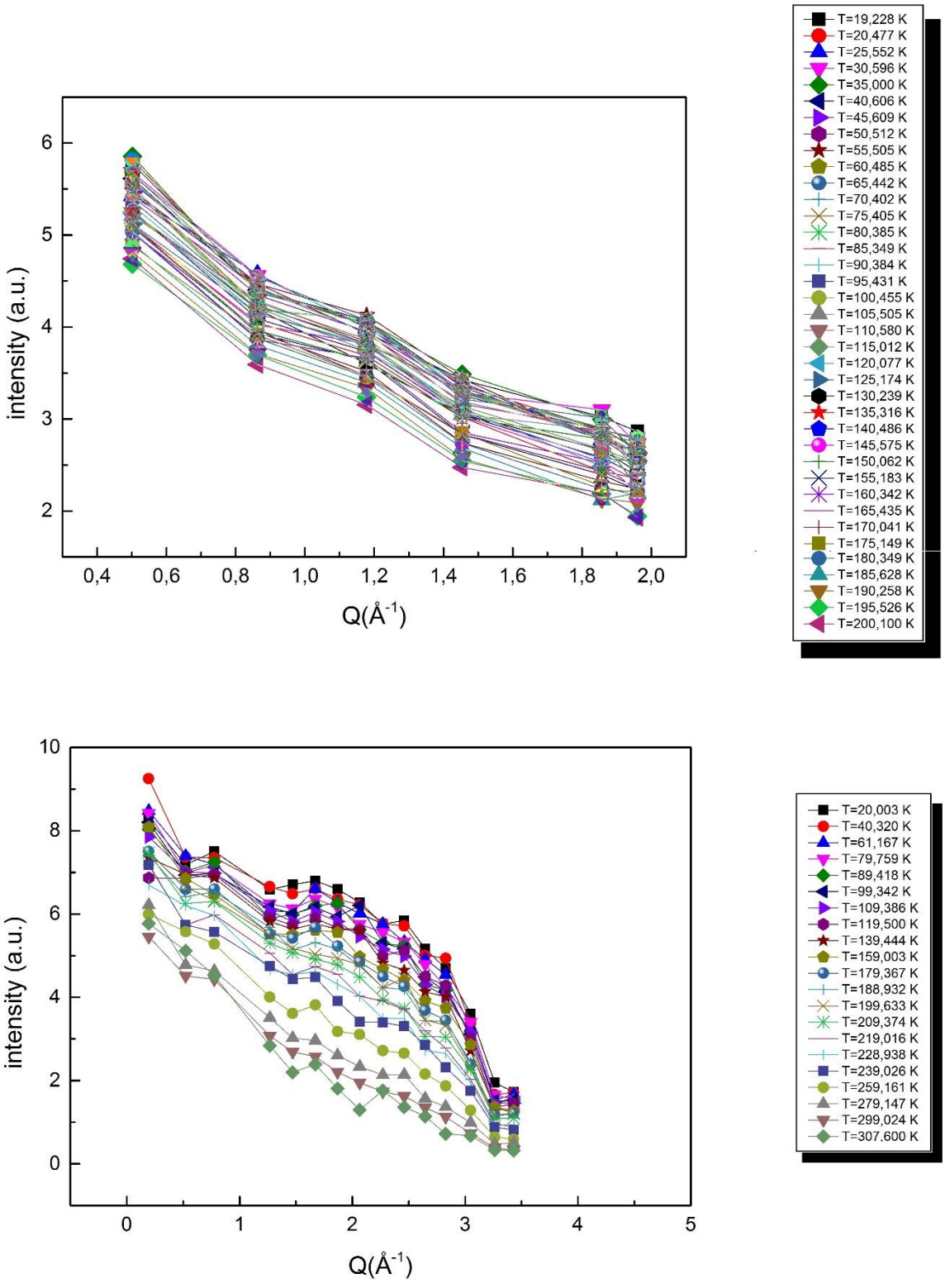

Fig. 5.11: Elastically scattered intensity profile of hydrated lysozyme (H_2O) sample as a function of the exchanged wavevector Q, in the range between 0.50 and 1.96 $Å^{-1}$, and at temperature values in the range from 19 K to 200 K, for IN10 and in the range between 0.19 and 4.66 $Å^{-1}$, and at temperature values in the range from 20 K to 308 K, for IN13. As it can be seen in all two cases, by increasing temperature, the scattered intensity at the higher temperature values, generally drops in Q fulfilling a decaying behavior.

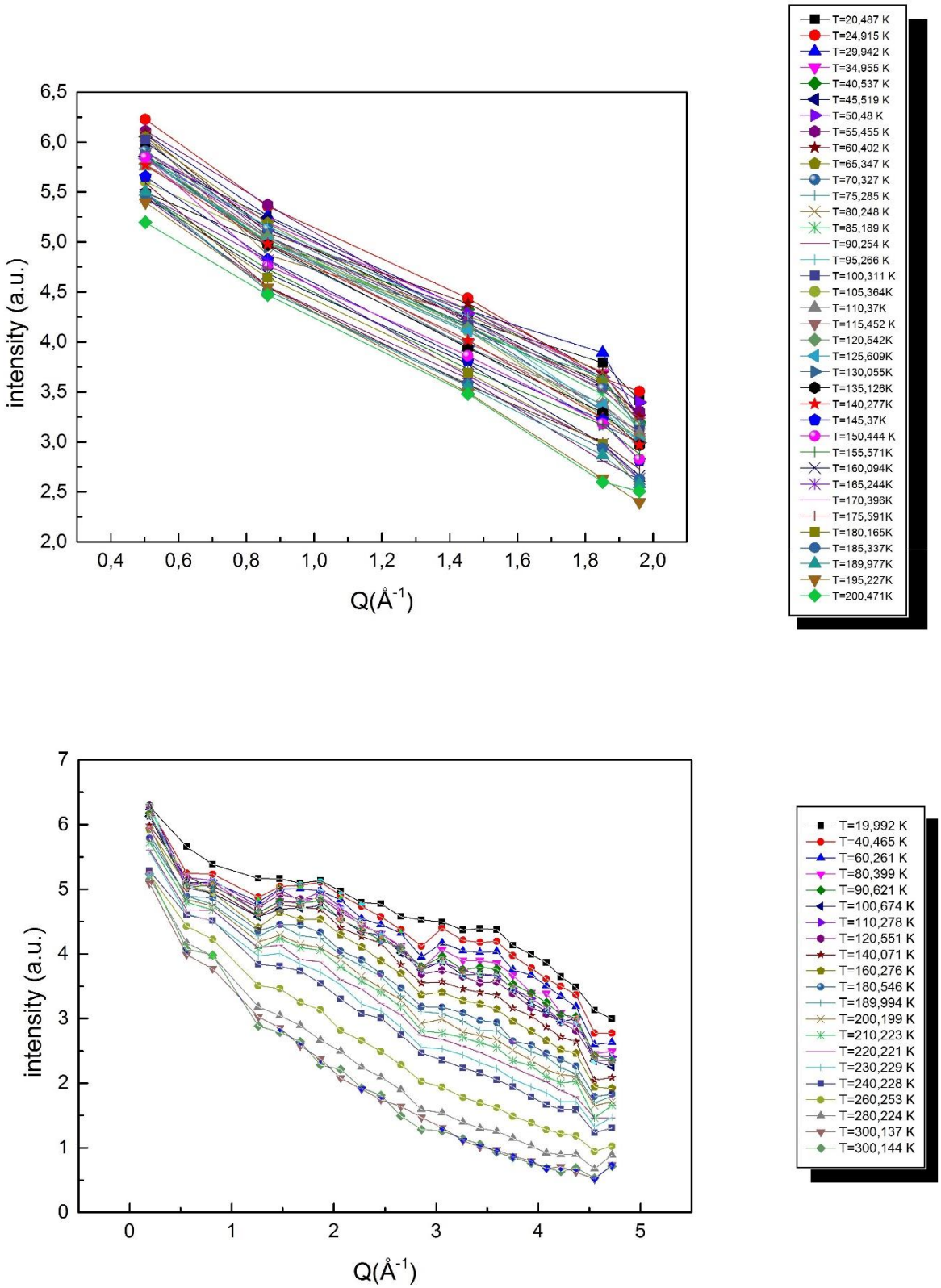

Fig. 5.12 Elastically scattered intensity profile of hydrated lysozyme (D_2O) sample as a function of the exchanged wavevector Q, in the range between 0.50 and 1.96 $Å^{-1}$, and at temperature values in the range from 20 K to 200 K, for IN10 and in the range between 0.19 and 4.66 $Å^{-1}$, and at temperature values in the range from 19 K to 300 K, for IN13. As it can be seen in all two cases, by increasing temperature, the scattered intensity at the higher temperature values, generally drops in Q fulfilling a decaying behavior.

Based on what has been seen so far, it can be seen that the IN10 spectrometer allows us to analyze the data in a temperature range much wider than the IN13 spectrometer does and, on the other hand, the IN13 spectrometer allows us to analyze the data in a Q range much wider than the IN10 spectrometer.

They give us the opportunity to study the same problem from two different angles.

Below are the graphical representations that show what we have just said. By way of example, data on water-hydrated lysozyme were plotted.

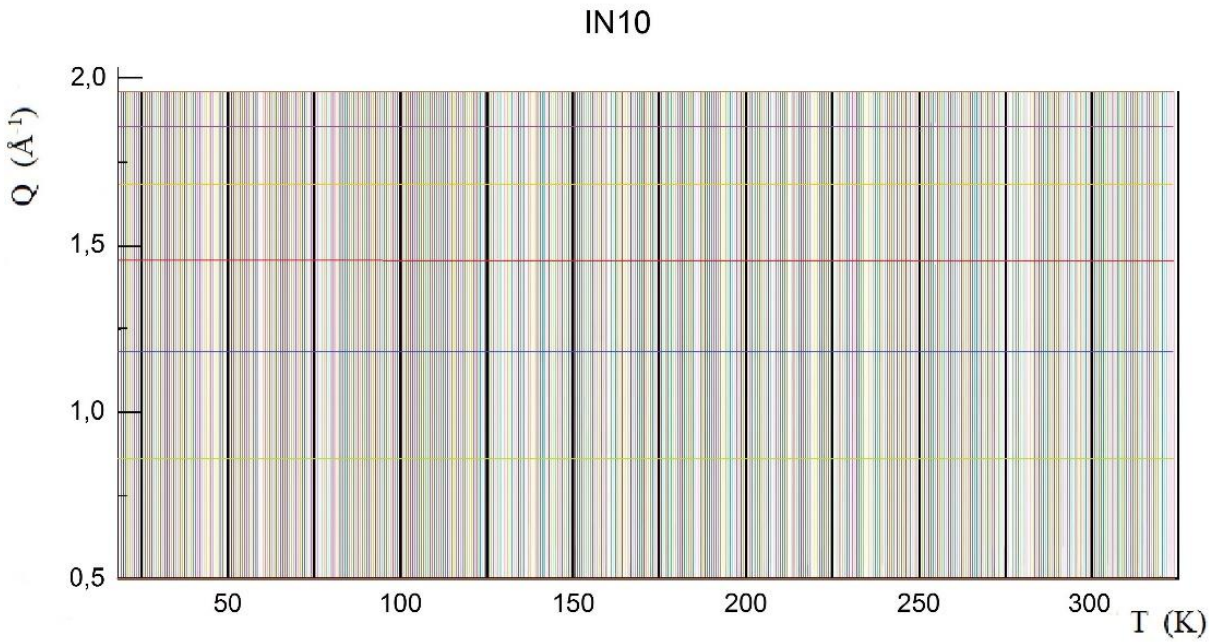

Fig. 5.13 On the axis of ascites the temperature values T analyzed, on the axis of the ordered values of the wavevector Q analyzed with the IN10 spectrometer for water-hydrated lysozyme. We can see how much the temperature values are numerically far superior to the values of the wavevector Q.

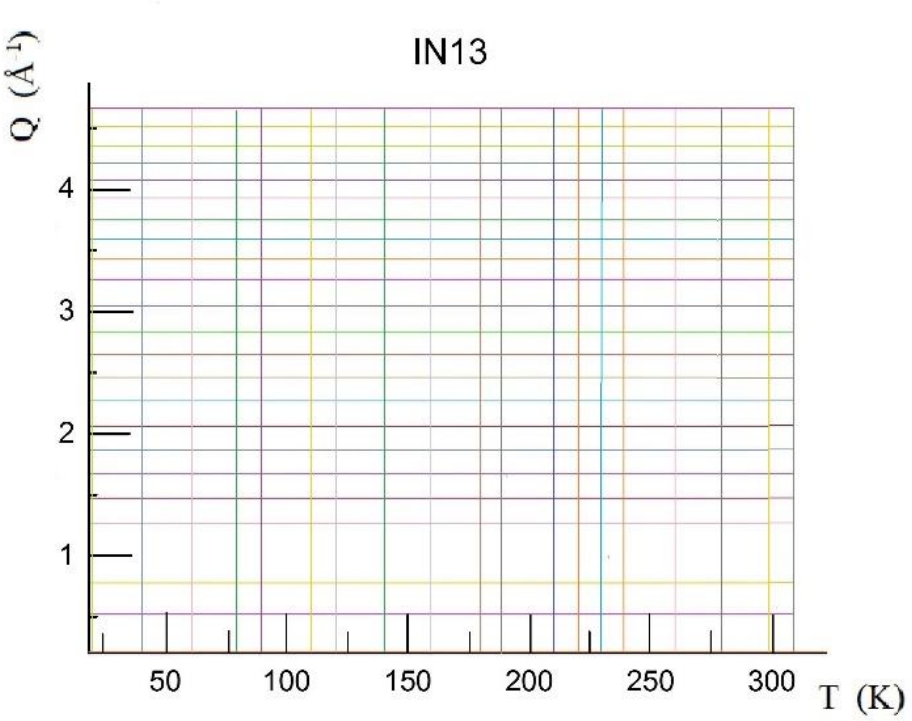

Fig. 5.14 On the axis of ascites the temperature values T analyzed, on the axis of the ordered values of the wavevector Q analyzed with the IN13 spectrometer for water-hydrated lysozyme. We can see how much the values of the wavevector Q are numerically far superior to the temperature values.

Below a figure that summarizes the capacity of the IN10 spectrometer to conduct a careful temperature analysis and the ability of the IN13 spectrometer to conduct a careful wavevector Q analysis.

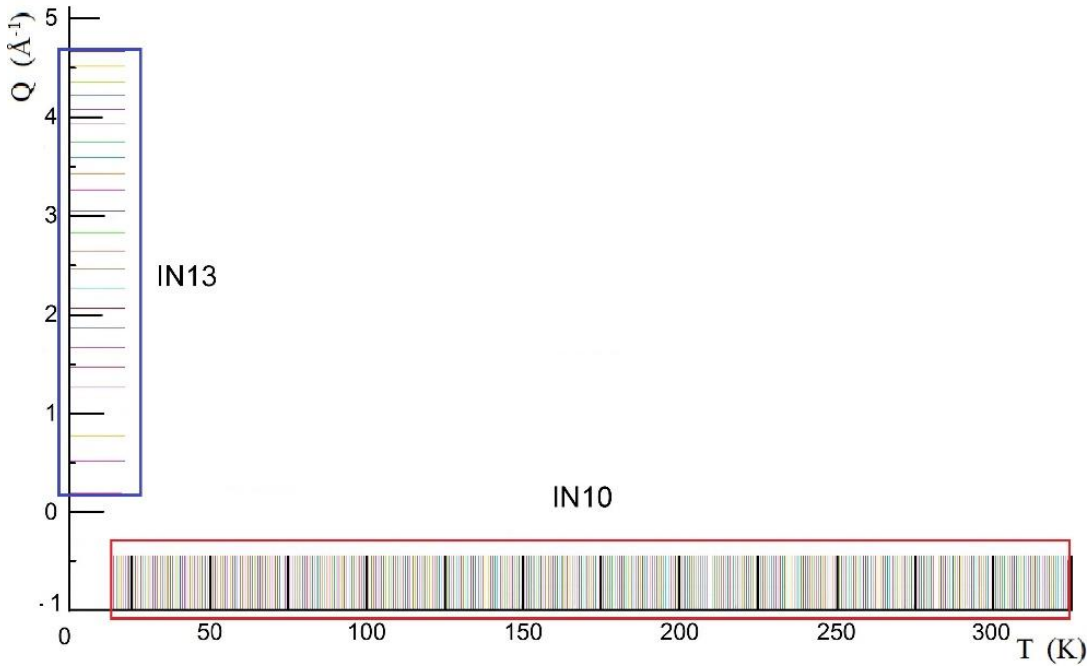

Fig. 5.15 On the axis of ascites the temperature values T analyzed with the IN10 spectrometer, on the axis of the ordered values of the wavevector Q analyzed with the IN13 spectrometer, for water-hydrated lysozyme.

5.2.3 Comparison between the MSD data obtained in experiments conducted on lysozyme with IN10 and IN13 spectrometers

By performing EINS experiments which give a direct connection with the scattering law evaluated at $= 0$, $S_R(\vec{Q}, \omega = 0)$, we know that the measured MSD corresponds to the integration in the time domain of the product of the system MSD times the resolution function. So the relation between the measured MSD (obtained by EINS it depends on the employed instrumental resolution) $\langle \vec{r}^2 \rangle_R$, and the system MSD (function of time) $\langle \vec{r}^2 \rangle(t)$, is:

$$\langle \vec{r}^2 \rangle_R = \int_{-\infty}^{\infty} \langle \vec{r}^2 \rangle(t) R(t) dt$$

One can make the following remarks:

- Considering two different systems and studying them with the same instrumental resolution yields, the comparison between the MSDs measured is:

$$\langle r^2 \rangle_{1,R} - \langle r^2 \rangle_{2,R} = \int_{-\infty}^{\infty} [\langle r^2 \rangle_1(t) - \langle r^2 \rangle_2(t)] R(t) dt \qquad (5.6)$$

So, on two different systems, using the same instrument working at the same resolution, the difference between the measured MSD does not correspond to the difference between their MSDs.

- Considering the same system and studying it at different instrumental resolutions yields, the comparison between the MSDs measured is:

$$\langle r^2 \rangle_{1,R} - \langle r^2 \rangle_{2,R} = \int_{-\infty}^{\infty} \langle r^2 \rangle(t) [R_1(t) - R_2(t)] dt \qquad (5.7)$$

We now compare the measured MSDs temperature behavior obtained for the same systems, that is, dry and hydrated (H2O and D2O with h = 0.4) lysozyme, respectively, by the IN13 spectrometer working at the energy resolution value of 8 μeV and by the IN10 spectrometer working at the energy resolution value of 1 μeV, without and with normalization. The MSD values have been obtained by employing the following common Q-range: 0.5 ÷ 2.0 Å^{-1}.

In agreement with:

$$\langle \vec{r}^2 \rangle_R = \int_{-\infty}^{\infty} \langle r^2 \rangle(t) R(t) dt$$

the MSD evaluated, without normalization, by IN10, in all the temperature ranges, is higher in respect to that evaluated by IN13. This is because that even at the lowest temperature values, where only vibrational contributions are expected to contribute, the measured MSD is the integral of the product between the resolution function and the system MSD.

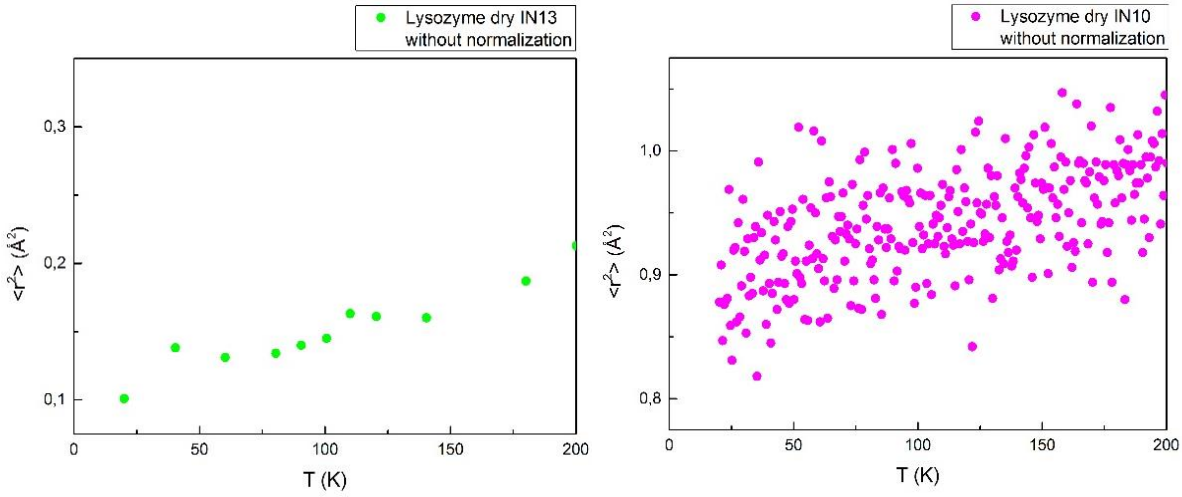

Fig. 5.16 Measured MSDs temperature behavior obtained from data collected by the IN13 and IN10 spectrometers on dry lysozyme samples without normalization.

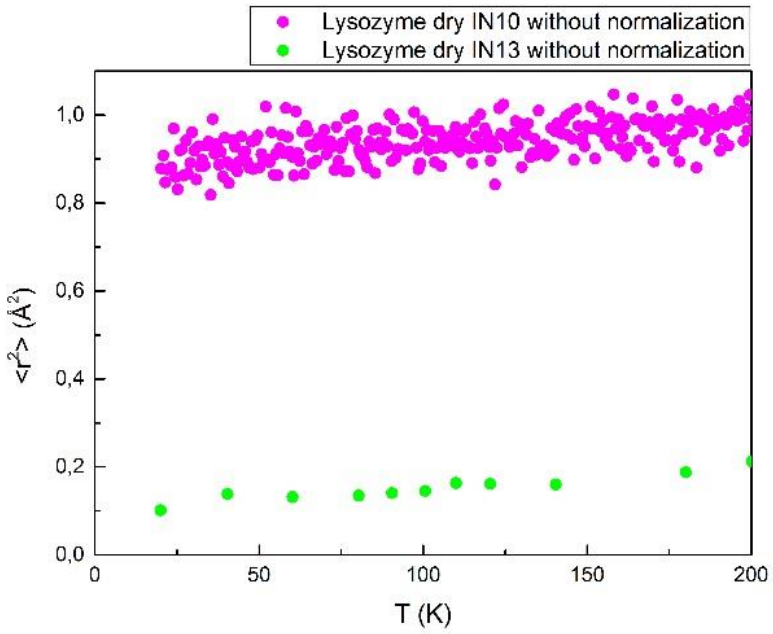

Fig. 5.17 Comparison between the measured MSDs temperature behavior obtained from data collected by the IN13 and IN10 spectrometers on dry lysozyme samples without normalization. It can be noticed that the value of the MSD obtained by the IN10 spectrometer is significantly higher than that achieved by IN13.

By proceeding to normalization of data obtained through the two different spectrometers, we note that at lower temperatures, the values of MSD are very similar. This is because only vibrational motions occur. Approximately in the low temperature range up to T = 80 K, the system MSD can be considered almost constant $\langle r^2 \rangle(t) \rightarrow \langle r^2 \rangle^{(V)}$ and, in such a case, the measured MSD by the following equation:

$$\langle \vec{r}^2 \rangle_R = \int_{-\infty}^{\infty} \langle r^2 \rangle(t) R(t) dt$$

results:

$$\langle r^2 \rangle_R = \int_{-\infty}^{\infty} \langle r^2 \rangle(t) R(t) dt = \int_{-\infty}^{\infty} \langle r^2 \rangle^{(V)} R(t) dt$$

$$\langle r^2 \rangle_R = \langle r^2 \rangle^{(V)} \int_{-\infty}^{\infty} R(t) dt \tag{5.8}$$

So, at the lowest temperature values, where only vibrational contributions are expected to contribute, the measured MSD is the integral of the product between the resolution function and the system MSD Then, starting from the last equation, it's possible to determine the system MSD at the lowest temperature values

$$\langle r^2 \rangle^{(V)} = \frac{\langle r^2 \rangle_R}{\int_{-\infty}^{\infty} R(t) dt} \tag{5.9}$$

What is remarkable is that by applying this procedure to the data collected on the same systems by the two spectrometers IN13 and IN10, working at a different energy resolution, we obtain at the lowest temperature values the same system MSD value

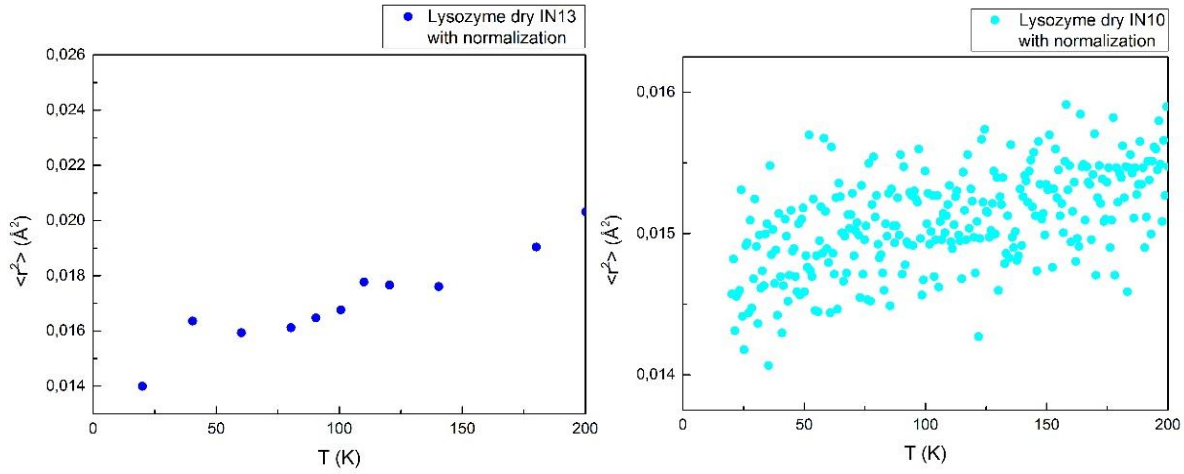

Fig. 5.18 Measured MSDs temperature behavior obtained from data collected by the IN13 and IN10 spectrometers on dry lysozyme samples with normalization.

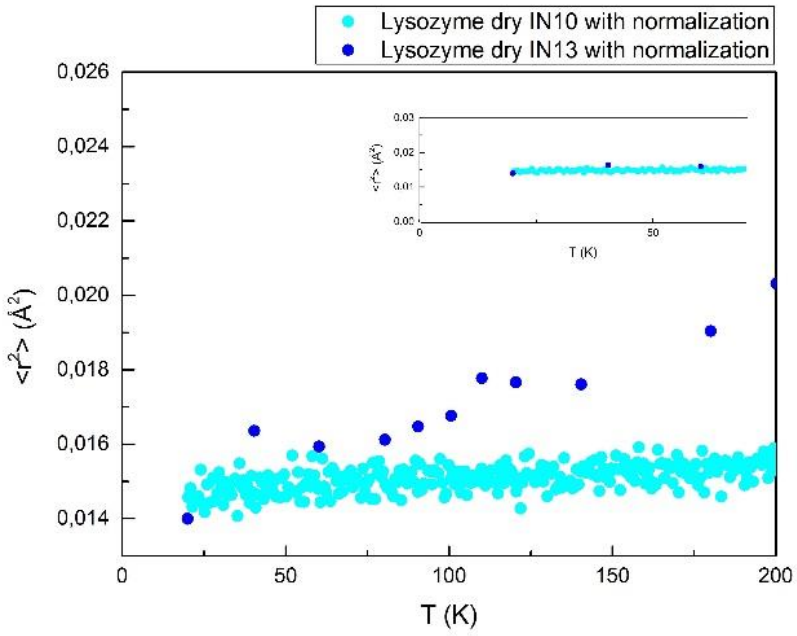

Fig. 5.19 Comparison between the measured MSDs temperature behavior obtained from data collected by the IN13 and IN10 spectrometers on dry lysozyme samples with normalization. It is possible to see that at lower temperatures the MSD values obtained with the two spectrometers are very similar.

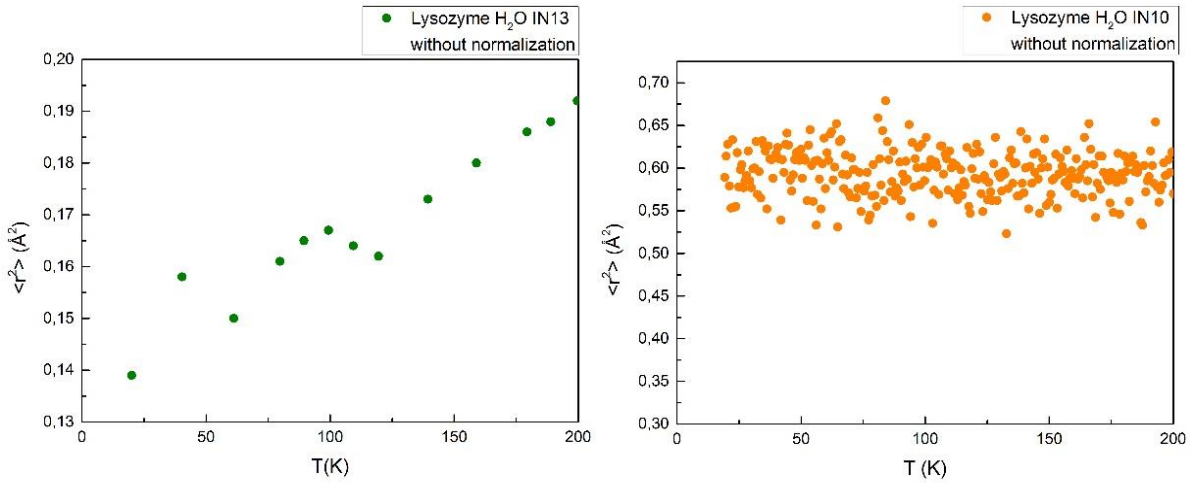

Fig. 5.20 Measured MSDs temperature behavior obtained from data collected by the IN13 and IN10 spectrometers on hydrated (H_2O) lysozyme samples without normalization.

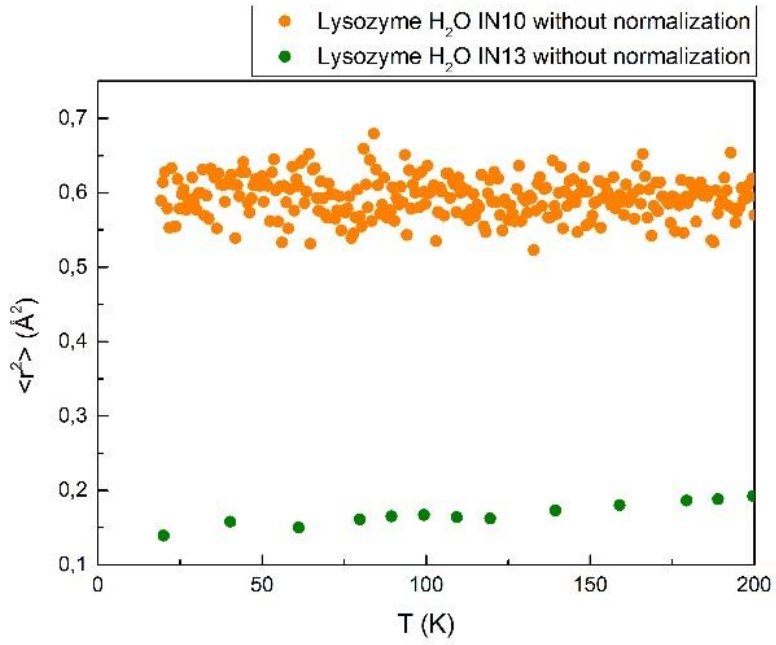

Fig. 5.21 Comparison between the measured MSDs temperature behavior obtained from data collected by the IN13 and IN10 spectrometers on hydrated (H_2O) lysozyme samples without normalization.

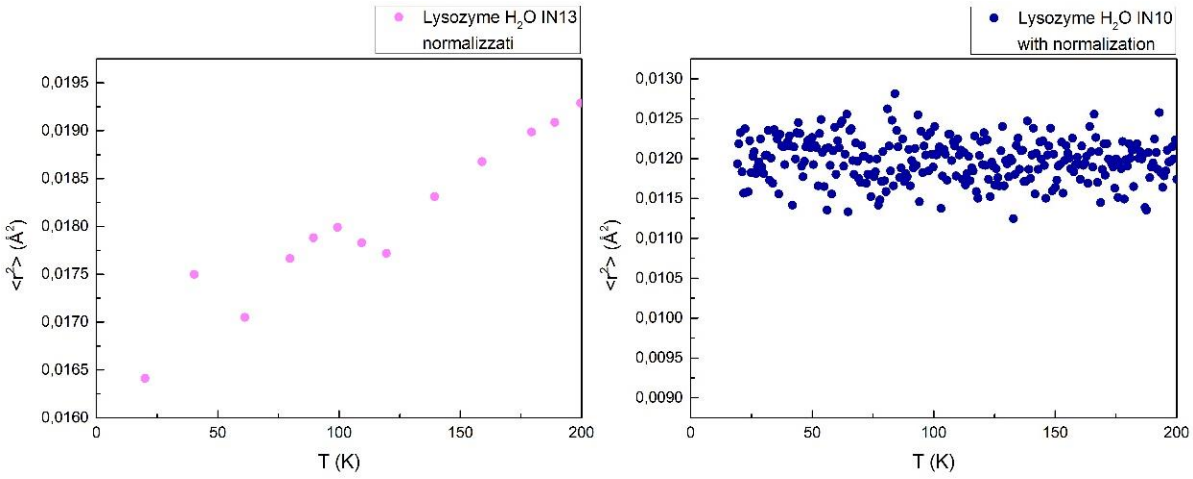

Fig. 5.22 Measured MSDs temperature behavior obtained from data collected by the IN13 and IN10 spectrometers on hydrated (H_2O) lysozyme samples with normalization.

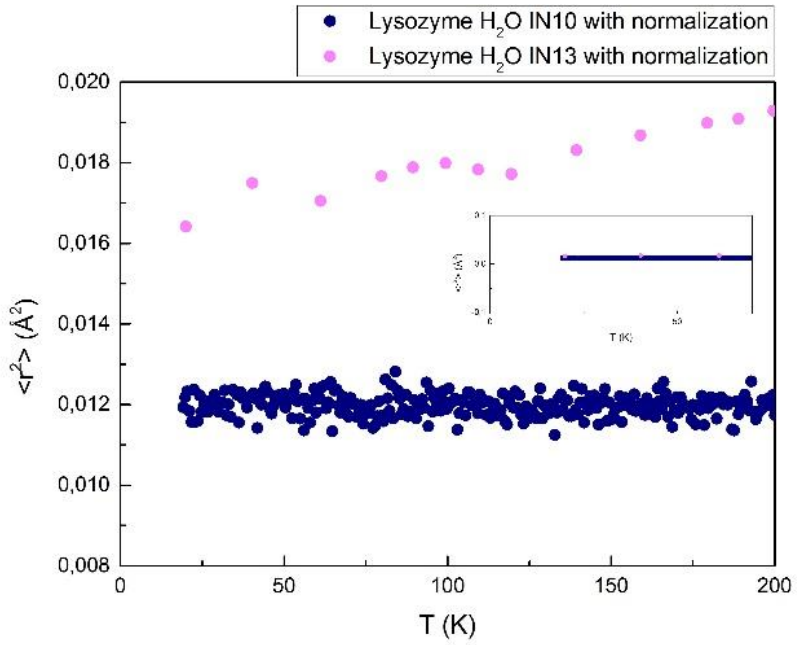

Fig. 5.23 Comparison between the measured MSDs temperature behavior obtained from data collected by the IN13 and IN10 spectrometers on hydrated (H_2O) lysozyme samples with normalization. It is possible to see that at lower temperatures the MSD values obtained with the two spectrometers are very similar.

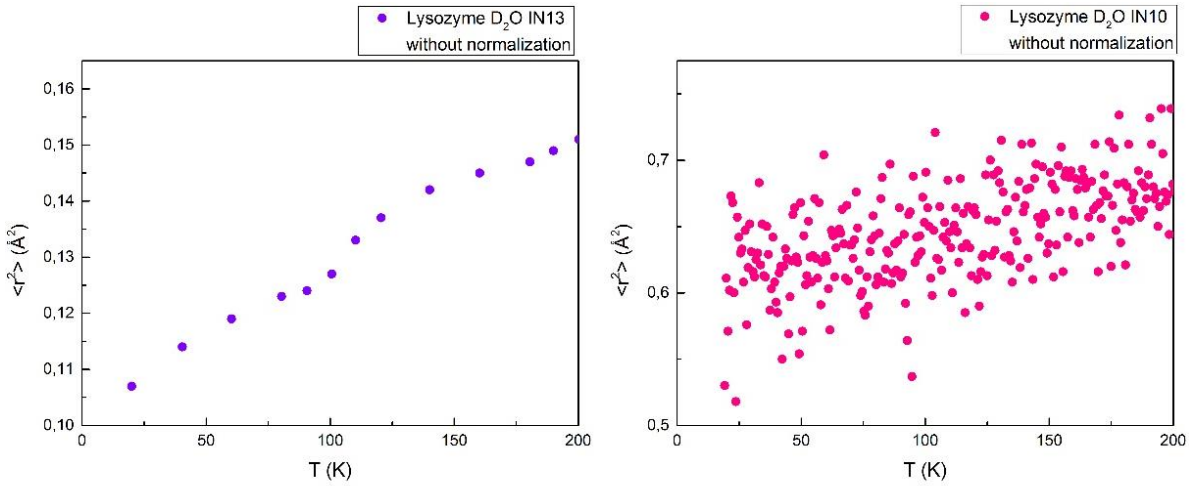

Fig. 5.24 Measured MSDs temperature behavior obtained from data collected by the IN13 and IN10 spectrometers on hydrated (D_2O) lysozyme samples without normalization.

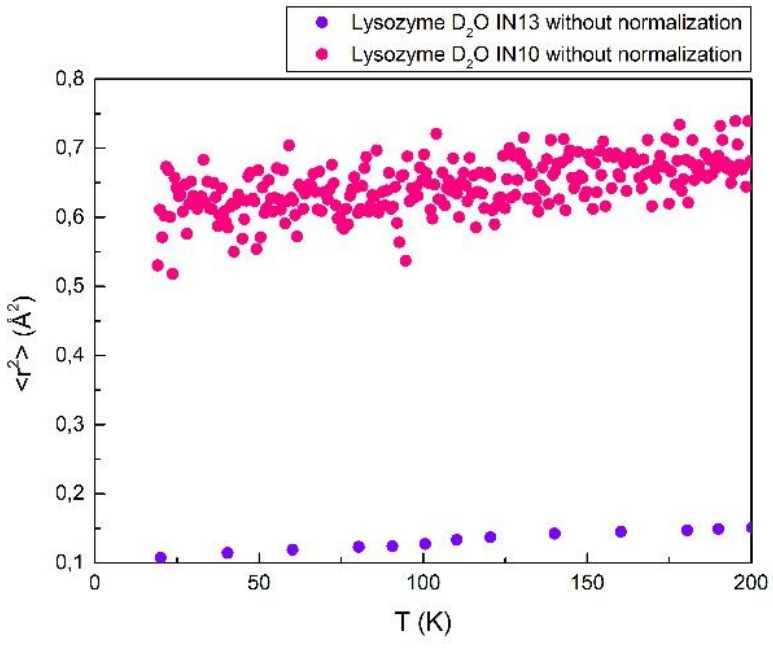

Fig. 5.25 Comparison between the measured MSDs temperature behavior obtained from data collected by the IN13 and IN10 spectrometers on hydrated (D_2O) lysozyme samples without normalization.

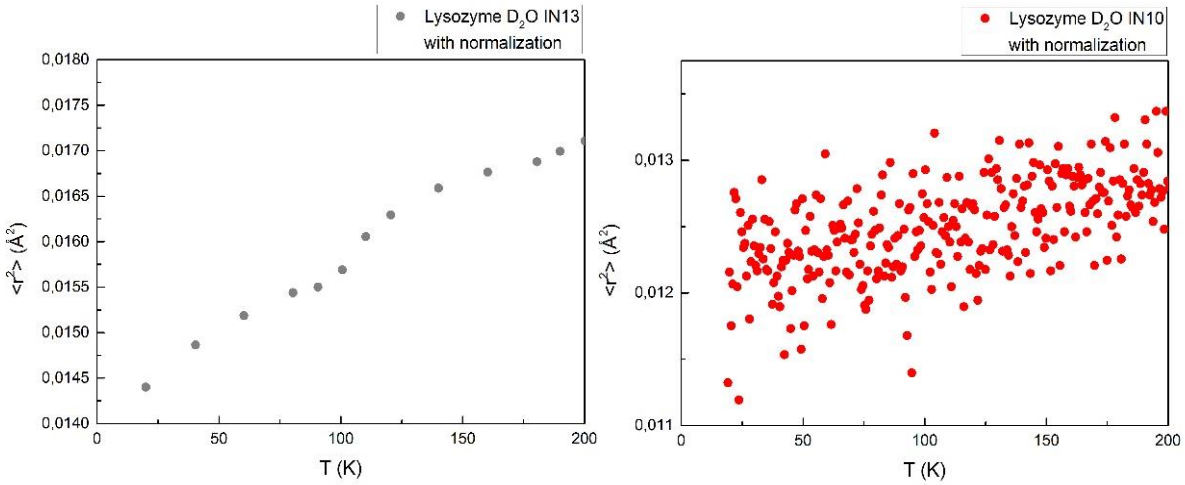

Fig. 5.26 Measured MSDs temperature behavior obtained from data collected by the IN13 and IN10 spectrometers on hydrated (D_2O) lysozyme samples with normalization.

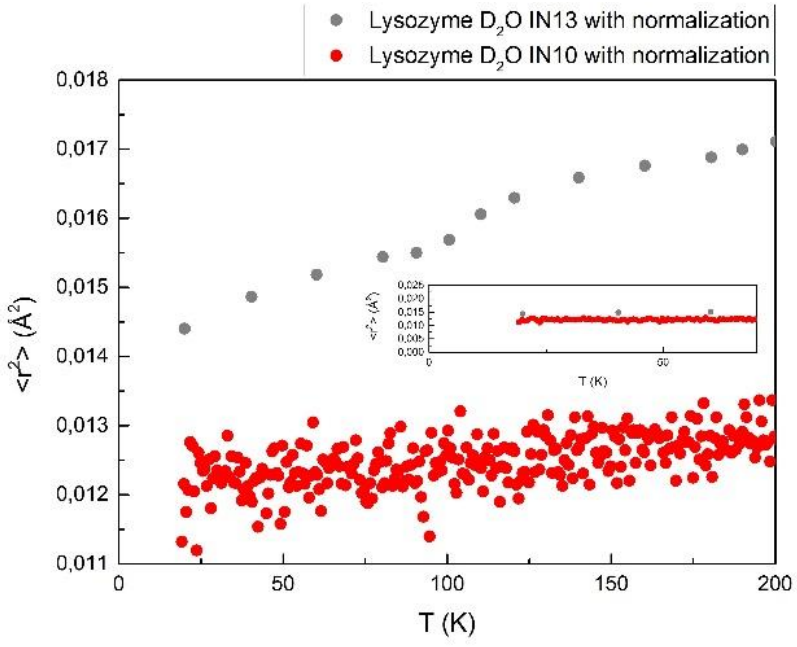

Fig. 5.27 Comparison between the measured MSDs temperature behavior obtained from data collected by the IN13 and IN10 spectrometers on hydrated (D_2O) lysozyme samples with normalization. It is possible to see that at lower temperatures the MSD values obtained with the two spectrometers are very similar.

Table 5.2: Vibrational MSDs and their roots, representative of Mean Displacements (MDs), for dry and hydrated (H_2O and D_2O) lysozyme samples

LYSOZYME DRY					
MSD_M^{IN10} ($Å^2$)	MSD_M^{IN13} ($Å^2$)	MSD^{IN10} ($Å^2$)	MSD^{IN13} ($Å^2$)	MD^{IN10} (Å)	MD^{IN13} (Å)
1,241	0,172	0,00029	0,00034	0,017	0,018
1,228	0,199	0,00030	0,00036	0,017	0,019
1,251	0,219	0,00030	0,00042	0,017	0,020

LYSOZYME/H_2O					
MSD_M^{IN10} ($Å^2$)	MSD_M^{IN13} ($Å^2$)	MSD^{IN10} ($Å^2$)	MSD^{IN13} ($Å^2$)	MD^{IN10} (Å)	MD^{IN13} (Å)
2,165	0,253	0,00052	0,00049	0,023	0,022
2,471	0,460	0,00060	0,00089	0,024	0,029
2,853	0,462	0,00069	0,00090	0,026	0,030

LYSOZYME/D_2O					
MSD_M^{IN10} ($Å^2$)	MSD_M^{IN13} ($Å^2$)	MSD^{IN10} ($Å^2$)	MSD^{IN13} ($Å^2$)	MD^{IN10} (Å)	MD^{IN13} (Å)
0,897	0,079	0,00022	0,00015	0,015	0,012
0,748	0,114	0,00018	0,00022	0,013	0,015
0,832	0,079	0,00020	0,00015	0,014	0,012

Table 5.3 Data provided by the spectrometer IN13

DRY

T (K)	MSD (Å²)	MSD (N) (Å²)
20,019	0,101	0,013991
40,41	0,138	0,016354
60,234	0,131	0,015933
80,434	0,134	0,016115
90,54	0,14	0,016472
100,659	0,145	0,016763
110,001	0,163	0,017773
120,453	0,161	0,017664
140,452	0,16	0,017609
180,066	0,187	0,019037
200,191	0,213	0,020317

H_2O

T (K)	MSD (Å²)	MSD (N) (Å²)
20,003	0,139	0,016413
40,32	0,158	0,017499
61,167	0,15	0,01705
79,759	0,161	0,017664
89,418	0,165	0,017882
99,342	0,167	0,01799
109,386	0,164	0,017828
119,5	0,162	0,017719
139,444	0,173	0,01831
159,003	0,18	0,018677
179,367	0,186	0,018986
188,932	0,188	0,019088
199,633	0,192	0,01929
209,374	0,193	0,01934

D_2O

T (K)	MSD (Å²)	MSD (N) (Å²)
19,992	0,107	0,0144
40,465	0,114	0,014864
60,261	0,119	0,015186
80,399	0,123	0,015439
90,621	0,124	0,015502
100,674	0,127	0,015688
110,278	0,133	0,016055
120,551	0,137	0,016294
140,071	0,142	0,016589
160,276	0,145	0,016763
180,546	0,147	0,016878
189,994	0,149	0,016993
200,199	0,151	0,017107

Table 5.4 Data provided by the spectrometer IN10

DRY			H_2O			D_2O		
T (K)	MSD (Å²)	MSD (N) (Å²)	T (K)	MSD (Å²)	MSD (N) (Å²)	T (K)	MSD (Å²)	MSD (N) (Å²)
20,183	0,878	0,014572	19,228	0,589	0,011935	19,19	0,53	0,011321
20,83	0,908	0,014819	19,827	0,614	0,012186	19,853	0,611	0,012156
21,497	0,847	0,014312	20,477	0,628	0,012324	20,487	0,571	0,011751
22,085	0,876	0,014555	21,129	0,579	0,011833	21,112	0,602	0,012066
22,728	0,879	0,01458	21,783	0,553	0,011564	21,731	0,673	0,012758
23,366	0,881	0,014597	22,386	0,633	0,012373	22,373	0,668	0,01271
24,007	0,969	0,015308	23,023	0,554	0,011575	23,034	0,6	0,012046
24,605	0,859	0,014413	23,666	0,555	0,011585	23,677	0,518	0,011193
25,247	0,831	0,014176	24,299	0,618	0,012225	24,267	0,657	0,012605
25,891	0,92	0,014916	24,896	0,578	0,011823	24,915	0,642	0,01246
26,534	0,922	0,014932	25,552	0,598	0,012026	25,557	0,63	0,012343
27,125	0,862	0,014438	26,199	0,604	0,012086	26,144	0,633	0,012373
27,76	0,942	0,015093	26,852	0,577	0,011813	26,786	0,608	0,012126
28,401	0,866	0,014472	27,44	0,585	0,011894	27,429	0,647	0,012509
29,059	0,891	0,014679	28,074	0,591	0,011955	28,074	0,576	0,011802
29,658	0,961	0,015245	28,727	0,62	0,012245	28,668	0,619	0,012235
30,28	0,919	0,014908	29,318	0,585	0,011894	29,315	0,652	0,012557
30,899	0,853	0,014363	29,96	0,577	0,011813	29,942	0,631	0,012353
31,504	0,929	0,014989	30,596	0,599	0,012036	30,569	0,616	0,012205
32,119	0,883	0,014613	31,244	0,6	0,012046	31,181	0,612	0,012166
32,777	0,898	0,014737	31,841	0,631	0,012353	31,822	0,625	0,012294
33,408	0,885	0,01463	32,464	0,569	0,011731	32,453	0,63	0,012343
34,017	0,93	0,014997	33,106	0,596	0,012006	33,101	0,683	0,012852
34,645	0,939	0,015069	33,745	0,565	0,011689	33,68	0,621	0,012255
35,256	0,818	0,014065	34,345	0,632	0,012363	34,303	0,652	0,012557
35,891	0,991	0,015481	35	0,627	0,012314	34,955	0,613	0,012176
36,491	0,912	0,014851	35,608	0,62	0,012245	35,556	0,612	0,012166
37,13	0,934	0,015029	36,24	0,552	0,011554	36,175	0,65	0,012538
37,774	0,887	0,014646	36,849	0,626	0,012304	36,825	0,629	0,012334
38,399	0,916	0,014884	37,47	0,611	0,012156	37,451	0,587	0,011915
38,964	0,86	0,014422	38,108	0,61	0,012146	38,034	0,603	0,012076
39,606	0,948	0,015141	38,691	0,588	0,011925	38,664	0,642	0,01246
40,247	0,893	0,014696	39,346	0,612	0,012166	39,302	0,608	0,012126
40,833	0,845	0,014295	39,98	0,617	0,012215	39,95	0,593	0,011975
41,477	0,885	0,01463	40,606	0,624	0,012284	40,537	0,585	0,011894
42,111	0,943	0,015101	41,193	0,611	0,012156	41,173	0,615	0,012196

42,743	0,928	0,014981	**41,838**	0,539	0,011417	**41,808**	0,62	0,012245
43,321	0,872	0,014522	**42,47**	0,61	0,012146	**42,429**	0,55	0,011533
43,957	0,894	0,014704	**43,114**	0,595	0,011996	**43,012**	0,62	0,012245
44,581	0,951	0,015165	**43,699**	0,628	0,012324	**43,649**	0,633	0,012373
45,214	0,915	0,014876	**44,323**	0,641	0,012451	**44,286**	0,626	0,012304
45,797	0,917	0,014892	**44,958**	0,627	0,012314	**44,921**	0,569	0,011731
46,428	0,893	0,014696	**45,609**	0,586	0,011904	**45,519**	0,597	0,012016
47,079	0,88	0,014588	**46,197**	0,573	0,011772	**46,15**	0,624	0,012284
47,7	0,939	0,015069	**46,836**	0,592	0,011965	**46,767**	0,659	0,012624
48,303	0,877	0,014563	**47,462**	0,61	0,012146	**47,363**	0,664	0,012672
48,935	0,943	0,015101	**48,093**	0,618	0,012225	**47,998**	0,627	0,012314
49,557	0,953	0,015181	**48,67**	0,619	0,012235	**48,639**	0,623	0,012275
50,184	0,88	0,014588	**49,314**	0,609	0,012136	**49,254**	0,554	0,011575
50,749	0,911	0,014843	**49,949**	0,622	0,012265	**49,838**	0,668	0,01271
51,374	0,901	0,014761	**50,512**	0,588	0,011925	**50,48**	0,571	0,011751
52,02	1,019	0,015698	**51,183**	0,612	0,012166	**51,103**	0,643	0,01247
52,606	0,898	0,014737	**51,81**	0,609	0,012136	**51,744**	0,606	0,012106
53,244	0,893	0,014696	**52,433**	0,562	0,011658	**52,332**	0,613	0,012176
53,861	0,961	0,015245	**53,024**	0,627	0,012314	**52,956**	0,654	0,012576
54,502	0,864	0,014455	**53,665**	0,645	0,012489	**53,588**	0,627	0,012314
55,084	0,911	0,014843	**54,298**	0,603	0,012076	**54,217**	0,608	0,012126
55,714	0,863	0,014447	**54,917**	0,561	0,011648	**54,803**	0,628	0,012324
56,344	0,924	0,014949	**55,505**	0,608	0,012126	**55,455**	0,671	0,012739
56,969	0,954	0,015189	**56,139**	0,533	0,011353	**56,084**	0,626	0,012304
57,55	0,913	0,014859	**56,77**	0,609	0,012136	**56,669**	0,611	0,012156
58,179	1,016	0,015675	**57,425**	0,587	0,011915	**57,286**	0,668	0,01271
58,82	0,95	0,015157	**58,015**	0,552	0,011554	**57,923**	0,591	0,011955
59,412	0,917	0,014892	**58,622**	0,605	0,012096	**58,563**	0,623	0,012275
60,029	0,905	0,014794	**59,263**	0,635	0,012392	**59,141**	0,704	0,013048
60,656	0,862	0,014438	**59,852**	0,576	0,011802	**59,775**	0,628	0,012324
61,285	1,008	0,015613	**60,485**	0,618	0,012225	**60,402**	0,624	0,012284
61,87	0,913	0,014859	**61,091**	0,609	0,012136	**61,035**	0,603	0,012076
62,501	0,895	0,014712	**61,734**	0,64	0,012441	**61,627**	0,572	0,011761
63,133	0,962	0,015253	**62,315**	0,643	0,01247	**62,238**	0,647	0,012509
63,759	0,865	0,014463	**62,952**	0,586	0,011904	**62,879**	0,643	0,01247
64,347	0,975	0,015356	**63,604**	0,601	0,012056	**63,518**	0,612	0,012166
64,972	0,963	0,015261	**64,234**	0,652	0,012557	**64,1**	0,634	0,012382
65,603	0,931	0,015005	**64,808**	0,531	0,011332	**64,728**	0,645	0,012489
66,236	0,889	0,014663	**65,442**	0,631	0,012353	**65,347**	0,648	0,012518
66,813	0,928	0,014981	**66,091**	0,633	0,012373	**65,941**	0,645	0,012489
67,46	0,896	0,01472	**66,717**	0,593	0,011975	**66,569**	0,663	0,012662
68,094	0,947	0,015133	**67,283**	0,576	0,011802	**67,203**	0,637	0,012412
68,686	0,935	0,015037	**67,93**	0,615	0,012196	**67,836**	0,611	0,012156

69,314	0,947	0,015133	**68,573**	0,592	0,011965	**68,44**	0,666	0,012691
69,921	0,966	0,015284	**69,14**	0,571	0,011751	**69,079**	0,609	0,012136
70,551	0,911	0,014843	**69,784**	0,566	0,0117	**69,699**	0,636	0,012402
71,158	0,933	0,015021	**70,402**	0,612	0,012166	**70,327**	0,636	0,012402
71,774	0,94	0,015077	**71,036**	0,598	0,012026	**70,908**	0,626	0,012304
72,414	0,929	0,014989	**71,649**	0,598	0,012026	**71,535**	0,64	0,012441
73,029	0,875	0,014547	**72,281**	0,565	0,011689	**72,178**	0,676	0,012786
73,654	0,973	0,01534	**72,891**	0,576	0,011802	**72,797**	0,649	0,012528
74,258	0,895	0,014712	**73,531**	0,595	0,011996	**73,397**	0,617	0,012215
74,9	0,925	0,014957	**74,146**	0,549	0,011523	**74,013**	0,598	0,012026
75,513	0,937	0,015053	**74,775**	0,576	0,011802	**74,657**	0,601	0,012056
76,106	0,873	0,01453	**75,405**	0,573	0,011772	**75,285**	0,586	0,011904
76,741	0,993	0,015497	**76,03**	0,579	0,011833	**75,878**	0,583	0,011874
77,373	0,872	0,014522	**76,626**	0,595	0,011996	**76,534**	0,612	0,012166
77,965	0,956	0,015205	**77,269**	0,539	0,011417	**77,174**	0,59	0,011945
78,59	0,999	0,015543	**77,911**	0,545	0,01148	**77,73**	0,631	0,012353
79,248	0,945	0,015117	**78,515**	0,567	0,01171	**78,362**	0,64	0,012441
79,875	0,964	0,015269	**79,139**	0,604	0,012086	**78,993**	0,658	0,012615
80,459	0,921	0,014924	**79,768**	0,568	0,01172	**79,633**	0,643	0,01247
81,11	0,909	0,014827	**80,385**	0,555	0,011585	**80,248**	0,606	0,012106
81,715	0,912	0,014851	**80,97**	0,659	0,012624	**80,882**	0,612	0,012166
82,363	0,896	0,01472	**81,644**	0,611	0,012156	**81,511**	0,645	0,012489
82,944	0,881	0,014597	**82,275**	0,58	0,011843	**82,15**	0,671	0,012739
83,57	0,939	0,015069	**82,897**	0,644	0,01248	**82,74**	0,687	0,01289
84,217	0,928	0,014981	**83,488**	0,562	0,011658	**83,373**	0,608	0,012126
84,858	0,966	0,015284	**84,077**	0,679	0,012814	**83,978**	0,618	0,012225
85,434	0,868	0,014488	**84,713**	0,631	0,012353	**84,551**	0,632	0,012363
86,075	0,97	0,015316	**85,349**	0,61	0,012146	**85,189**	0,63	0,012343
86,716	0,937	0,015053	**85,961**	0,572	0,011761	**85,824**	0,697	0,012983
87,358	0,922	0,014932	**86,61**	0,584	0,011884	**86,489**	0,607	0,012116
87,934	0,937	0,015053	**87,242**	0,62	0,012245	**87,093**	0,615	0,012196
88,575	0,962	0,015253	**87,876**	0,567	0,01171	**87,74**	0,637	0,012412
89,227	0,929	0,014989	**88,49**	0,577	0,011813	**88,386**	0,617	0,012215
89,822	1,001	0,015559	**89,132**	0,573	0,011772	**89,033**	0,639	0,012431
90,447	0,895	0,014712	**89,783**	0,607	0,012116	**89,611**	0,664	0,012672
91,085	0,99	0,015473	**90,384**	0,562	0,011658	**90,254**	0,612	0,012166
91,713	0,903	0,014778	**91,017**	0,593	0,011975	**90,869**	0,615	0,012196
92,329	0,923	0,01494	**91,654**	0,584	0,011884	**91,511**	0,644	0,01248
92,966	0,921	0,014924	**92,29**	0,608	0,012126	**92,115**	0,592	0,011965
93,592	0,967	0,015292	**92,885**	0,587	0,011915	**92,767**	0,564	0,011679
94,239	0,964	0,015269	**93,544**	0,651	0,012547	**93,404**	0,659	0,012624
94,829	0,92	0,014916	**94,183**	0,543	0,011459	**93,993**	0,661	0,012643
95,45	0,968	0,0153	**94,807**	0,63	0,012343	**94,625**	0,537	0,011396

96,111	0,961	0,015245	**95,431**	0,578	0,011823	**95,266**	0,688	0,012899
96,703	0,958	0,015221	**96,053**	0,611	0,012156	**95,918**	0,623	0,012275
97,338	1,006	0,015598	**96,698**	0,6	0,012046	**96,506**	0,642	0,01246
97,963	0,926	0,014965	**97,337**	0,624	0,012284	**97,172**	0,628	0,012324
98,62	0,877	0,014563	**97,94**	0,58	0,011843	**97,81**	0,643	0,01247
99,208	0,89	0,014671	**98,576**	0,628	0,012324	**98,437**	0,631	0,012353
99,878	0,986	0,015442	**99,233**	0,601	0,012056	**99,024**	0,672	0,012748
100,519	0,939	0,015069	**99,796**	0,585	0,011894	**99,674**	0,653	0,012567
101,129	0,966	0,015284	**100,455**	0,636	0,012402	**100,311**	0,691	0,012927
101,719	0,921	0,014924	**101,112**	0,6	0,012046	**100,964**	0,664	0,012672
102,346	0,932	0,015013	**101,739**	0,603	0,012076	**101,575**	0,65	0,012538
102,995	0,964	0,015269	**102,344**	0,61	0,012146	**102,223**	0,611	0,012156
103,641	0,893	0,014696	**102,992**	0,535	0,011375	**102,87**	0,598	0,012026
104,23	0,925	0,014957	**103,631**	0,574	0,011782	**103,446**	0,647	0,012509
104,895	0,964	0,015269	**104,268**	0,607	0,012116	**104,082**	0,721	0,013205
105,542	0,884	0,014621	**104,851**	0,601	0,012056	**104,736**	0,626	0,012304
106,11	0,941	0,015085	**105,505**	0,569	0,011731	**105,364**	0,625	0,012294
106,769	0,925	0,014957	**106,158**	0,626	0,012304	**105,965**	0,665	0,012682
107,401	0,948	0,015141	**106,755**	0,626	0,012304	**106,625**	0,617	0,012215
108,046	0,931	0,015005	**107,404**	0,593	0,011975	**107,259**	0,642	0,01246
108,627	0,946	0,015125	**108,047**	0,616	0,012205	**107,891**	0,653	0,012567
109,281	0,956	0,015205	**108,677**	0,611	0,012156	**108,494**	0,639	0,012431
109,921	0,973	0,01534	**109,295**	0,574	0,011782	**109,144**	0,685	0,012871
110,584	0,923	0,01494	**109,917**	0,62	0,012245	**109,788**	0,646	0,012499
111,163	0,917	0,014892	**110,58**	0,6	0,012046	**110,37**	0,634	0,012382
111,824	0,938	0,015061	**111,237**	0,606	0,012106	**111,016**	0,6	0,012046
112,453	0,963	0,015261	**111,829**	0,57	0,011741	**111,677**	0,651	0,012547
113,048	0,968	0,0153	**112,473**	0,603	0,012076	**112,323**	0,664	0,012672
113,684	0,929	0,014989	**113,12**	0,563	0,011669	**112,905**	0,646	0,012499
114,319	0,924	0,014949	**113,705**	0,577	0,011813	**113,559**	0,623	0,012275
114,975	0,891	0,014679	**114,36**	0,598	0,012026	**114,219**	0,686	0,01288
115,582	0,985	0,015434	**115,012**	0,568	0,01172	**114,867**	0,634	0,012382
116,217	0,951	0,015165	**115,655**	0,584	0,011884	**115,452**	0,66	0,012634
116,854	0,925	0,014957	**116,262**	0,58	0,011843	**116,092**	0,585	0,011894
117,499	1,001	0,015559	**116,906**	0,624	0,012284	**116,724**	0,637	0,012412
118,091	0,935	0,015037	**117,552**	0,555	0,011585	**117,388**	0,665	0,012682
118,743	0,97	0,015316	**118,201**	0,547	0,011502	**117,996**	0,634	0,012382
119,377	0,959	0,015229	**118,799**	0,599	0,012036	**118,645**	0,613	0,012176
120,014	0,927	0,014973	**119,436**	0,617	0,012215	**119,279**	0,662	0,012653
120,636	0,896	0,01472	**120,077**	0,588	0,011925	**119,876**	0,664	0,012672
121,27	0,941	0,015085	**120,682**	0,628	0,012324	**120,542**	0,659	0,012624
121,919	0,842	0,01427	**121,356**	0,587	0,011915	**121,165**	0,61	0,012146
122,52	0,926	0,014965	**122,013**	0,619	0,012235	**121,85**	0,59	0,011945

123,16	1,015	0,015667	**122,624**	0,57	0,011741	**122,414**	0,616	0,012205
123,826	0,958	0,015221	**123,242**	0,549	0,011523	**123,051**	0,627	0,012314
124,459	1,024	0,015737	**123,895**	0,591	0,011955	**123,713**	0,629	0,012334
125,054	0,95	0,015157	**124,51**	0,586	0,011904	**124,344**	0,689	0,012908
125,698	0,949	0,015149	**125,174**	0,563	0,011669	**124,95**	0,613	0,012176
126,37	0,927	0,014973	**125,773**	0,583	0,011874	**125,609**	0,655	0,012586
127,008	0,933	0,015021	**126,423**	0,572	0,011761	**126,262**	0,7	0,013011
127,605	0,957	0,015213	**127,072**	0,562	0,011658	**126,859**	0,628	0,012324
128,242	0,986	0,015442	**127,724**	0,605	0,012096	**127,519**	0,689	0,012908
128,891	0,93	0,014997	**128,305**	0,636	0,012402	**128,164**	0,632	0,012363
129,482	0,98	0,015395	**128,98**	0,562	0,011658	**128,774**	0,654	0,012576
130,137	0,881	0,014597	**129,634**	0,593	0,011975	**129,383**	0,692	0,012936
130,795	0,963	0,015261	**130,239**	0,589	0,011935	**130,055**	0,683	0,012852
131,419	0,956	0,015205	**130,9**	0,573	0,011772	**130,708**	0,715	0,01315
132,02	0,98	0,015395	**131,527**	0,596	0,012006	**131,354**	0,676	0,012786
132,68	0,904	0,014786	**132,18**	0,593	0,011975	**131,951**	0,627	0,012314
133,3	0,913	0,014859	**132,819**	0,523	0,011246	**132,598**	0,661	0,012643
133,978	0,946	0,015125	**133,433**	0,576	0,011802	**133,248**	0,663	0,012662
134,574	0,909	0,014827	**134,078**	0,612	0,012166	**133,839**	0,628	0,012324
135,208	1,01	0,015629	**134,717**	0,621	0,012255	**134,483**	0,624	0,012284
135,863	0,927	0,014973	**135,316**	0,582	0,011864	**135,126**	0,608	0,012126
136,45	0,918	0,0149	**135,981**	0,605	0,012096	**135,767**	0,646	0,012499
137,111	0,932	0,015013	**136,635**	0,606	0,012106	**136,393**	0,672	0,012748
137,777	0,907	0,01481	**137,222**	0,567	0,01171	**137,058**	0,639	0,012431
138,429	0,911	0,014843	**137,863**	0,567	0,01171	**137,698**	0,684	0,012861
139,048	0,97	0,015316	**138,526**	0,643	0,01247	**138,34**	0,619	0,012235
139,659	0,92	0,014916	**139,19**	0,582	0,011864	**138,933**	0,712	0,013122
140,309	0,963	0,015261	**139,81**	0,571	0,011751	**139,62**	0,661	0,012643
140,951	0,982	0,015411	**140,486**	0,6	0,012046	**140,277**	0,666	0,012691
141,559	0,977	0,015371	**141,082**	0,634	0,012382	**140,839**	0,678	0,012805
142,207	0,958	0,015221	**141,731**	0,552	0,011554	**141,488**	0,626	0,012304
142,849	0,986	0,015442	**142,364**	0,602	0,012066	**142,183**	0,679	0,012814
143,497	0,996	0,01552	**143,002**	0,582	0,011864	**142,801**	0,713	0,013131
144,103	0,954	0,015189	**143,648**	0,616	0,012205	**143,433**	0,61	0,012146
144,756	1,003	0,015574	**144,256**	0,595	0,011996	**144,078**	0,686	0,01288
145,405	0,946	0,015125	**144,902**	0,618	0,012225	**144,717**	0,697	0,012983
146,003	0,898	0,014737	**145,575**	0,587	0,011915	**145,37**	0,657	0,012605
146,673	1,013	0,015652	**146,205**	0,547	0,011502	**145,956**	0,642	0,01246
147,32	0,974	0,015348	**146,823**	0,6	0,012046	**146,622**	0,652	0,012557
147,983	0,943	0,015101	**147,458**	0,611	0,012156	**147,261**	0,695	0,012964
148,549	0,948	0,015141	**148,12**	0,634	0,012382	**147,884**	0,66	0,012634
149,211	0,929	0,014989	**148,79**	0,556	0,011596	**148,517**	0,657	0,012605
149,875	0,974	0,015348	**149,385**	0,601	0,012056	**149,179**	0,63	0,012343

150,536	0,969	0,015308	**150,062**	0,56	0,011637	**149,831**	0,637	0,012412
151,143	1,019	0,015698	**150,7**	0,569	0,011731	**150,444**	0,691	0,012927
151,79	0,97	0,015316	**151,312**	0,586	0,011904	**151,096**	0,682	0,012843
152,434	0,901	0,014761	**151,973**	0,588	0,011925	**151,765**	0,612	0,012166
153,032	0,97	0,015316	**152,617**	0,616	0,012205	**152,39**	0,678	0,012805
153,676	1,006	0,015598	**153,242**	0,553	0,011564	**152,981**	0,636	0,012402
154,323	0,962	0,015253	**153,862**	0,593	0,011975	**153,659**	0,696	0,012974
154,983	0,987	0,01545	**154,509**	0,612	0,012166	**154,309**	0,661	0,012643
155,601	0,946	0,015125	**155,183**	0,602	0,012066	**154,974**	0,71	0,013104
156,233	0,957	0,015213	**155,823**	0,596	0,012006	**155,571**	0,616	0,012205
156,904	0,931	0,015005	**156,431**	0,583	0,011874	**156,251**	0,688	0,012899
157,549	0,995	0,015512	**157,094**	0,621	0,012255	**156,884**	0,692	0,012936
158,142	1,047	0,015912	**157,731**	0,579	0,011833	**157,484**	0,642	0,01246
158,797	0,969	0,015308	**158,365**	0,588	0,011925	**158,166**	0,687	0,01289
159,477	0,991	0,015481	**159,022**	0,597	0,012016	**158,809**	0,692	0,012936
160,093	0,923	0,01494	**159,683**	0,588	0,011925	**159,496**	0,662	0,012653
160,705	0,95	0,015157	**160,342**	0,57	0,011741	**160,094**	0,658	0,012615
161,364	0,976	0,015363	**160,955**	0,611	0,012156	**160,725**	0,686	0,01288
162,068	0,906	0,014802	**161,622**	0,587	0,011915	**161,379**	0,678	0,012805
162,683	0,926	0,014965	**162,262**	0,59	0,011945	**162,051**	0,638	0,012421
163,3	0,919	0,014908	**162,908**	0,598	0,012026	**162,671**	0,685	0,012871
163,965	1,038	0,015844	**163,532**	0,565	0,011689	**163,318**	0,693	0,012946
164,617	0,99	0,015473	**164,216**	0,636	0,012402	**163,951**	0,687	0,01289
165,228	0,992	0,015489	**164,841**	0,604	0,012086	**164,593**	0,679	0,012814
165,879	0,942	0,015093	**165,435**	0,585	0,011894	**165,244**	0,682	0,012843
166,539	0,99	0,015473	**166,107**	0,652	0,012557	**165,904**	0,657	0,012605
167,166	0,976	0,015363	**166,774**	0,622	0,012265	**166,556**	0,642	0,01246
167,817	0,974	0,015348	**167,45**	0,566	0,0117	**167,147**	0,684	0,012861
168,434	0,925	0,014957	**168,041**	0,604	0,012086	**167,8**	0,663	0,012662
169,122	0,983	0,015418	**168,692**	0,542	0,011449	**168,486**	0,712	0,013122
169,732	1,02	0,015706	**169,382**	0,582	0,011864	**169,128**	0,666	0,012691
170,369	0,894	0,014704	**170,041**	0,614	0,012186	**169,742**	0,616	0,012205
171,026	0,962	0,015253	**170,626**	0,575	0,011792	**170,396**	0,668	0,01271
171,71	0,991	0,015481	**171,272**	0,614	0,012186	**171,059**	0,656	0,012595
172,326	0,957	0,015213	**171,939**	0,595	0,011996	**171,671**	0,677	0,012795
172,961	0,979	0,015387	**172,569**	0,594	0,011985	**172,33**	0,689	0,012908
173,662	0,941	0,015085	**173,23**	0,589	0,011935	**173,004**	0,673	0,012758
174,242	0,943	0,015101	**173,892**	0,585	0,011894	**173,671**	0,673	0,012758
174,898	0,976	0,015363	**174,556**	0,559	0,011627	**174,277**	0,714	0,01314
175,55	0,989	0,015465	**175,149**	0,595	0,011996	**174,938**	0,62	0,012245
176,201	0,918	0,0149	**175,852**	0,548	0,011512	**175,591**	0,666	0,012691
176,831	0,942	0,015093	**176,497**	0,591	0,011955	**176,258**	0,709	0,013094
177,516	1,035	0,015821	**177,157**	0,583	0,011874	**176,882**	0,647	0,012509

178,146	0,894	0,014704
178,804	0,989	0,015465
179,412	0,958	0,015221
180,088	0,984	0,015426
180,733	0,98	0,015395
181,389	1,009	0,015621
182,037	0,962	0,015253
182,679	0,99	0,015473
183,35	0,88	0,014588
183,975	0,989	0,015465
184,63	1,001	0,015559
185,266	0,984	0,015426
185,942	0,944	0,015109
186,538	0,989	0,015465
187,205	0,965	0,015277
187,889	0,974	0,015348
188,534	1,013	0,015652
189,153	0,974	0,015348
189,808	0,989	0,015465
190,48	0,918	0,0149
191,109	0,945	0,015117
191,76	0,995	0,015512
192,406	0,978	0,015379
193,082	0,93	0,014997
193,698	0,995	0,015512
194,351	1,008	0,015613
195,029	1,006	0,015598
195,696	0,987	0,01545
196,299	1,032	0,015798
196,979	0,992	0,015489
197,633	0,941	0,015085
198,245	1,014	0,01566
198,906	0,964	0,015269
199,591	1,045	0,015897
200,262	0,99	0,015473
200,856	0,993	0,015497
201,551	0,963	0,015261

177,751	0,617	0,012215
178,442	0,546	0,011491
179,113	0,594	0,011985
179,769	0,586	0,011904
180,394	0,614	0,012186
181,043	0,596	0,012006
181,708	0,606	0,012106
182,331	0,561	0,011648
182,971	0,611	0,012156
183,678	0,614	0,012186
184,324	0,596	0,012006
184,967	0,604	0,012086
185,628	0,595	0,011996
186,3	0,601	0,012056
186,979	0,536	0,011385
187,592	0,533	0,011353
188,284	0,603	0,012076
188,941	0,572	0,011761
189,583	0,585	0,011894
190,258	0,59	0,011945
190,907	0,62	0,012245
191,58	0,603	0,012076
192,194	0,582	0,011864
192,858	0,654	0,012576
193,564	0,578	0,011823
194,232	0,56	0,011637
194,847	0,574	0,011782
195,526	0,58	0,011843
196,155	0,606	0,012106
196,782	0,591	0,011955
197,445	0,592	0,011965
198,078	0,61	0,012146
198,779	0,595	0,011996
199,431	0,619	0,012235
200,1	0,57	0,011741

177,549	0,682	0,012843
178,208	0,734	0,013323
178,806	0,638	0,012421
179,502	0,655	0,012586
180,165	0,683	0,012852
180,797	0,621	0,012255
181,409	0,68	0,012824
182,061	0,712	0,013122
182,735	0,654	0,012576
183,392	0,67	0,012729
184,01	0,675	0,012777
184,702	0,663	0,012662
185,337	0,661	0,012643
185,995	0,692	0,012936
186,677	0,657	0,012605
187,318	0,683	0,012852
187,987	0,662	0,012653
188,618	0,68	0,012824
189,291	0,671	0,012739
189,977	0,689	0,012908
190,608	0,732	0,013305
191,245	0,712	0,013122
191,908	0,68	0,012824
192,557	0,671	0,012739
193,193	0,675	0,012777
193,859	0,65	0,012538
194,539	0,665	0,012682
195,227	0,739	0,013369
195,808	0,705	0,013057
196,499	0,676	0,012786
197,181	0,669	0,01272
197,842	0,674	0,012767
198,467	0,644	0,01248
199,138	0,739	0,013369
199,811	0,682	0,012843
200,471	0,677	0,012795

Conclusions

In the present thesis the attention is focused to the Mean Square Displacement (MSD) experimental determination from the neutron intensity data scattered according to the wavevector Q at different energy-resolution values. The data analyzed were collected in previous Elastic Incoherent Neutron Scattering measure carried out at the Large Scale Facility of the Institut Laue Langevin (ILL) on dry and hydrated lysozyme.

The instruments used were the IN10 and IN13 spectrometers. These spectrometers are characterized by a relatively high energy of the incident neutrons (16 meV) and allow to span a quite wide range of momentum transfer with two different energy resolutions. More specifically, for the IN13 spectrometer, the incident wavelength was 2.23 Å, the *Q*-range was 0.28 ÷ 4.27 $Å^{-1}$, and the elastic energy resolution was 8 μeV, which corresponds to an elastic time resolution of 516 ps; for the IN10 spectrometer, the incident wavelength was 6.27 Å, the *Q*-range was 0.30 ÷ 2.00 $Å^{-1}$, and the elastic energy resolution (fwhm) was 1 μeV, which corresponds to an elastic time resolution of 4136 ps.

From this study it was deduced that the Mean Square Displacement obtained with the IN10 spectrometer is always higher than that obtained with IN13 spectrometer. Thus, at a higher resolution, a smaller Mean Square Displacement corresponds and vice versa at a lower resolution a larger Mean Square Displacement corresponds.

Furthermore, the validity limits of Gauss's approximation for MSD evaluation has been also theoretically investigated. The data, appropriately normalized, has been analyzed according to the wave vector exchanged at different temperatures in order to extract the values of the Mean Square Displacement to the two different resolutions. There are several papers in the literature in which Mean Square Displacement is evaluated. However, calculation is often made taking into account different Q ranges and different energy resolution values (ie different resolution times). Furthermore, the data is often normalized so that it does not make direct or even possible comparison between the values obtained with different instruments or in different experimental conditions.

It is therefore important to examine the various possible procedures for normalizing the data and see what does not change the calculation of Mean Square Displacement.

The comparison, in particular, has been performed at very low temperatures ($T < 80$ K). In such a case occur only vibrational motions and the MSD system can be considered almost constant $\langle r^2 \rangle (t) \rightarrow \langle r^2 \rangle^{(V)}$.

In particular it has been shown that even though a normalization consisting of a multiplication of intensity data does not produce any change in MSD, the same procedure can not be applied directly when data logarithms are considered in a Guinier plot.

The systems investigated were dry and hydrated lysozyme (H_2O and D_2O). Lysozyme is part of the innate immune systema possesses bacteriolytic able to hydrolyze peptidoglycan in the cell wall of the bacteria. It is a natural enzyme, found in human tears, saliva, and other body fluids, secreted by epithelial cells, macrophages, astrocytes and microglia. It causes the bacterial wall of some bacteria to reduce the surface negative electrical charge so as to make the phagocytosis of the bacterium easier.

For this type of study, a wide range of experimental techniques is usually employed. Indeed, the simultaneous use of several experimental techniques, affecting several regions of the energy-momentum plan, is valuable in studying and understanding this complex phenomenology which affects systems characterized by a dynamic structure that can be parameterized by means of appropriate space-time scales.

Aknoweledgements

I would like to thank everyone who has made this experience for me possible and unforgettable.
My first duty and huge pleasure is to address a special thank you to my PhD thesis supervisor Professor Salvatore Magazù for his excellent guidance, patience, precious support and advice during the entire course and for welcoming me in his research group.
My sincere thanks also go to Dr.ssa Maria Teresa Caccamo, who has given me lots of constructive suggestions and comments.
I would like to thank the Department of Physics and Earth Science of Messina University for allowing me to use their research laboratories during my PhD course.
I would also like to thank Prof. Lorenzo Torrisi for his presence and availability.
I warmful thank you to Dr.ssa Paola Donato for her patience and courtesy.
I would also like to thank the members of my research group: Ing. Antonio Cannuli, Dr. Giuseppe Castorina, Dr. Franco Colombo.
Last, but not least, I am deeply grateful to my family, my mother and my father who sustained and encouraged me with their affection and helped me in difficult moments. My husband and my daughter Laura who fills my days with her smiles.

References

[1] F. Volino, Spectroscopic Methods for the Study of Local Dynamics in Polyatomic Fluids, Microscopic Structure and Dynamics of Liquids, NATO Advanced Study Institutes Series Volume 33, 1978, pp 221-300 and reference therein.

[2] D. Gabor. Theory of communication. Journal of the IEE, 93:429–457, 1946.

[3] J. B. Allen. Short term spectral analysis, synthesis, and modification by discrete Fourier transform. IEEE Transactions on Acoustics, Speech, Signal Processing, ASSP-25: 235 – 238, 1977.

[4] H. Frauenfelder, G. Chen, J. Berendzen, P.W. Fenimore, H. Jansson, B.H. McMahon, I.R. Stroe, J. Swenson, R.D. Young, Proc. Natl. Acad. Sci. USA, 2009, 106, 5129-5134.

[5] S. A. Lusceac, M. Vogel, J. Phys. Chem. B, 2010, 114, 10209-10216.

[6] L. Fu, S. Villette, S. Petoud, F. Fernandez-Alonso, M.L. Saboungi, J.Phys. Chem. B, 2011, 115, 1881-1888.

[7] G. Schirò, C. Caronna, F. Natali, A. Cupane, J. Am. Chem. Soc., 2010, 132, 1371-1376.

[8] S. Khodadadi, J.E. Curtis, A.P. Sokolov, More than one dynamic crossover in protein hydration water, J. Phys. Chem. B 115 (2011) 6222-6226.

[9] S. Capaccioli, K.L. Ngai, S. Ancherbak, A. Paciaroni, J. Phys. Chem. B, 2012, 116, 1745-1757.

[10] S. Magazù, F. Migliardo, A. Benedetto, J. Phys. Chem B, 2010, 114, 9268-9274.

[11] Zaccai, G. Science 2000, 288, 1604–1607.

[12] Doster, W.; Cusack, S.; Petry, W. Nature 1989, 337, 754–756.

[13] Smith, J. C.; Q. Rev. Biophys.1991, 24, 227–291.

[14] Bicout, D. J.; Zaccai, G. Biophys. J. 2001, 80, 1115–1123.

[15] Réat, V.; Dunn R.; Ferrand, M. ; Finney, J. L.; Daniel, R. M.; Smith, J. C. Proc. Natl. Acad. Sci. USA. 2000, 97, 9961–9966.24

[16] L. Van Hove, Phys. Rev. 95, 249 (1954).

[17] S. Magazù, F. Migliardo, A. Benedetto, E. Calabrò, R. La Torre, M.T. Caccamo Bioprotective Effects of Sucrose and Trehalose on Proteins Edited by S. Magazù (Nova Science Publishers Inc, 2013).

[18] A. Rahman, S. Singwi, A. Sjolander, Phys. Rev. 126, 986 (1962).

[19] S. Magazù, F. Migliardo, M.T.F. Telling, Food Chem. 106, 1460 (2008).

[20] I.V. Blazhnov, S. Magazù, G. Maisano, N.P. Malomuzh, F. Migliardo, Phys. Rev. E, 73, 031201 (2006).

[21] S. Magazù, F. Migliardo, F. Affouard, M. Descamps, M.T.F. Telling, J. Chem. Phys. 132, 123 (2010).

[22] Gregory, R. B. *Protein-Sol*V*ent Interactions*; Dekker: New York,1995.

[23] Teeter, M. M. *Annu. Re*V. *Biophys. Biophys. Chem.* 1991, *20*, 577.

[24] Careri, G. *Prog. Biophys. Mol. Biol.* 1998, *70*, 223.

[25] S.Magazu, ,F. Migliardo, A Benedetto *J. Phys. Chem. B* 2010, *114*, 9269

[26] G. E. Uhlenbeck and L. S. Ornstein "On the Theory of the Brownian Motion" Phys. Rev. 36, 823 – Published 1 September 1930

[27] Einstein, A. Über die von der molekularkinetischen Theorie der Wärme geforderte Bewegung von in ruhenden Flüssigkeiten suspendierten Teilchen. Ann. Phys. 17 (1905).
[28] Einstein, A. Theoretische Bemerkungen Über die Brownsche Bewegung. Zeitschrift für Elektrochemie und angewandte physikalische Chemie 13, 41-42, doi:10.1002/bbpc.19070130602 (1907).
[29] Michalet X. Mean square displacement analysis of single-particle trajectories with localization error: Brownian motion in an isotropic medium. Phys Rev E, Stat, Nonlinear, Soft Matter Phys. 2010;82(4 Pt 1):041914. doi: 10.1103/PhysRevE.82.041914.
[30] A. Benedetto, S. Magazù, G. Maisano and F. Migliardo, International Conference on Complexity, Metastability and Nonextensivity, in: Complexity, Metastability and Nonextensivity, S. Abe, H. Herrmann, P. Quarati, A. Rapisarda and C. Tsallis, eds, Catania, Italy, 2007.
[31] S. Magazù, G. Maisano, F. Migliardo and A. Benedetto, Phys. Rev. E 77 (2008), 061802.
[32] S. Magazù, G. Maisano, F. Migliardo and A. Benedetto, J. Phys. Chem. 112 (2008), 8936–8942.
[33] S. Magazù, G. Maisano, F. Migliardo and A. Benedetto, J. Mol. Struct. 882 (2008), 1.
[34] S. Magazù, G. Maisano, F. Migliardo and A. Benedetto, Phys. Rev. E 79 (2009), 041915.
[35] S. Magazù, G. Maisano, F. Migliardo and A. Benedetto, Biochim. Biophys. Acta 1804 (2010), 49.
[36] S. Magazù, G. Maisano, F. Migliardo, G. Galli, A. Benedetto, D. Morineau, F. Affouard and M. Descamps, J. Chem. Phys. 129 (2008), 155103.
[37] Magazù S, Maisano G, Migliardo F and Benedetto A 2008 *J. Molec. Struct.* **882** 140
[38] Magazù S, Maisano G, Migliardo F and Benedetto A 2009 *Phys. Rev. E* **79** 041915
[39] A Benedetto, S Magazù, F Migliardo1, C Mondelli and M A Gonzalez Journal of Physics: Conference Series 340 (2012) 012093
[40] L. Helmfors et al. Protective properties of lysozyme on β-amyloid pathology: implicationsfor Alzheimer disease / Neurobiology of Disease 83 (2015) 122–133
[41] Fleming, A., 1922. On a remarkable bacteriolytic element found in tissues and secretions. Proc. R. Soc. Lond. B Biol. Sci. 93, 306–317.
[42] Ganz, T., 2004. Antimicrobial polypeptides. J. Leukoc. Biol. 75 (1), 34–38.
[43] Joël Janin. Cyrus Chothia Domains in proteins: Definitions, location, and structural principles; Methods in Enzymology Volume 115, 1985, Pages 420-430
[44] W. Kauzmann Some Factors in the Interpretation of Protein Denaturation Advances in Protein Chemistry Volume 14, 1959, Pages 1-63
[45] Claus W. Heizmann, Günter Fritz and Beat W. Schäfer PROTEINS: STRUCTURE, FUNCTIONS AND PATHOLOGY [Frontiers in Bioscience 7, d1356-1368, May 1, 2002]

[46] The Genetic Control of Tertiary Protein Structure: Studies With Model Systems Charles J. Epstein, Robert F. Goldberger, and Christian B. Anfinsen CSH Simposia on quantitative biology
[47] The origin, evolution and structure of the protein worldGustavo Caetano-Anollés, Minglei Wang, Derek Caetano-Anollés, Jay E. MittenthalBiochemical Journal Feb 01, 2009, 417 (3) 621-637;
[48] Matthews, B. W. in The Proteins Vol. 3, 3rd edn (eds Neurath, H. & Hill, R. L.) 403−590 (Academic, New York, 1977).
[49] Simpson, R. J., Begg, G. S., Dorow, D. S. & Morgan, F. J. Biochemistry 19, 1814−1819 (1980).
[50] Kester, W. R. & Matthews, B. W. J. biol. Chem. 252, 7704−7710 (1977)
[51] https://www.ill.eu/instruments-support/instruments-groups/instruments/in10/
[52] https://www.ill.eu/instruments-support/instruments-groups/instruments/in13/description/instrument-layout/
[53] Alefeld, B.; Kollmar, A.; Dasannachrya, B. A. J. Chem. Phys. 1976, 63, 4415.
[54] Tokuhisa, A.; Joti, Y.; Nakagawa, H.; Kitao, A.; Kataoka, M. Phys. ReV. E 2007, 75, 041912.
[55] Meinhold, L.; Clement, D.; Tehei, M.; Daniel, R.; Finney, J. L.; Smith, J. C. Biophys. J. 2008, 94, 4812.
[56] Kneller, G. R.; Hinsen, K. J. Chem. Phys. 2009, 131, 045104.
[57] Gabel, F.; Bellissent-Funel, M. C. Biophys. J. 2007, 92, 4054.
[58] Kneller, G. R.; Calandrini, V. J. Chem. Phys. 2007, 126, 125107.
[59] Becker, T.; Smith, J. C. Phys. ReV. E 2003, 67, 021904.
[60] Becker, T.; Hayward, J. A.; Finney, J. L.; Daniel, R. M.; Smith, J. C. Biophys. J. 2004, 87, 1436.